UNIVERSITÀ DEGLI STUDI DI MILANO

Scuola di Dottorato in Scienze Biologiche e Molecolari

XXVI Ciclo

THE AUXILIARY SUBUNIT TRIP8b ANTAGONIZES THE BINDING OF cAMP TO HCN2 CHANNELS THROUGH AN ALLOSTERIC MECHANISM

Andrea Cosimo Saponaro

PhD Thesis

Scientific tutor: Prof. Anna Moroni

Academic year: 2012 - 2013

CONTENTS

PART I

Abstract

In neurons, hyperpolarization-activated cyclic nucleotide-regulated (HCN1-4) channels are the molecular determinants of the I_h current, which controls several cognitive processes. Unique among the voltage-gated ion channel superfamily, HCN channels are modulated by the direct binding of cAMP to their cytoplasmic cyclic nucleotide binding domain (CNBD). Thus, cyclic nucleotide-dependent conformational changes of CNBD are determinant in the regulation of HCN channel opening. The rearrangements induced by cAMP in HCN CNBD are not yet elucidated, since for this protein is known only the cAMP-bound form. HCN channels are further regulated by their association with the auxiliary protein TRIP8b, which preferentially binds to the cAMP-unbound CNBD and opposes cAMP regulation. Recently, we proposed a cyclic allosteric model to explain the mutual antagonistic effect of TRIP8b and cAMP. Here, to validate this model, we first determined the model structure of the human HCN2 CNBD in the cAMP-unbound form using NMR methodologies. By comparing the cAMP-unbound and cAMP-bound structures we highlighted all the conformational changes allosterically coupled to the channel opening transition. Subsequently, we mapped the TRIP8b binding site onto the cAMP-unbound CNBD. Our results show that cAMP and TRIP8b do not compete for the same binding region, and support our allosteric antagonistic model for the dual regulation of HCN channels by cAMP and TRIP8b.

1 STATE OF THE ART

1.1 I_h current

I_h is a mixed cationic (Na^+ and K^+) current activated by the hyperpolarization of the plasma membrane and regulated by cyclic nucleotides (cAMP and cGMP) (Fig. 1) [1]. Given its peculiar voltage dependence, which is contrary to the vast majority of the voltage-gated current activated upon membrane depolarization, it was called with the name of "funny current" (I_f) in the heart cells [2], and with the names of "queer current" (Iq) [3] or "hyperpolarization activated current" (I_h) in neurons [4]. In this work the term I_h will be used.

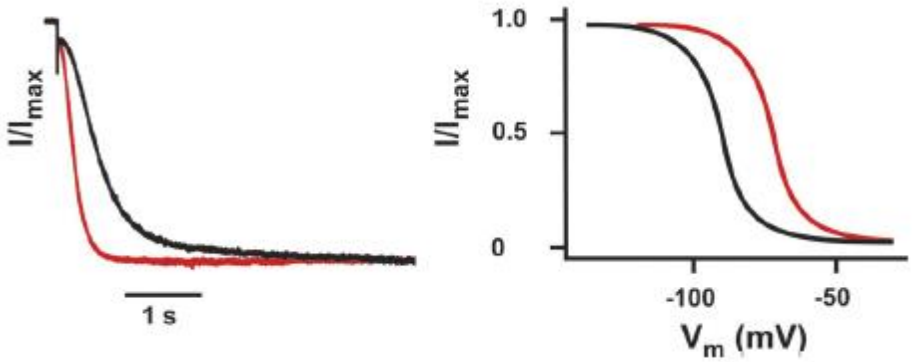

Fig. 1: Biophysical properties of I_h current.
Left: I_h activates faster in the presence (red) than in the absence (black) of cAMP at maximal activation voltage (-140mV). Right: activation curve of I_h in the absence (black) and presence (red) of cAMP. In the presence of cAMP, the activation curve of I_h is shifted to the right [5].

I_h current controls, among other functions, the resting membrane potential, the regulation of dendritic integration and the pacemaking activity (in both heart and brain). Since I_h has a reversal potential of around -20 mV, at physiological ionic conditions and resting potential it is partially open and inwardly directed and consequently sets the level of the resting membrane potential at a somewhat depolarized level [5]. Furthermore, I_h current seems to function as a slow "voltage clamp", counteracting both hyperpolarizing and depolarizing inputs, respectively

by producing a depolarizing inward current, due to its activation, or by facilitating the hyperpolarization, because of its deactivation [6]. In neurons, this ability to oppose to excitatory and inhibitory stimuli is crucial for the modulation of the amplitude and passive propagation of the excitatory postsynaptic potentials (EPSPs) and inhibitory postsynaptic potentials (IPSPs) [7, 8] (Fig. 2A). Moreover, I_h current contributes to the genesis of the action potential in the SAN cells and Purkinje cardiac fibers [9], as well as in neuronal cells, such as the talamocortical relay neurons [10] and the hippocampal stratum oriens interneurons [11]. The activation of I_h current at negative voltages, due to the repolarization phase of the action potential, generates an excitatory inward current, which drives the membrane potential to the threshold for firing a subsequent action potential (Fig. 2B).

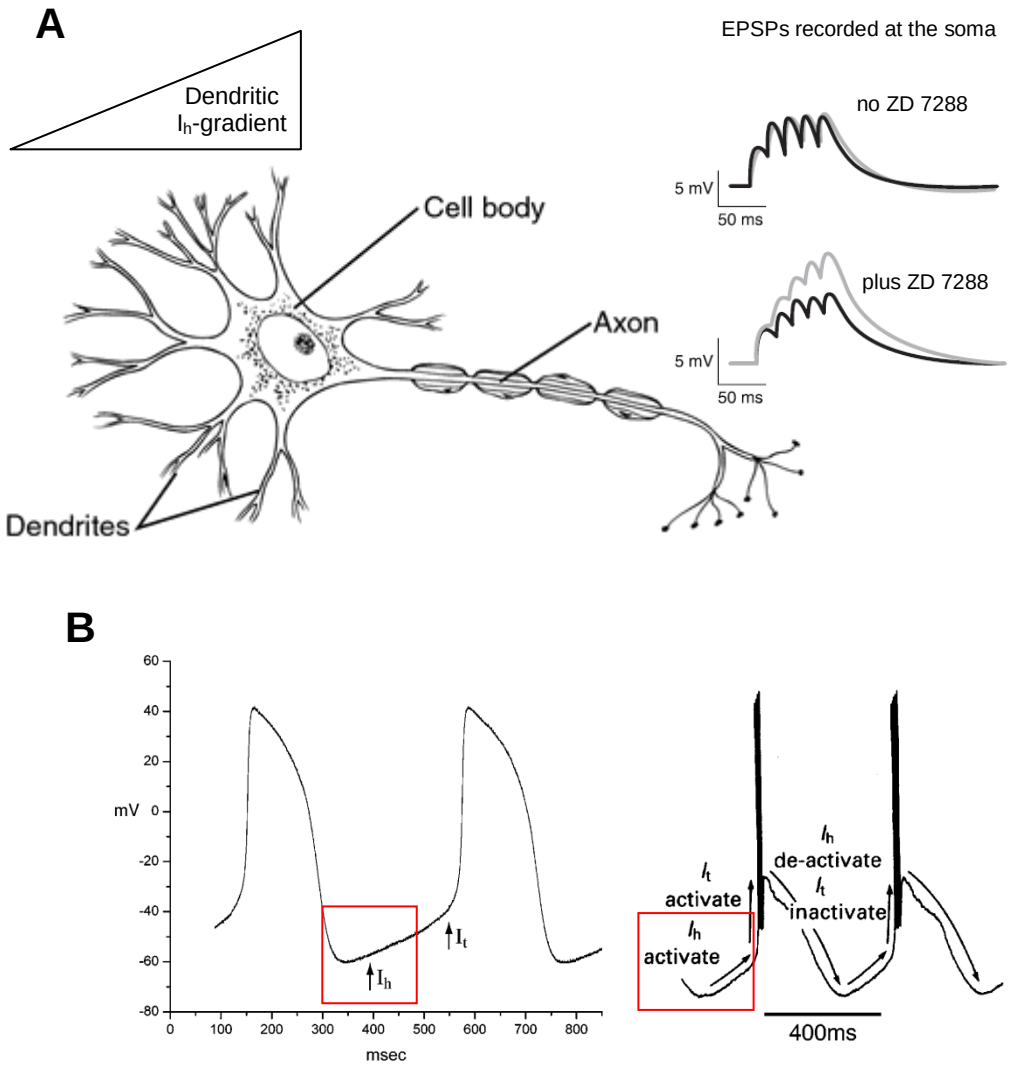

Fig. 2: Multiple functions of I_h in neurons and cardiac myocytes:
A, The somato-dendritic gradient of I_h effectively filters the propagation of inputs through dendrites and then normalizes their temporal summation at the soma. Right: Summation of EPSPs from proximal (black trace) and distal (gray trace) dendrites recorded at the soma after propagation. The voltage recordings are shown before (top panel) and after (bottom panel) inhibition of I_h by the selective I_h blocker ZD 7288 [image modified from Ref. 5]. B, Pacemaking function of I_h in a cardiac sinoatrial node myocyte (left) and in a thalamocortical relay neuron (right). In both cells, I_h activation following an action potential produces a slow depolarization that triggers an action potential through activation of calcium channels (I_t current). Red box indicates the temporal shadow of action of the I_h current [image modified from Ref. 1].

1.2 HCN channels

Hyperpolarization-activated cyclic nucleotide-gated (HCN1-4) channels are the molecular determinants of I_h current. HCN channels belong to the superfamily of the voltage-gated K^+ (Kv) channels [12]. Thus, the "core" unit of these channels reflects the typical architecture of the voltage-gated K^+ channel, which is constituted by the assembly of four α-subunits, integrally embedded in the cell membrane to create an ion-conducting pore. In mammals four protein isoforms (HCN1-4) were found [13], which are able to organize either in homo or hetero-tetramers [14]. HCN channels are expressed mainly in the central nervous system and heart. All the four isoforms are present in the brain, even though with different expression profiles: of all HCN3 shows the weakest expression, by contrast HCN2 presents the widest expression profile, in particular reaching high levels in the thalamus. The second brain isoform is HCN1, that shows a more selective expression profile compared with HCN2. HCN1 is highly expressed in the hippocampus, neocortex, cerebellar cortex and neuronal stem cells. HCN4 isoform, which expression is generally low, is restricted to specific regions, such as thalamus nuclei and mitral cells of the olfactory bulb [15, 16]. All the four isoforms are present in cardiac tissues, though HCN4 is the predominant, accounting for >80% of the total HCN mRNA in the SAN, the pacemaker region of the heart [16, 17]. The α-subunit of HCN channels has six transmembrane segments (S1-S6), of which, segment S4 forms the voltage sensor domain, while S5-S6 comprise the pore region. HCN channel have both intracellular N- and C-termini. The N-terminus is different in every isoform, while the C-terminal tail contains the CNBD (cyclic nucleotide binding domain), which determines the modulation of the HCN channel activity by the cyclic nucleotides. Right upstream of the CNBD the C-linker domain is present, which connects the CNBD to the pore region, and therefore conveys the regulation of channel gating exerted by the CNBD (Fig. 3) [5]. The amino acid sequence of the C-linker/CNBD region is highly conserved among the four isoforms [1, 5].

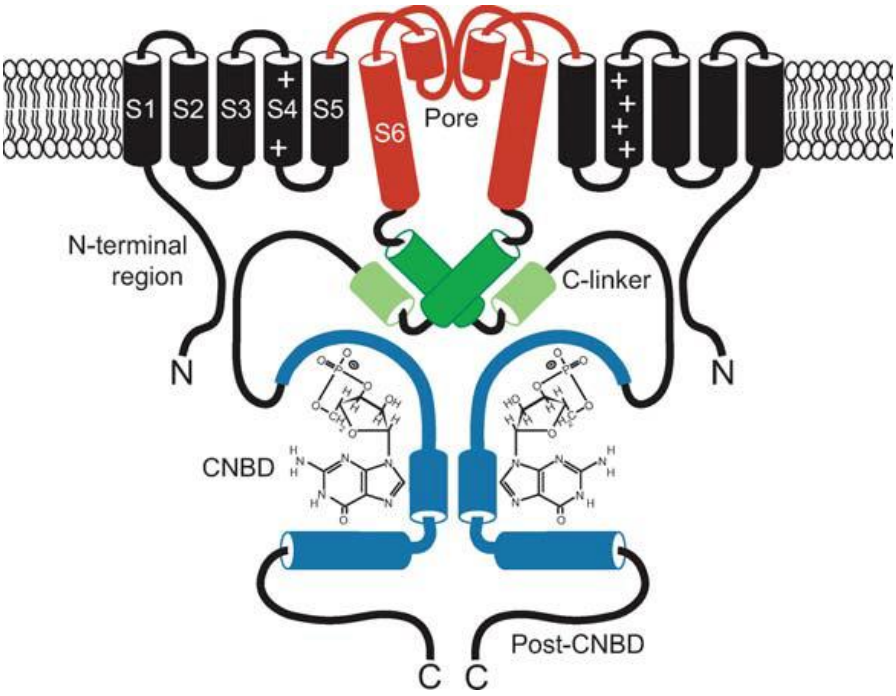

Fig. 3: Topology of HCN channels. Two of the four subunits of an HCN channel are shown. The transmembrane segments (S1–S6) are shown in black, except for the pore region (S6 and pore loop), which is shown in red. The voltage sensor (S4) is indicated by positive charges. The C-terminal region contains the cyclic nucleotide binding domain (CNBD, blue, shown with cAMP bound) and the C-linker (green), which connects the CNBD to the pore [5].

1.3 The role of the cyclic nucleotide

HCN channels are directly modulated by cAMP and cGMP, which enhance channel opening in hyperpolarization by binding to the CNBD. In HCN channels CNBD exerts a tonic inhibition on the channel pore, shifting the gating in absence of the cyclic nucleotide to more negative potentials (Fig. 1). This inhibition is released by ligand binding, with a consequent increase of the open probability at hyperpolarizing voltages and a shift of the voltage dependence of activation at more depolarizing potentials [18] (Fig. 1 and 4B). The inhibitory effect of CNBD is supported by the fact that the deletion of this domain causes the same effect of facilitation in channel opening, that is determined by cAMP binding [18]. The proposed mechanism of HCN channel opening is complex, requiring the allosteric interactions between four domains: the pore, the S4 voltage sensor, the C-linker, and the CNBD (Fig. 4A). Each domain is in equilibrium between two possible conformations. The pore can be closed or open, the voltage sensor and

the C-linker can be resting or activated, and the CNBD can be unbound or bound to ligand. The domains are then coupled to each other, indicating that the conformation of one module affects the conformation of another module [19]. Hence, the opening transition of the channel is allosterically coupled to a conformational change both in the voltage sensor (S4) domain, due to hyperpolarization of the membrane potential and in the CNBD, caused by cyclic nucleotide binding [20]. Despite the complexity of the mechanism of channel opening, it can be asserted that the closed-to-open transition of the channel reflects the transition from the cAMP-unbound to the bound conformation of the CNBD, which indeed stabilizes the closed and open state of the channel, respectively [18-20] (Fig. 4B).

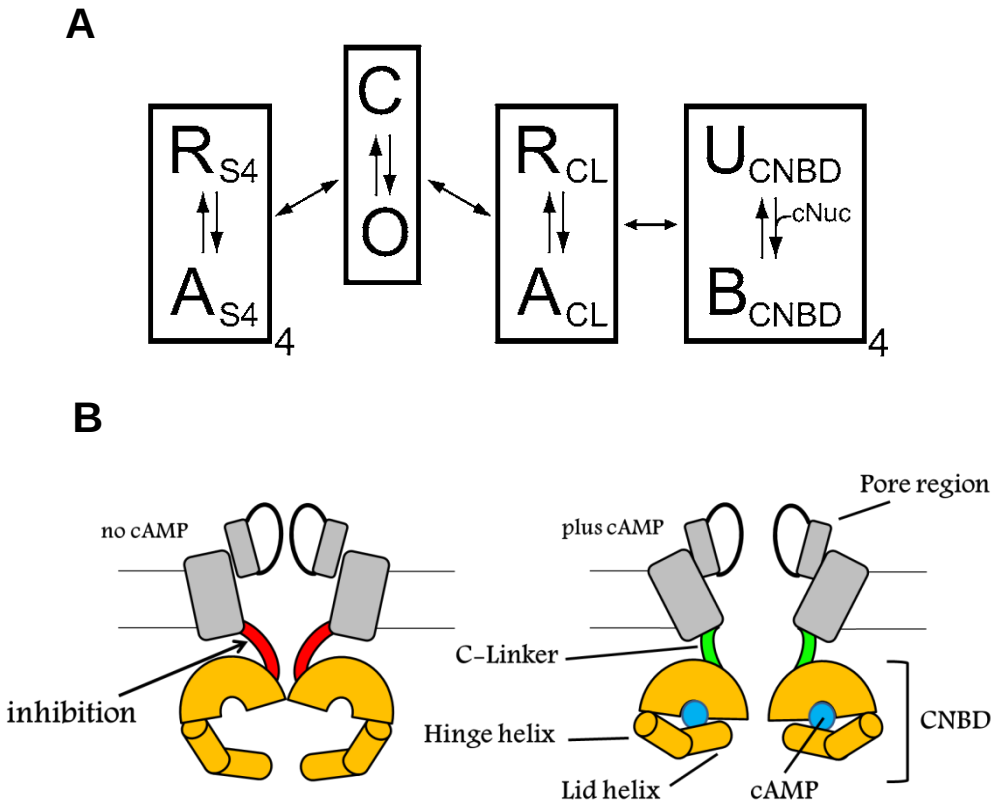

Fig. 4: Molecular mechanism of cAMP modulation of HCN channel opening.
A, Proposed activation mechanism for HCN channels. Voltage sensor (S4), C-linker (CL). States are shown as closed (C), open (O), resting (R), activated (A), unbound (U), and bound with ligand (B). Boxes around states indicate separable gating modules. Single-headed arrows indicate equilibrium between states, and double-headed arrows indicate coupling between gating modules [19]. B, Effect of cAMP on the HCN channel. The figure illustrates two adjacent α-subunits of the four comprising the channel. The core transmembrane domain (S1-S6) is

indicated in grey. In orange is represented the cyclic nucleotide-binding domain (CNBD), as a semicircular region (b-roll) and two cylinders (B/C helix element) (see Par. 1.5 for a detailed explanation of the CNBD elements). Left, the CNBD in the cAMP-unbound conformation inhibits the gating of the core transmembrane domain by a strain coupled through the C-linker (indicated in red). Right, in the presence of cAMP (blue circle), a conformational change in the CNBD leads to relief of strain on the C-linker (indicated in green), which promotes channel opening [image modified from Ref. 18].

1.4 The role of TRIP8b

In addition to cAMP, HCN channels are further regulated by proteins such as TRIP8b (TPR-containing Rab8b interacting protein), a cytoplasmic β-subunit of neuronal HCN channels, which regulates ion channel trafficking and gating [21-23]. TRIP8b is subjected to alternative splicing at its N-terminus, giving rise to different isoforms with diverse effects on HCN channel trafficking. In contrast, all TRIP8b isoforms inhibit HCN channel opening by antagonizing the effect of cAMP (Fig. 5) [21]. TRIP8b directly binds the cytoplasmic C-terminal region of HCN through two distinct sites conserved in all isoforms: the tetratricopeptide repeat (TPR) domain, which binds the last three aminoacids (SNL) of HCN [24], and an 80 amino acid sequence located in its central core (miniTRIP8b), that interacts with the CNBD domain [25]. It has been argued that, whereas the TPR domain stabilizes the interaction between HCN channels and TRIP8b, miniTRIP8b is necessary and sufficient to antagonize the cAMP-induced effect on channel opening (Fig. 6) [25, 26]. Furthermore, it was demonstrated that miniTRIP8b fragment also reduces the maximal current through the channel in the absence of cAMP (Fig. 7B) [26].

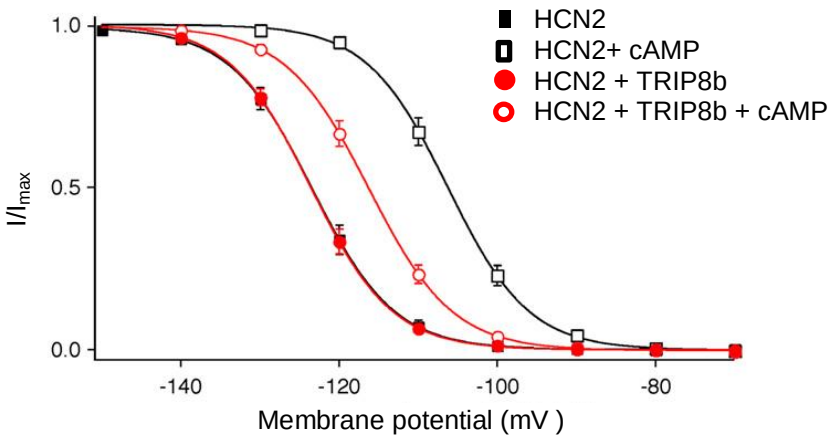

Fig. 5: TRIP8b antagonizes the cAMP-induced effect on HCN channel opening. Steady-state activation curves of HCN2 channels (black) and HCN2 and TRIP8b channels (red) before (filled symbols) and after application of 100 µM cAMP (open symbols). The right shift of the curve of activation due to cAMP is significantly reduced for HCN2 that is in complex with TRIP8b, indicating that TRIP8b is able to partially inhibits the cAMP effect [image modified from Ref. 22].

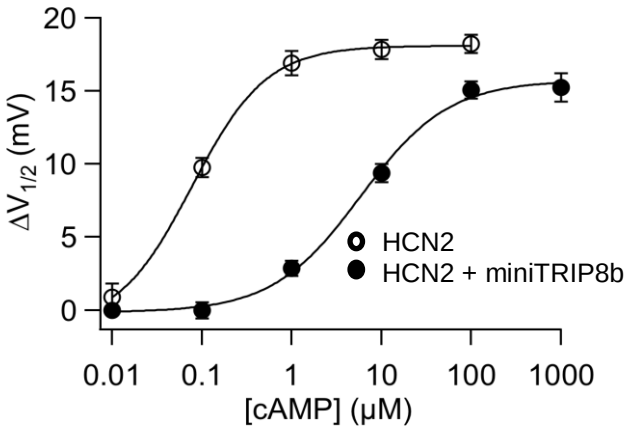

Fig. 6: Effects of miniTRIP8b on action of cAMP on HCN2 channel voltage gating.
(A) Shift in $V_{1/2}$ as a function of [cAMP] in the absence (open circles) or presence (filled circles) of 4 µM miniTRIP8b. Solid lines show fits of the Hill equation, which yield: ΔV_{max}= 18.1 mV for HCN2; ΔV_{max}= 15.8 mV for HCN2 plus 4 µM miniTRIP8b. for HCN2 co-expressed with TRIP8b ΔV_{max}= 14.2 mV [image modified from Ref. 26].

Although the interaction of TRIP8b with HCN channels has been characterized at both the functional and biochemical level, high-resolution structural data of the TRIP8b-HCN CNBD

complex have not yet been obtained, preventing the development of a decisive molecular model to explain the mutual inhibitory effect of TRIP8b and cAMP. In a recent work it was shown that cAMP acts by competitively displacing TRIP8b from HCN CNBD [27]. Furthermore it has been suggested that TRIP8b and cAMP compete for the same binding site, as the mutation of a conserved Arginine residue of the cyclic nucleotide binding site (R538E in human HCN1 and R591E in human HCN2), which is known to severely decrease the affinity of the CNBD for the cAMP, abolishes the interaction with TRIP8b [27]. On the contrary, we have shown that the interaction of HCN1 and TRIP8b is maintained in the HCN1 R538A mutant and strongly decreased, but not abolished, in the R538E mutant and that miniTRIP8b effect on HCN2 R591E mutant is not altered (Fig. 7) [26]. Moreover, our electrophysiological results demonstrated that the mutual antagonistic effects of TRIP8b and cAMP are better described by a cyclic allosteric mechanism rather than a direct competition of the two ligands [26]. These data strongly support the hypothesis that TRIP8b and cAMP binding sites do not overlap, and indeed structural data of the TRIP8b-CNBD complex are now required to validate the allosteric antagonism between the ligands.

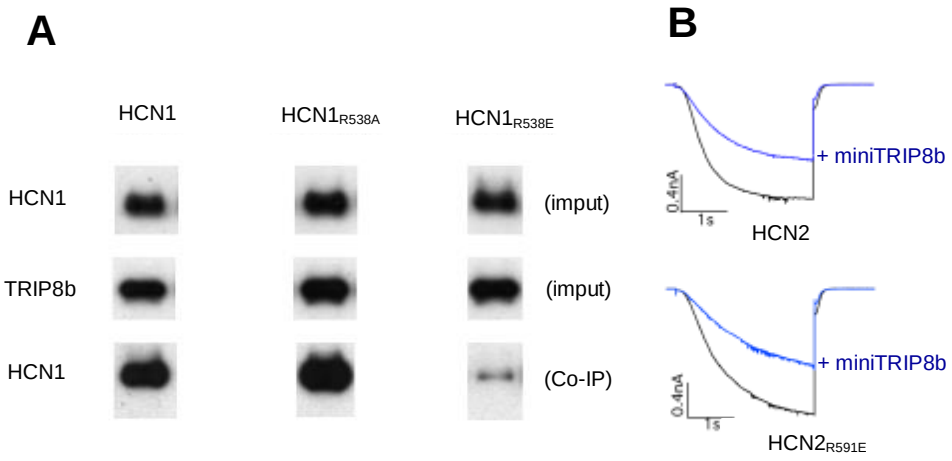

Fig. 7: TRIP8b does not bind to the cyclic nucleotide binding site of the CNBD.
A, The effect of mutations in the HCN1 CNBD residue R_{538} on TRIP8b binding. Western blot analysis shows binding of HCN1, $HCN1_{R538A}$ and $HCN1_{R538E}$ mutants to wild-type TRIP8b assessed by coimmunoprecipitation from Xenopus *oocyte extracts co-expressing TRIP8b and HCN1. The top row shows the HCN1 input signal using an anti-HCN1 antibody. The middle row*

shows the TRIP8b input signal using an anti-TRIP8b antibody. The bottom row shows the amount of HCN1 protein coimmunoprecipitated with the TRIP8b antibody (western blot probed using anti-HCN1 antibody). Note that exposure times are directly comparable along each row, but not down each column. B, TRIP8b reduces maximal current by interacting to the CNBD. Currents through HCN2 WT and R591E mutant channel before (black trace) and after (blue trace) the application of 4 μM miniTRIP8b to inside-out patches (no cAMP present). The effect of miniTRIP8b on the maximal current reduction is not altered by R591E mutation highlighting that TRIP8b and cAMP binding sites do not overlap [images modified from Ref. 26].

1.5 The CNB domain

The CNBD is a structural domain found in several different kinds of prokaryotic and eukaryotic cyclic nucleotide-binding proteins: from the bacterial MloK1 channel [28] to the mammalian PKA enzyme [29]. It consists of an N-terminal helical bundle, followed by an 8-stranded antiparallel β-roll, and two terminal α-helices (Hinge and Lid). The cyclic nucleotide binding site (known as PBC, Phosphate Binding Cassette) is a pocket formed by the β-roll of the CNBD (Fig. 8) [30]. In HCN channels, the first two helices of the N-terminal helical bundle have been conventionally associated to the upstream C-linker sequence (Fig. 8A). Although only the structure of the cAMP-bound form of HCNs CNBD is known [31, 32], structural data coming from other CNBDs in the cAMP-unbound configuration demonstrate that the cyclic nucleotide induces the reorientation of the N-terminal helical bundle, as well as of the Hinge and Lid helices (Fig. 9). These movements are essential for the CNBD to perform its function. Once the cyclic nucleotide binds the PBC, this interaction causes the approach of the hinge and lid helices to the β-roll. In the new position adopted, the lid helix is able to interact with the base of the cyclic nucleotide and this binding stabilizes its own orientation and that of the hinge helix. Furthermore, the new conformation adopted by the hinge-Lid helix element causes the reorientation of the N-terminal helical bundle. The movement of the N-terminal helical bundle is important for cyclic nucleotide signalling, as it gives rise to conformational changes, that are translated into activation mechanisms specific for the different cyclic nucleotide-regulated proteins [30].

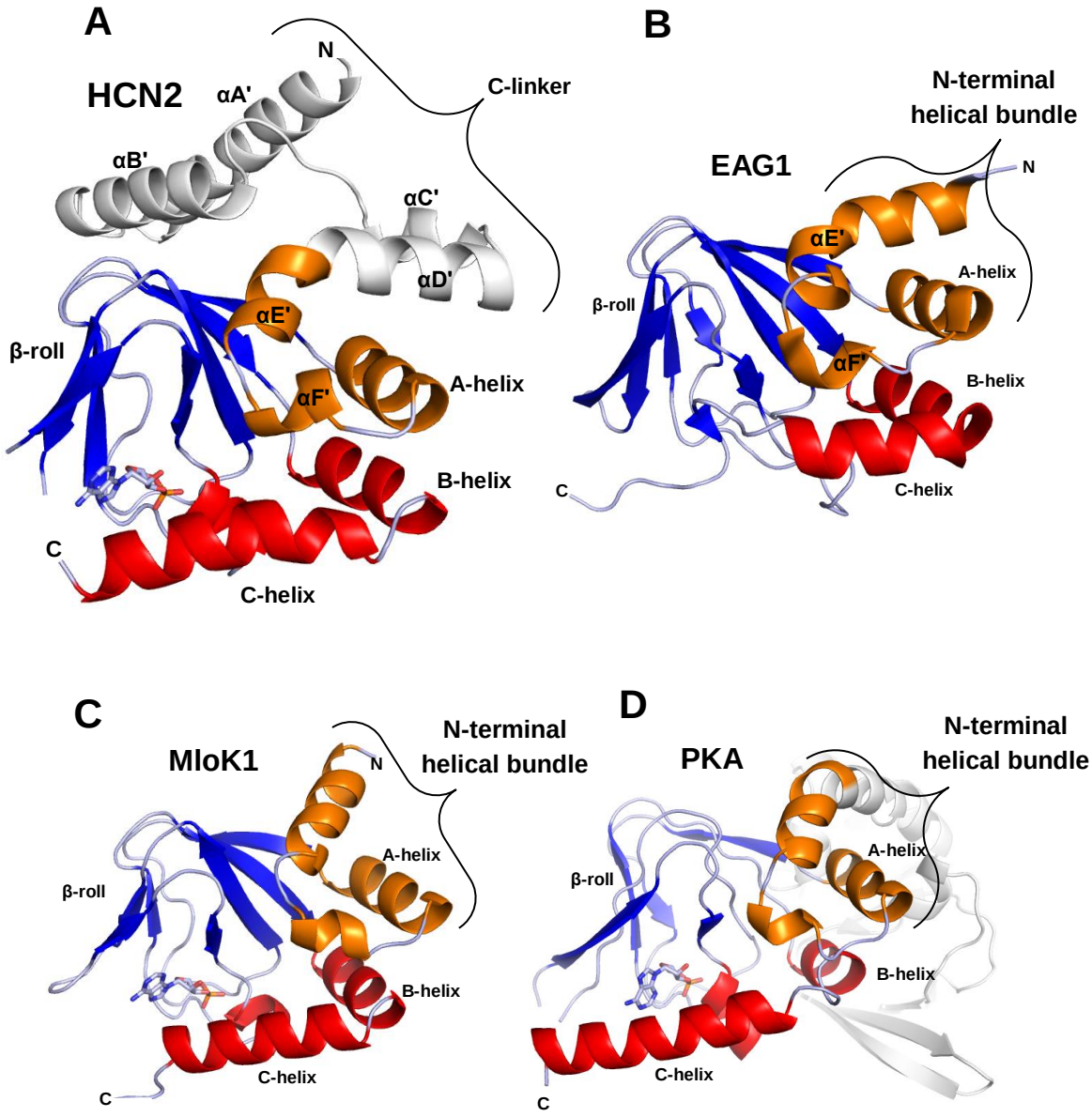

Fig. 8: The structural elements and topology of CNBD-containing proteins are universally conserved.

A, HCN2 CNBD in the cAMP-bound conformation. B, CNBD of EAG1 channel, which belongs to the voltage-gated potassium channel family together with EAG and ELK channels. C, CNBD from the prokaryotic cyclic nucleotide-gated channel MloK1 in the cAMP-bound conformation. D, cAMP-bound CNBD site B of protein kinase A (PKA). The evolutionarily conserved elements of these four proteins are coloured: N-terminal helical bundle in orange, 8 β-strands in blue, B and C-helix in red. Structures were generated from the Protein Data Bank accession codes 3U10 (HCN2, Ref. 31), 4F8A (EAG1, Ref. 33), 2KXL (MloK1, Ref. 28) and 1RL3 (PKA, Ref. 29) using PyMOL.

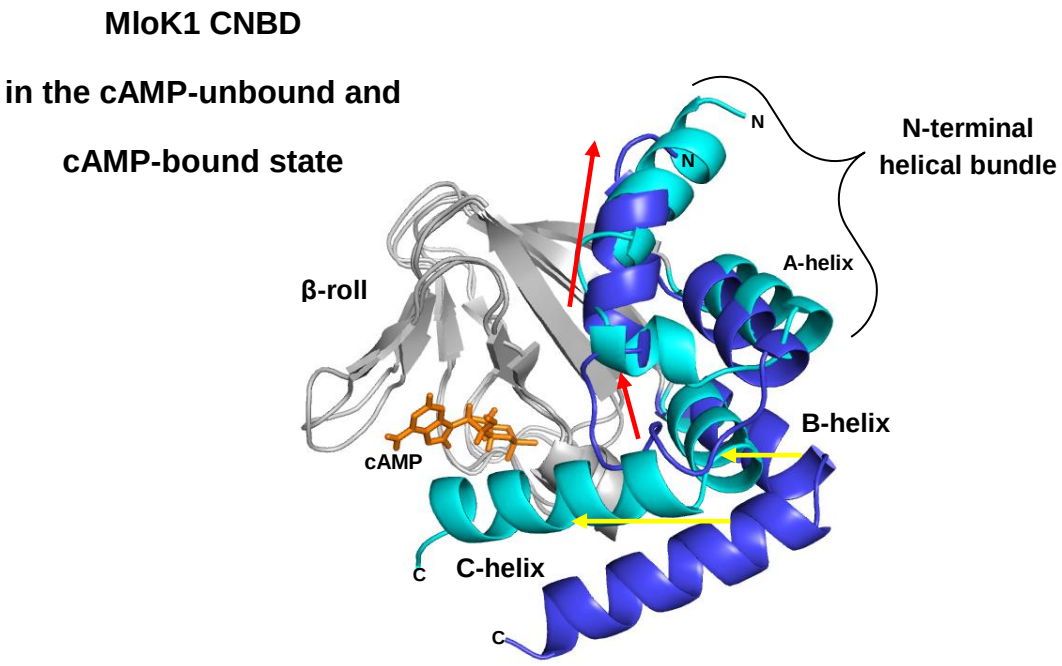

Fig. 9: Universally conserved movements of the CNBD protein caused by cyclic nucleotide binding.
A, Superimposition of the CNBD in the cAMP-unbound and -bound conformations from the prokaryotic MloK1 channel. β -roll subdomain of both forms is coloured gray, while the N-terminal helical bundle and the B/C-helices are coloured in light blue (cAMP-bound form) and blue (cAMP-unbound form), respectively . cAMP is in orange. Red arrows indicate movements of the N-terminal helical bundle and yellow arrows movement of the B/C-helices. Both groups of movements are consequence of the binding of cAMP to the PBC. Structures were generated from the Protein Data Bank accession codes 2KXL (cAMP-unbound CNBD) and 2K0G (cAMP-bound CNBD) using PyMOL.

1.6 The binary cAMP-TRIP8b regulatory system

In the central nervous system cAMP signaling is important for the regulation of different cognitive processes [34, 35] and emotional aspects [36]. Moreover, HCN channels have been shown to mediate long-term memory processes [37] and misregulation of I_h occurs in several neurological disorders [38-40]. Several works established a direct connection between cAMP and HCN channels in the development of neuronal functions, as in the case of the prefrontal cortex, in which cAMP-modulation of HCN channel activity is involved in the regulation of

working memory networks [41]. As for cAMP, a role in the regulation of HCN-mediated neuronal activity has been robustly established for TRIP8b [42, 43] and the combined effect of cAMP and TRIP8b as well. For example, in the hippocampus and entorhinal cortex HCN channels control the development of place and grid cells, respectively, which are critical for spatial memory and navigation [44, 45]. In these two regions of the brain HCN channels show a dorsoventral gradient of sensitivity for cAMP. In particular, in the hippocampus it was highlighted that this different response to cAMP is due to a dorsoventral gradient of expression of TRIP8b (Fig. 10) [44]. The increased expression of TRIP8b in the dorsal region, compared to the distal region, corresponds to a decreased cAMP sensitivity of I_h in dorsal cells, and viceversa for the ventral cells. Thus, the binary cAMP-TRIP8b modulation of HCN channels is relevant for the spatial and temporal development of the hippocampus properties. Moreover, such mechanism of HCN channel regulation accounts for the peculiar role of cAMP in the ventral hippocampus, where cyclic nucleotide levels are specifically increased during strong emotional conditions [36]. The high similarity with the hippocampus in the spatial profile of cAMP-dependent modulation of HCN channels led to argue the involvement of the cAMP-TRIP8b regulatory pathway also for I_h current present in the enthorinal cortex [45]. Indeed, the combined action of cAMP and TRIP8b signaling in the modulation of HCN channels is becoming even more crucial for the understanding of an increasing number of physiological functions and diseases affecting cognition.

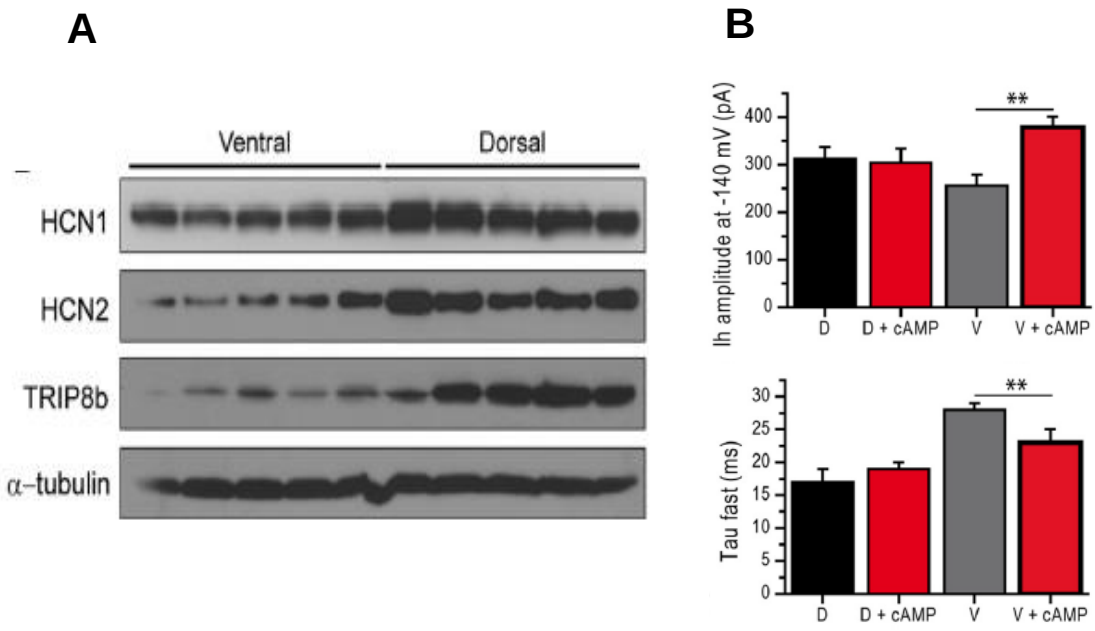

Fig. 10: The dorsoventral distribution of TRIP8b as a molecular substrate for the different sentitivity of I_h to cAMP in the hippocampus [44].

A, Western blots of HCN1, HCN2, and TRIP8b proteins from ventral and dorsal hippocampus demonstrate that HCN1, HCN2, and TRIP8b protein levels are significantly larger in dorsal than ventral hippocampus. B, Application of cAMP increases I_h amplitude and kinetics and resonance in ventral place cells. Histograms of I_h current properties before and after cAMP. Note the cAMP-dependent increase in amplitude and faster kinetics in ventral, but not dorsal place cells.

2 AIMS OF THE PROJECT

Assuming that HCN CNBD undergoes the same extensive spatial rearrangements upon cAMP binding as for the known CNBD-containing proteins, one plausible hypothesis for the explanation of the mutual allosteric antagonism of TRIP8b and cAMP is that each of the two ligands stabilizes the CNBD in a conformation that decreases the affinity for the antagonist. A conclusive validation of this assumption requires the structural description of the complex between HCN CNBD and TRIP8b. Thus the main purpose of this work was to obtain structural information on this protein complex. Since our efforts to crystallize the CNBD-TRIP8b complex failed, we employed soluble NMR methodologies. First, we set out to obtain the structure of the human HCN2 CNBD in the cAMP-unbound form. The determination of the cAMP-unbound CNBD structure was essential to clarify all of the conformational changes occurring in the transition from the cAMP-unbound to the bound state of the CNBD. Furthermore, since we established that TRIP8b binds preferentially the cAMP-unbound form of the CNBD, the determination of this CNBD conformation was a necessary prerequisite for the study of the TRIP8b binding site on HCN CNBD. The second goal of the project was to identify the TRIP8b binding region on the CNBD, using NMR titration experiments. Finally, the identification of the TRIP8b binding site on CNBD led to the description of a molecular mechanism of competition occurring between cAMP and TRIP8b that supported the proposed model of the mutual allosteric antagonism.

3 RESULTS

3.1 cAMP destabilizes the miniTRIP8b-HCN2 Clinker/CNBD complex

Electrophysiological experiments have shown that the antagonistic role of TRIP8b on the cAMP-dependent effect on HCN currents is due to miniTRIP8b fragment, the 80 amino acid core moiety of the full length protein [26]. Furthermore, we and others have previously shown that TRIP8b preferentially interacts with HCN channel having their CNBD in the cAMP-unbound conformation and that such interaction decreases at increasing cAMP concentrations [25-27]. We decided to investigate if this behavior is maintained also in vitro, between the isolated HCN C-linker/CNBD and miniTRIP8b proteins, using a direct biochemical analysis. To this end, we co-expressed in *E. coli* the HCN2 C-terminal region including the C-linker and the CNBD tagged with the His_6-MBP sequence (herafter $CNBD_{c\text{-}linker}$), with the miniTRIP8b fragment tagged with the Strep sequence. The bacterial lysate was supplemented with increasing cAMP concentrations (from 0 to 1 mM) and the complex subsequently purified by means of the Nickel affinity column. As expected, increasing cAMP concentration in the lysate decreased the amount of miniTRIP8b protein co-purified with $CNBD_{c\text{-}linker}$, highlighting the destabilizing effect of the cyclic nucleotide on the TRIP8b-CNBD interaction (Fig. 1). These results confirmed that miniTRIP8b and cAMP are competing for the binding to CNBD, and that TRIP8b preferentially binds the cAMP-unbound conformation of the CNBD. The question remains whether a direct (for the same binding site) or an indirect (allosteric) competition event occurs between the two ligands. To answer this question we employed soluble NMR methodologies to obtain the structure of the HCN2 CNBD in the cAMP-unbound conformation and subsequently map the TRIP8b binding site on it.

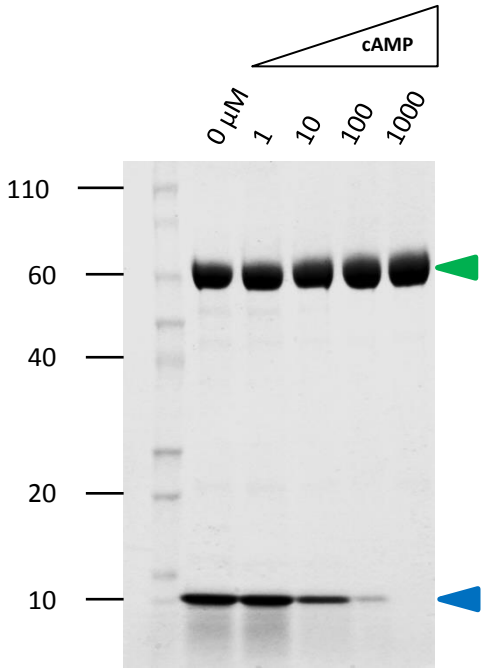

Fig. 1: cAMP disrupts the miniTRIP8b-CNBD$_{c\text{-}linker}$ complex formation.
Coomassie blue staining following SDS-PAGE separation of the complex eluted from a Nickel affinity column, after pre-incubation with increasing cAMP concentrations (indicated on the top) . Green arrowhead marks the position of CNBD$_{c\text{-}linker}$, while blue arrowhead that of miniTRIP8b. Numbers to the left refers to molecular weight markers (kDa), loaded in the first lane.

3.2 Biochemical characterization of the miniTRIP8b-CNBD complex

Since the most usual soluble NMR techniques restricts the analysis to proteins below 30-40 kDa, we prepared a shorter construct of the C-linker + CNBD fragment, removing the first three α-helices (A'-C') of the C-linker (hereafter CNBD, residues 521-672 of the human HCN2 channel). This was also necessary in order to prevent the C-linker-driven tetramerization of the protein at the high concentrations required for the NMR experiments [31, 46]. First we tested the capability of the CNBD to interact with miniTRIP8b. To this end, we coexpressed it with the strep-tagged miniTRIP8b in *E.coli* and purified the complex by means of a strep-tactin affinity column. As shown in Fig. 2A the CNBD efficiently co-purifies with miniTRIP8b, confirming that neither the complete C-linker domain, nor the oligomerization of the HCN2 protein are required for the interaction with miniTRIP8b sequence. In order to validate this assay, but

mostly to obtain biochemical information about the stoichiometry and the affinity constant of miniTRIP8b-CNBD interaction, we performed isothermal titration calorimetry (ITC) on the complex. Titration of miniTRIP8b fragment onto the CNBD produced exothermic binding signals, which can be fit with a single-site binding model. The generated binding curve (Fig. 2B) yields a binding affinity of 1.3 µM, and a binding stoichiometry ≈1. This result is in agreement with the 1:1 stoichiometry recently determined between HCN2 channel and full-length TRIP8b [24].

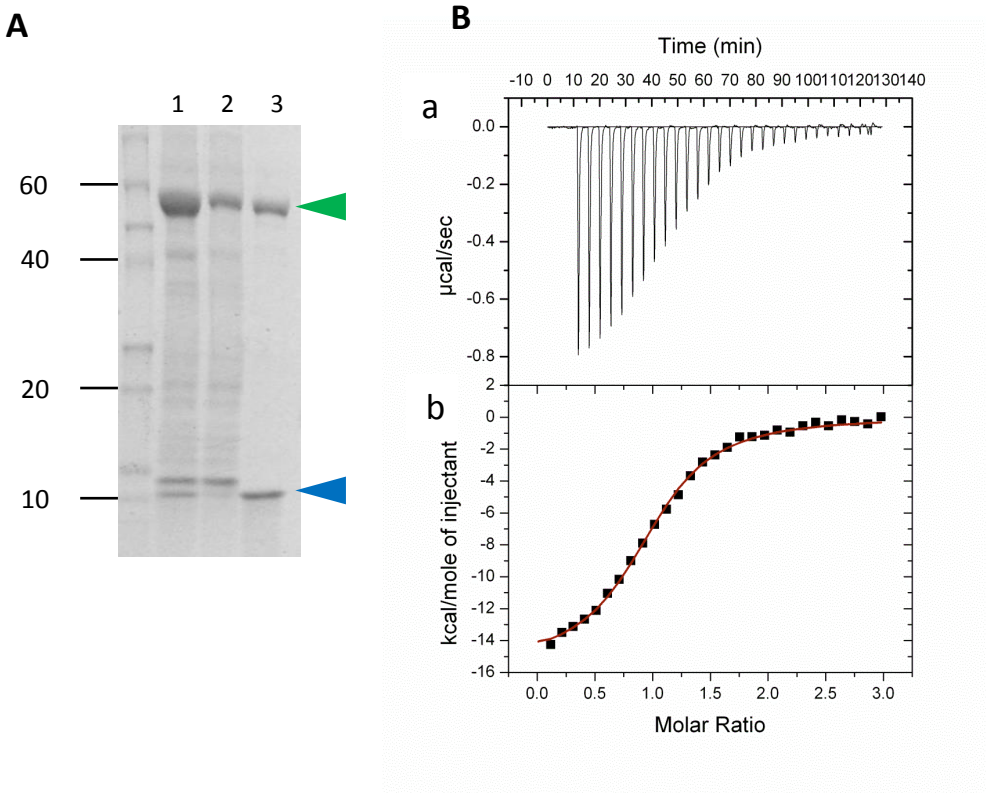

Fig. 2: Interaction between CNBD and miniTRIP8b.
A, Coomassie Blue staining following SDS-PAGE separation of the complex purified on a strep tactin affinity column by means of the Strep tag of miniTRIP8b,: lysate (1), flow-through (2), eluate (3). Green arrowhead marks the position of CNBD, while blue arrowhead Strep-miniTRIP8b. Numbers indicate molecular weight markers (kDA), loaded in the first lane. B, Isotermal titration calorimetry Interaction of miniTRIP8b to CNBD. (a) Heat changes during successive injections of 1 µl of miniTRIP8b (200 µM) to the CNBD protein (20µM). (b) Binding curve obtained by data in (a). The peaks have been integrated, normalized to the miniTRIP8b concentration and plotted against the molar ratio of miniTRIP8b to the CNBD. The solid line represents a nonlinear least-square fit to a single–site binding model, which yields a K_d of 1.30 ± 0.03 µM and a stoichiometric ratio N of 0.982 ± 0.006 (n = 3).

3.3 cAMP-unbound structure of the CNBD and comparison to the bound form

In order to acquire double and triple resonance NMR spectra of the human HCN2 CNBD in the cAMP-unbound conformation, we have produced and purified [^{15}N, ^{13}C], or [^{15}N] isotopically enriched protein (see PART III). All spectra of the CNBD show a single set of resonance signals, indicating that the protein is pure and adopts a single conformation. Moreover, the linewidths of the NMR spectra reflect a monomeric form, in line with the removal of the first three α-helices (A'-C') of the C-linker, which drives tetramerization of the protein. Using a combination of the collected spectra (see PART III), we were able to identify 91% of the backbone and 76% of the side chain atom resonances. No residue-specific assignments could be made for residues 534-535, 619 and 666-667. These residues are located in highly dynamic regions (Fig. 5B) and this can explain the absence of signal. For residues 579, 595, 633, 658 no amide backbone resonances could be observed. The lack of HN signals can be due to the fact that all these residues are expected to be solvent-exposed and not participating in hydrogen bonding. Fig 3 shows the assigned [^{1}H, ^{15}N] HSQC spectrum of the cAMP-unbound CNBD. [^{1}H, ^{15}N] HSQC correlates ^{15}N with the attached ^{1}H, and is considered the protein fingerprint, with the amide groups of the protein backbone and side-chain being visualized in the spectrum as spherical signals, except that of proline residues, which lack H^{N} and of the first residue.

A **[^{1}H, ^{15}N] HSQC of cAMP-unbound CNBD**

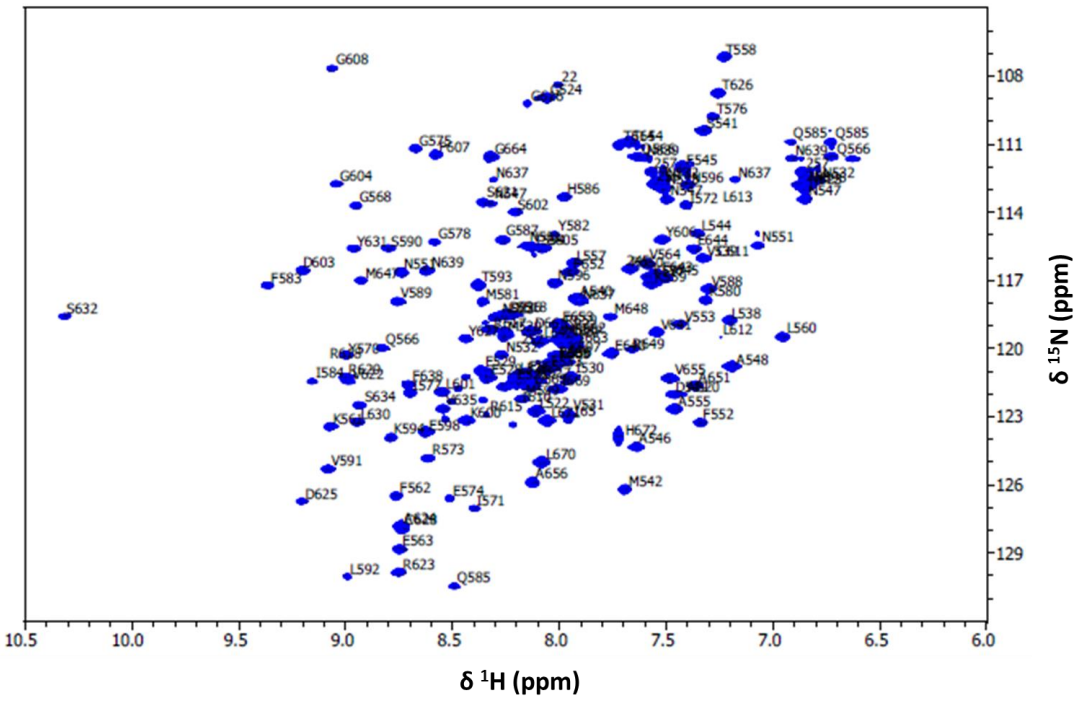

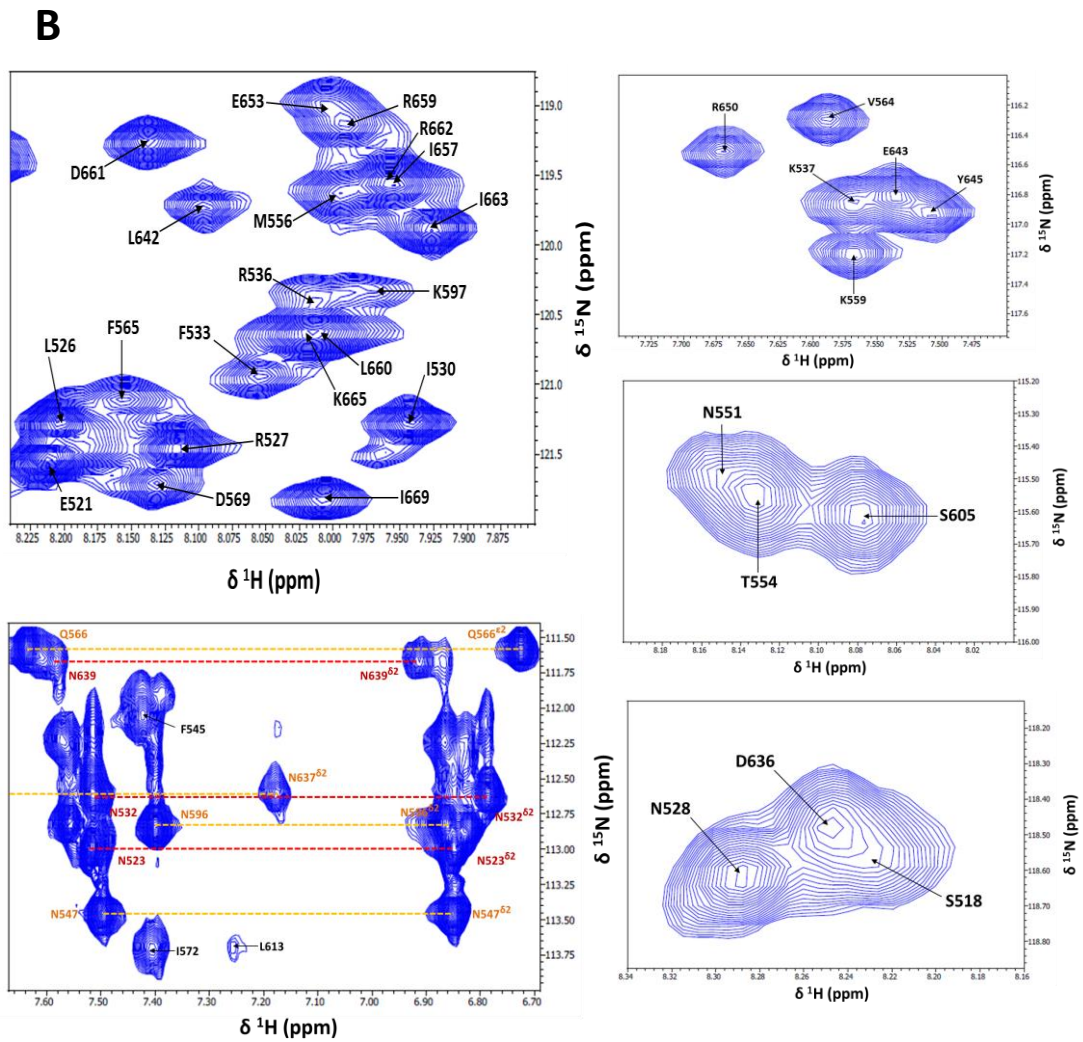

Fig. 3: HN resonances assignment of the cAMP-unbound CNBD.
A, [^{1}H, ^{15}N] HSQC spectrum of the ^{15}N-labeled cAMP-unbound CNBD (protein concentration = 1 mM) acquired in 150 mM KCl, 20 mM phosphate buffer, pH 7.0, at 298K, in a 600 MHz spectrometer equipped with a cryoprobe. B, small regions of the [1H, 15N] HSQC spectrum of the ^{15}N-labeled cAMP-unbound CNBD. Signals of the side-chain amide groups of asparagine and glutamine residues are connected by horizontal lines. Backbone and side- chain resonance assignments are indicated by one-letter amino acid code and the sequence number.

The first stage of the classical NMR structure determination process involves assignment of the ^{1}H, ^{15}N, and ^{13}C NMR resonances of the polypeptide backbone atoms. The second stage focuses on the assignment of the side chain atom resonances. This is a crucial step in the structure determination process, as it allows to obtain interproton distance restraints needed to generate the tertiary structure [47]. The spectra of CNBD for the assignment of side chain atom resonances exhibit a remarkable degree of resonance overlap, which have complicated the analysis. Thus, to date interproton distance restraints identified are not enough to generate a solid NMR structure of the cAMP-unbound CNBD. NMR signals are highly sensitive to local structure and indeed resonance values of the ^{1}H, ^{15}N, and ^{13}C belonging to the polypeptide backbone reflect a wide array of structural factors, such as backbone conformations and secondary structures (Φ and Ψ dihedral angles), hydrogen bond strength, and the position of aromatic rings [48-50]. Fig. 4 shows the secondary structure prediction of cAMP-unbound CNBD based on the $^{13}C^{\alpha}$, $^{13}C^{\beta}$, $^{13}C'$, ^{15}N, $^{1}H^{\alpha}$, and $^{1}H^{N}$ chemical shifts.

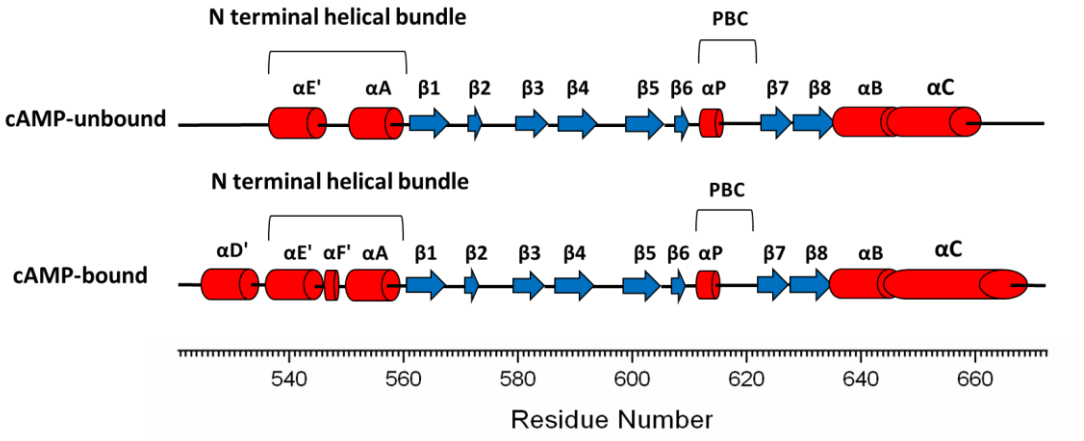

Fig. 4: Comparison of the secondary structure elements between cAMP-unbound and bound CNBD.
Secondary structure prediction for the cAMP-unbound CNBD calculated on the $^{13}C^{\alpha}$, $^{13}C^{\beta}$, $^{13}C'$, ^{15}N, $^{1}H^{\alpha}$, and $^{1}H^{N}$ chemical shifts using TALOS+ (upper line) and secondary structure elements of the cAMP-bound CNBD from the X-ray structure [31, 32] (lower line). Red cylinders indicate α-helices and blue arrows β-strands.

The comparison of the predicted secondary structures of the cAMP-unbound form to the secondary structures of cAMP-bound form coming from the X-ray structure [31, 32], suggests that the typical topology of HCN CNBD is maintained in the ligand-unbound state, with the exception of the absence of the F'-helix (within the N-terminal helical bundle) and the second half of the C-helix. Moreover, residues 521-532 forming D'-helix, which belong to the end of the C-linker, appear to be unstructured. Misfolding of the D'-helix can be explained by the absence of the C-linker. In order to obtain the cAMP-unbound CNBD structure using the NMR data already collected, we used CS-ROSETTA structure calculation program [51]. The unfolded residues 521-532 were removed from the calculation. Generation of a protein structure using CS-ROSETTA involves two separate stages. First, the query protein is divided in small segments and for each of these a polypeptide fragment from Protein Data Bank (PBD) is selected, based on the combined use of the amino acid sequence pattern and $^{13}C^{\alpha}$, $^{13}C^{\beta}$, $^{13}C'$, ^{15}N, $^{1}H^{\alpha}$, and $^{1}H^{N}$ chemical shifts. CS-ROSETTA is able to predict chemical shifts of C^{α},C^{β}, C', N, H^{α}, and H^{N} atoms for known protein structures available in the PDB, allowing to significantly increase the accuracy of selected fragments over the use of sequence information alone. The selected fragments are then used for *de novo* structure generation, using the ROSETTA RASREC protocol [52]. During CS-ROSETTA structure generation, the input chemical shifts are further used to re-score the generated structures. Evaluation of the agreement between the models and the input experimental data provides an important selection criterion for eliminating structures whose backbone angles have diverged from those of the original input fragments during the Rosetta optimization procedure. Furthermore, we used residual dipolar coupling (RDC) orientation data to improve the accuracy of the model generation [53]. RDCs provide orientation restraints, as they give information about the angle of a specific bond vector (in our case the backbone HN bond) relative to the external magnetic field, and thus display the relative orientation of parts of the molecule that are far apart in the structure. The decision on whether the CS-ROSETTA structure generation process has converged is based on how well the coordinates of the lowest energy structures agree with one another. In Fig. 5A the all atom energy of the generated models is plotted as a function of the C^{α} RMSD relative to the model with the lowest energy. This diagram shows the presence of about 20 structures that have less than 2 Å C^{α} RMSD from the lowest energy model. Indeed, the structure generation process is considered successful as it converged to a unique structural model, represented in Fig. 5B by

the 10 lowest energy models, all differing less than 1.5 Å Cα RMSD from the lowest energy model.

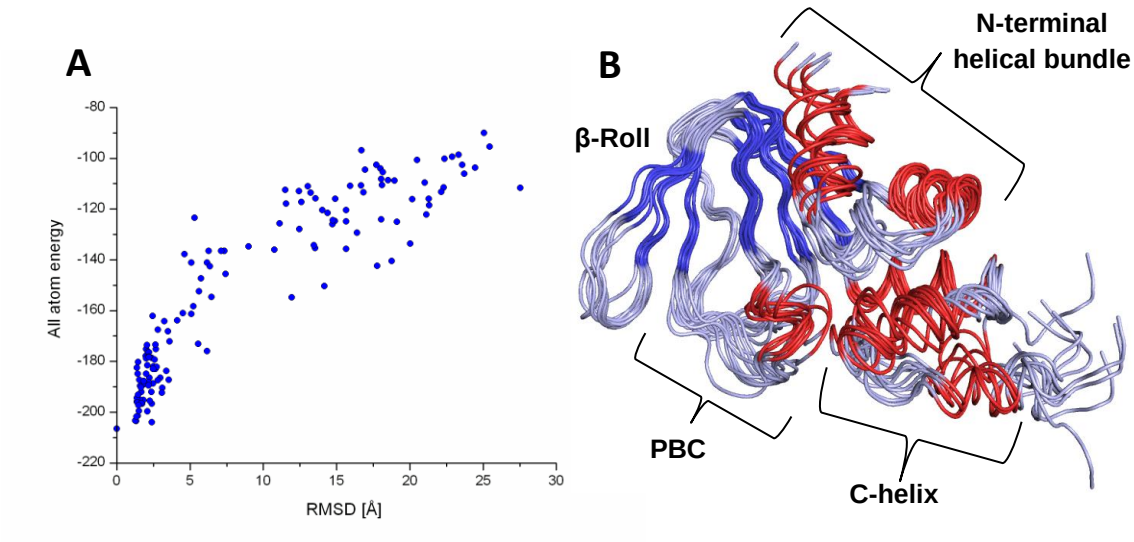

Fig. 5: CS-ROSETTA structure generation process.
A, Plots of CS-ROSETTA all atom energy versus C^{α} RMSD of CS-ROSETTA models relative to the lowest-energy model. B, Superimposition of the ten lowest energy structures generated by CS-ROSETTA calculation. A-helices are colored red, β-strands blue and loop regions grey.

Fig. 6A shows the lowest energy structure of cAMP-unbound CNBD, which resembles the general architecture of the CNBD proteins. It is constituted by an eight-stranded antiparallel β-roll, containing a short helix (P) and the following loop, collectively called PBC. The β-roll is connected at the N-terminus through β-1 to the N-terminal helical bundle, composed of a helix-turn-helix motif (helices E' and A) connected by a short loop, and through β-8 to the C-terminal helices B and C, also termed "hinge + lid". A remarkable observation is that the C-helix loses its secondary structure character in the central portion and is split into two. The accuracy of CS-ROSETTA approach is adversely affected by the presence of long disordered loops [51] and this explains the alternative conformations adopted by the C-terminal portion of the C-helix in the 10 models, compared to the well folded regions like the β-roll (Fig. 5B). By analysing ^{15}N and ^{13}C NOESY spectra no interproton distance restraints between residues in the N- and C-terminal part of the C-helix, as well as between the B-helix and the C-terminal

portion of the C-helix were found to support the helix-turn-helix conformation. We then concluded that the CS-ROSETTA model structure accounts for the low-ordered state adopted by the C-terminal half of the C-helix (Fig. 4 and 6A, residues 656-663), but not for its orientation. This structural instability is confirmed by the NMR relaxation data. Fig. 6B shows steady-state {1H}-15N-NOE experiments for the HN backbone signals of cAMP-unbound CNBD residues. Heteronuclear NOEs are sensitive to dynamics processes occurring in the subnanosecond time scale. In the absence of rapid internal motions of the protein backbone, NOE values are close to 0.8, whereas internal motions decrease NOE values proportionally to the increase in the mobility of the residues [54]. As highlighted in the diagram, residues 656-663 forming the C-teminal half of the C-helix undergo an increase in motions on subnanosecond time scale compared to the ones forming the N-terminal portion (residue 647-655), indicating substantial flexibility of the second half of the C-helix. One caveat of CS-ROSETTA is the tendency to generate secondary structures for disordered regions. This caveat is due the fact that ROSETTA all-atom energy function favors the formation of intramolecular hydrogen bonds [51]. Since $^{13}C^{\alpha}$, $^{13}C^{\beta}$, $^{13}C'$, ^{15}N, $^{1}H^{\alpha}$, and $^{1}H^{N}$ chemical shifts of residues 656-663 do not predict helical structure (Fig. 4), and steady-state {1H}-15N-NOEs indicate a flexible region, we consider the helical folding of residues 661-663 in the CS-ROSETTA model structure to be an artifact (Fig. 6A). Notably, no heteronuclear NOE values were reported for most of the residues forming the PBC (609-616) because of the low intensity of their HN signals. NMR results suggest that PBC undergoes a conformational exchange phenomenon in absence of the ligand, probably shifting between cAMP-unbound and cAMP-bound-like conformations. Residues forming PBC show low ^{1}H-^{1}H NOEs content, which confirms their dynamic behaviour. This agrees with the CS-ROSETTA models, which fail to converge to a single conformation for this region (Fig. 5B). Such a behaviour is in line with the role of the PBC as binding site of the cyclic nucleotide, which is prone to undergo conformational changes that are crucial for the rearrangement of the entire CNBD.

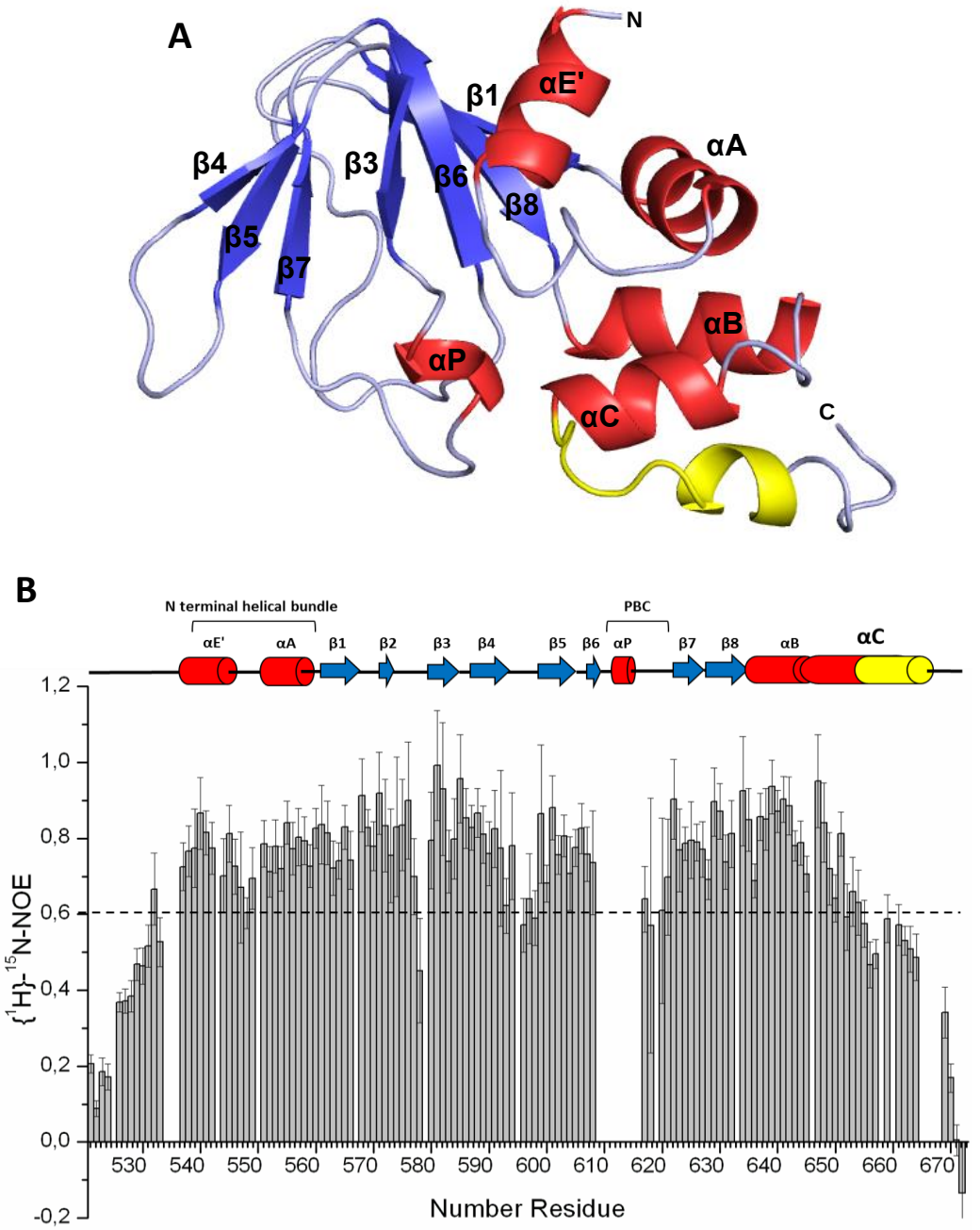

Fig. 6: CS-ROSETTA model structure and NMR relaxation analysis.
A, Ribbon representation of lowest energy model of cAMP-unbound CNBD. Secondary structure elements are labelled. A-helices are colored red, ß-strands
blue, loop regions grey and the C-terminal flexible potion of C-helix (residues 656-663) yellow. B, NMR relaxation analysis of picosecond-to-nanosecond (ps-ns) time-scale motions of cAMP-unbound CNBD. Steady-state heteronuclear {^{1}H}-^{15}N-NOE values of amide resonances at 298 K, 18.8 T, plotted against residue number. Secondary structure elements are shown on top of the graph: blue arrows indicate ß-strand, red cylinders indicate α-helices. The yellow cylinder

indicates the flexible part of the C-helix. The spectra for the heteronuclear {^{1}H}-^{15}N-NOE calculation were acquired in 150 mM KCl, 20 mM phosphate buffer, pH 7.0, at 298K, in a 600 MHz spectrometer equipped with a cryoprobe.

Superimposition of the cAMP-unbound model structure with the cAMP-bound X-ray structure [32] reveals the major rearrangements occurring in the CNBD upon ligand binding (Fig. 7). Notably, no significant differences are observed in the β-roll. Panel 7A shows that this fold is rather stable and the eight β-strands undergo only minor displacement upon ligand binding (C^{α} RMSD of 0.45 Å between cAMP-unbound and –bound forms). On the contrary, remarkable rearrangements are observed in the helical components of the CNBD. In details, we highlighted three regions involved in the conformational changes caused by ligand binding: the PBC, the N-terminal helical bundle and the hinge + lid helices (B and C) (Fig. 7B-D). Fig 7B shows a close look of the PBC in the unbound (dark green) and bound (light green) form. It is known that the phosphate-sugar moiety of cyclic nucleotide directly interacts with conserved residues of PBC (Glu_{582}, Cys_{584}, Arg_{591} and Thr_{592} for human HCN2), causing the tightening of this element. The rearrangement in the PBC in turn forces the movements of the helical components at the N- and C-termini of the β-roll. The PBC tightening directly controls the orientation of the B-helix by a conserved Leu-Phe regulatory system. In the absence of cAMP, the position adopted by a leucine (585 in HCN2) of the PBC sterically prevents the movement of a phenilalanine (611 in HCN2) of the B-helix. cAMP binding forces the leucine in a new conformation, which allows the phenilalanine to occupy the position previously adopted by the leucine [30]. Though in the ten model structures PBC does not assume a stable conformation (Fig. 5B), for eight of them Leu_{585} displays a typical position of a ligand-unbound CNBD (highlighted by the arrow in panel B), suggesting that both the tightening of the PBC and the Leu-Phe regulatory system is conserved in HCN CNBD. B (hinge) and C (lid) helices, as a single element, move closer to the β-roll cavity. As shown by Fig. 7C, the position of the two helices relative to each other is quite similar in the cAMP-unbound and bound structures, as the angle between the two helices does not remarkably change (48.6° and 54° respectively). The new position adopted by B and C helices is stabilized by the interaction of cyclic nucleotide with Arg_{659} of the C-helix (Fig. 7C). As shown in Fig. 7D, the conformational change of the PBC is indirectly forcing the movement of the N-terminal helical bundle, because, by moving closer to the β-roll, the C-helix displaces the N-terminal helical bundle. The reorientation of the N-terminal helical bundle is coupled to a

restructuration of the loop connecting helices E' and A, which becomes the F'-helix in the cAMP-bound form (Fig. 7D). Though the cAMP-unbound model structure in this region does not show secondary structure, heteronuclear NOE values around 0.7 (see Fig. 6B, N terminal helical bundle) indicate that the loop between the first and the second helices of the N-terminal helical bundle has some rigidity.

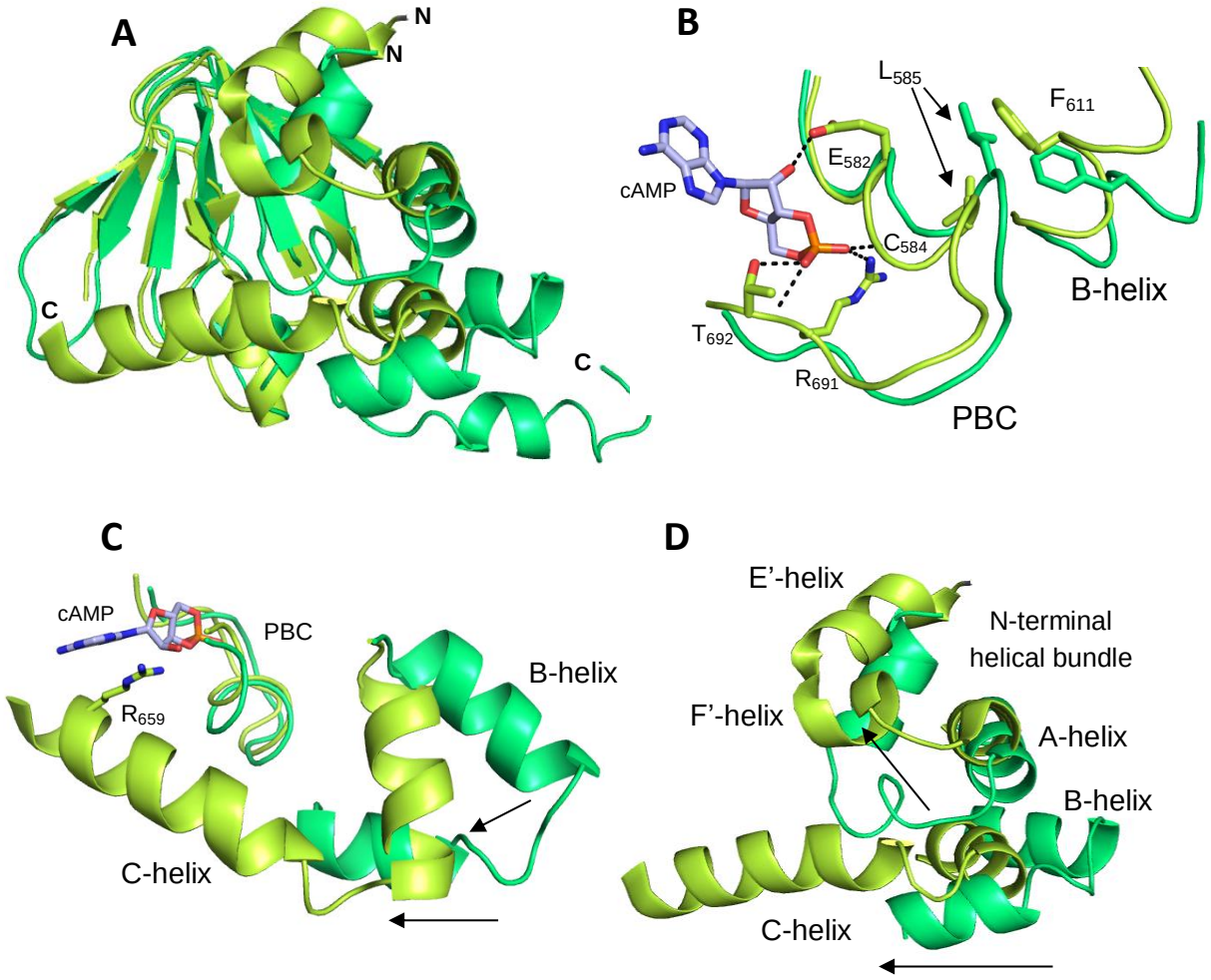

Fig. 7: Conformational changes following cyclic nucleotide binding.
A, Superposition of CS-ROSETTA cAMP-unbound (dark green) and X-ray cAMP-bound (light green, Ref. 32) CNBD structures. B, close view of the PBC. The phosphate-sugar moiety of cAMP binds E_{582}, C_{584}, R_{591} and T_{592} of PBC, inducing its rearrangement. In the absence of cAMP, L_{585} of PBC occupies the space that is filled by F_{611} of the B-helix in the cAMP-bound conformation. C, translation movement of the B/C-helix element upon binding of cAMP to PBC. D, close view

of the N- and C-helical components of CNBD. The movement of the B/C-helix element forces the N-terminal helical bundle to adopt a new position.

3.4 TRIP8b binding site on CNBD

Protein-protein interaction changes the chemical environment of the residues that compose the protein interfaces and, hence, affects the chemical shifts of the nuclei in that area. Thus, to identify the TRIP8b binding site on cAMP-unbound CNBD we used the chemical shift perturbation method, which allows to monitor changes of the chemical shifts of a labelled protein when the unlabeled interacting partner is titrated in [55]. Backbone amide resonance signals were used to monitor the chemical shifts changes and hence [^{1}H, ^{15}N] HSQC spectra were collected to follow the perturbation of their chemical shifts. We titrated unlabeled miniTRIP8b onto ^{15}N-labeled CNBD. The titration was performed maintaining the concentration of CNBD constant and increasing the amount of miniTRIP8b, bringing the miniTRIP8b/CNBD molar ratio from 0 to 2. With increasing amounts of miniTRIP8b, the CNBD amide resonances lost intensity and a new set of resonances started appearing, indicating that the complex is in the slow-exchange regime in the NMR time scale. At a ratio of 2.0 it is clear that a single set of amide resonances is observed (Fig. 8).

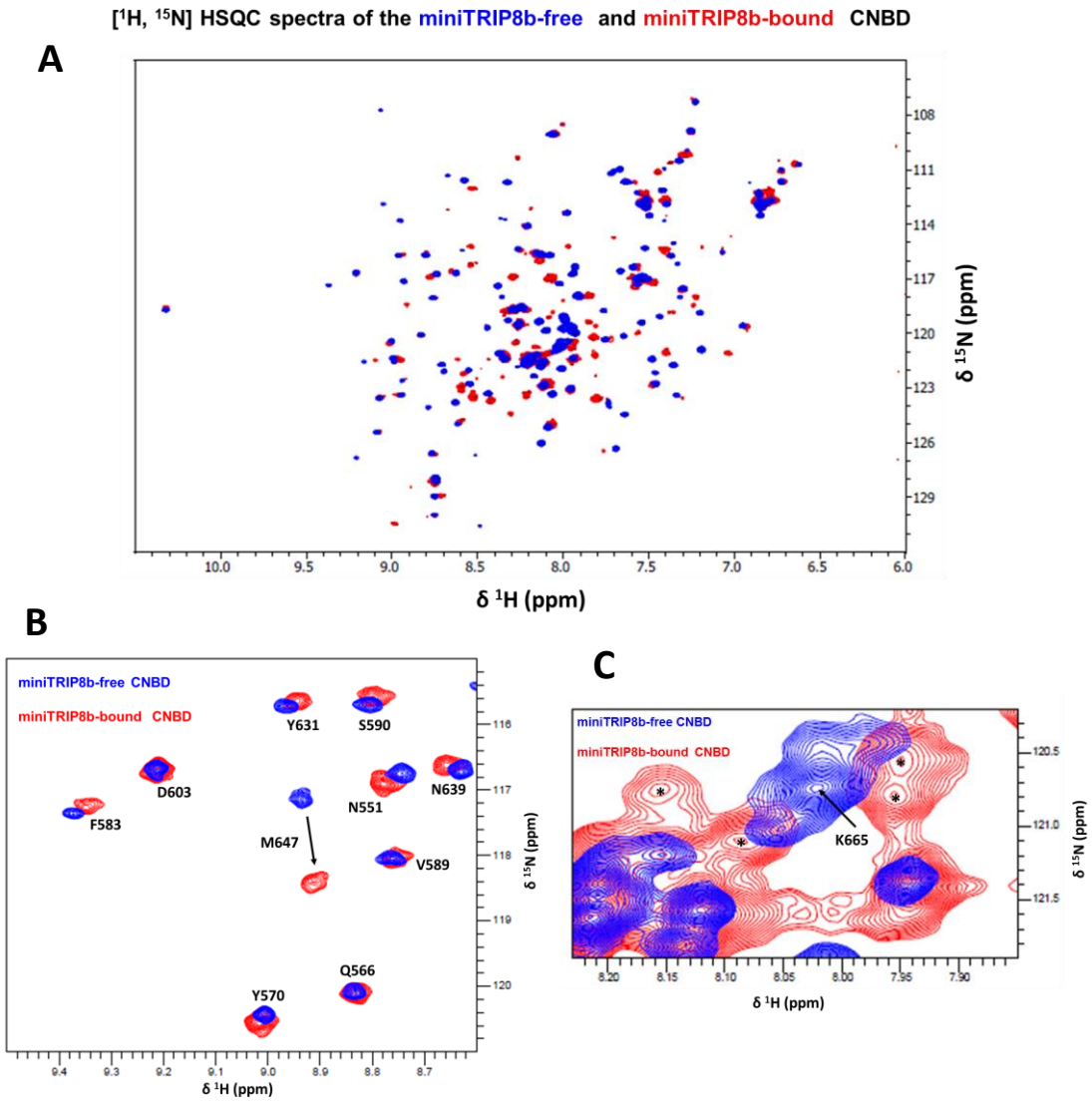

*Fig. 8: Chemical shift perturbation of CNBD amide HN signals due to miniTRIP8b interaction. A, Superimposition of the [^{1}H, ^{15}N] HSQC of miniTRIP8b-free CNBD (blue) and miniRTIP8b-bound CNBD (red, last point of the titration). B and C, Small regions of the superimposed spectra of panel A. B, amide HN peaks are labeled in order to illustrate different degree of miniTRIP8b-induced changes in chemical shift. C, * indicate possibly chemical shift changes for amide HN signal of residue Lysine 665. The spectra were acquired in 150 mM KCl, 20 mM phosphate buffer, pH 7.0, at 298K, in a 600 MHz spectrometer equipped with a cryoprobe.*

The slow chemical exchange regime generally corresponds to a complex having a K_d < 10 µM [55]. Our NMR data are therefore consistent with the K_d of miniTRIP8b-CNBD complex determined using ITC (Fig. 2). Fig. 9A shows the backbone amide chemical shift change for the

residues of CNBD upon miniTRIP8b interaction. Under the titration conditions, 129 HN cross peaks were observable in the CNBD spectrum out of the expected 150. Since miniTRIP8b-CNBD complex is prone to precipitate at the high concentrations required for the NMR experiments, we were not able to carry out the assignment procedure for the HN resonances of the miniTRIP8b-bound state of CNBD. Thus, making the assumption that new resonances appearing close to the "free" resonances correspond to their bound state [55, 56], we have unambiguously identified pairs of resonances from the two spectra with small chemical shift difference ($\Delta\delta_{HN}$) (86 residues) (see example in Fig. 8B). Certain resonances were characterized as significantly shifted based on the fact that no other bound state resonances could be identified within a $\Delta\delta_{HN}$ < 0.1 ppm (29 residues) (see example in Fig. 8B, M_{647}). An additional set of resonances (14 residues) were impossible to be unambiguously identified due to the presence of multiple unassigned bound resonances in their close vicinity (see example in Fig. 8C, K_{665}). These were characterized as ambiguous and were not included in the subsequent analysis (identified with a * in Fig. 9A). A threshold of 0.1 ppm was chosen to identify residues primarily involved in the binding (Fig. 9A). The majority of residues with a remarkable chemical shift change cluster in two regions of the CNBD sequence: the loop between E' and A α-helices of the N-terminal helical bundle (hereafter "N-bundle loop"), and the region which includes the C-helix plus the C-terminal peptide of the construct (hereafter "C-helix/stretch"). A schematic representation of these two regions, highlighted in red, is shown on the top of Panel A of Fig. 9, displaying the secondary structure of the CNBD. Figure 9B shows a ribbon representation of the cAMP-unbound CNBD, highlighting the TRIP8b interaction sites on the tertiary structure. Notably, both in the cAMP-unbound and bound configurations, the N-bundle loop and the C-helix/stretch are positioned on the same plane (Fig. 9B, C). Furthermore, in the quaternary structure they are not involved in the interaction between adjacent subunits and generate a surface that is exposed to the solvent (Fig. 9C). Therefore, we can assume that these two elements form a plausible binding region, accessible to the soluble TRIP8b protein. This confirms the electrophysiological result showing the effect of TRIP8b even in the presence of saturating concentrations of cAMP [26]. Notably, Figure 9A shows that the majority of residues forming the β-roll, as well as A and B helices are not significantly affected by the miniTRIP8b presence, suggesting that TRIP8b may act by stabilizing the cAMP-unbound conformation of the CNBD. Though miniTRIP8b binding does not appear to significantly alter the β-roll structure, some residues positioned in flexible regions adjacent to β-strands display a

remarkable chemical shift change (Fig. 9A), possibly due to local rearrangements of the H-bond network upon miniTRIP8b-CNBD binding.

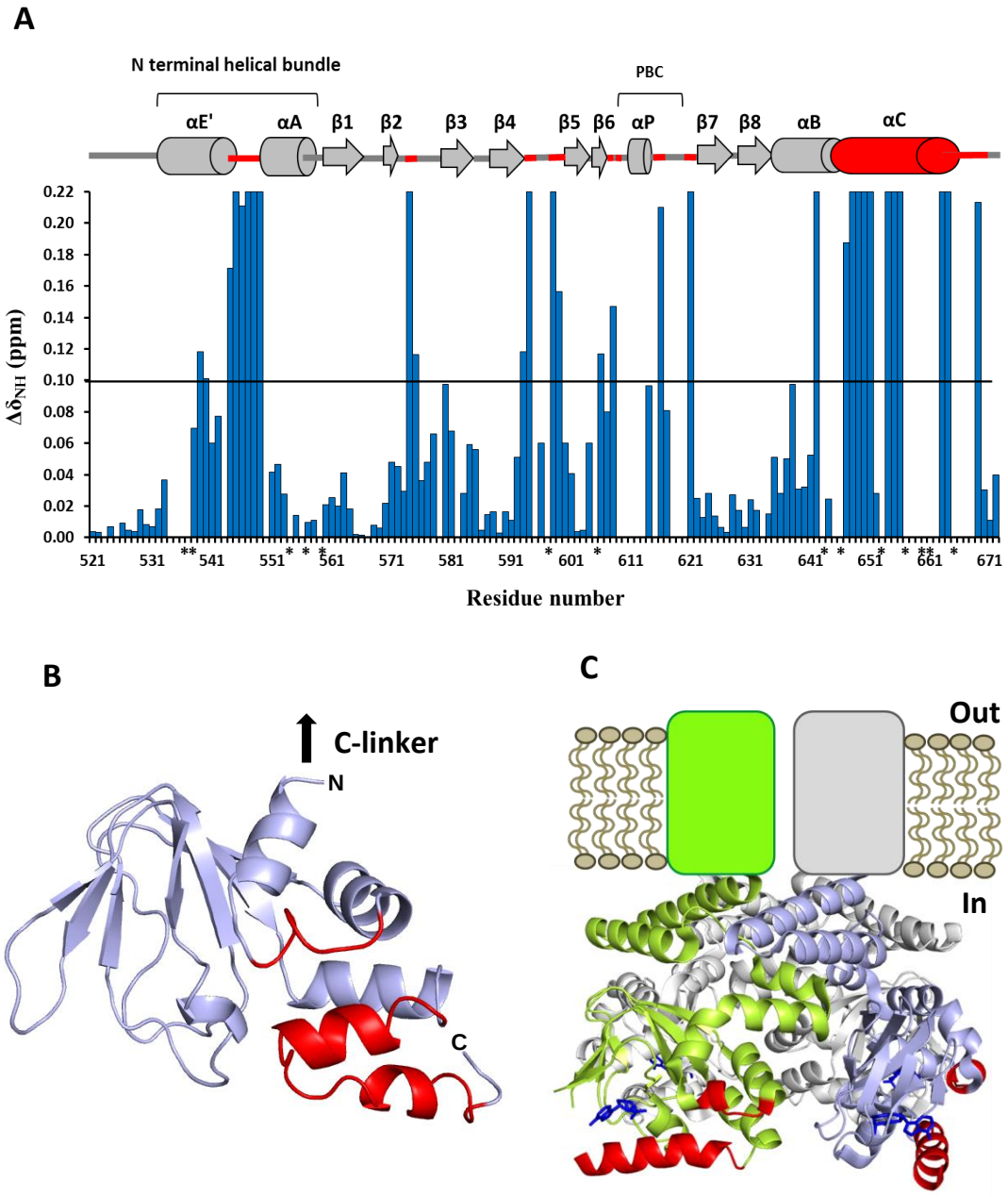

Fig. 9: Titration of miniTRIP8b onto the cAMP-unbound form of CNBD.
A, Chemical shift changes of the HN backbone resonances in the [^{1}H, ^{15}N] HSQC spectrum of CNBD caused by the presence of miniTRIP8b. The maximum value of chemical shift difference measured is attributed to all HN cross-peaks showing more than 0.1ppm of chemical shift difference for each possible options (remarkable chemical shift change). Residues for which no

results are shown correspond to prolines (525, 543, 550, 567, 646) and residues not detected in the miniTRIP8b-free form of CNBD (534, 535, 579, 582, 595, 609-613, 615, 618-620, 633, 658, 660, 662, 666-668). Asterisk indicates ambiguous residues not identified in the miniTRIP8b-bound state due to the presence of multiple unassigned bound resonances in their close vicinity (536, 537, 554, 556, 559, 597, 605, 643, 645, 653, 657, 659, 661, 665). Chemical shift changes of the HN resonances are plotted against CNBD residue numbers. At the top of the graph the secondary structure of the cAMP-unbound form of CNBD is represented. Cylinders represent α-helices, while arrows β-strands. The regions formed by residues strongly affected by the presence of miniTRIP8b are colored red. B, Ribbon representation of the cAMP-unbound CNBD showing in red the N-bundle loop and C-helix/stretch. C, ribbon representation of C-linker/CNBD (cAMP-bound form) in its tetrameric conformation. The N-bundle loop and C-helix/stretch are colored red in two of the four subunits. cAMP molecules are blue sticks.

3.5 Structural characterization of miniTRIP8b

The identification of TRIP8b residues involved in the binding to CNBD would be equally interesting in order to complete the structural information about CNBD-TRIP8b complex. To this end, the assigned [^{1}H, ^{15}N] HSQC spectrum of miniTRIP8b is required and subsequently the miniTRIP8b structure to map onto it the CNBD binding site. First of all, [^{1}H, ^{15}N] HSQC spectrum of miniTRIP8b was acquired to test the feasibility of the NMR approach for this polypeptide. [^{1}H, ^{15}N] HSQC is a relative simple and fast NMR spectrum that can be used as a preliminary test to discriminate between folded and unfolded proteins [57]. Fig. 10 shows [^{1}H, ^{15}N] HSQC spectra of miniTRIP8b and CNBD (cAMP-unbound and bound state). The comparison of the miniTRIP8b spectrum with the CNBD spectra highlights a different degree in folding between miniTRIP8b and CNBD. In the case of CNBD most of the HN signals are spread all over the spectrum, which is an indication of folding, whereas miniTRIP8b HN signals mainly collapses to the center of the spectrum.

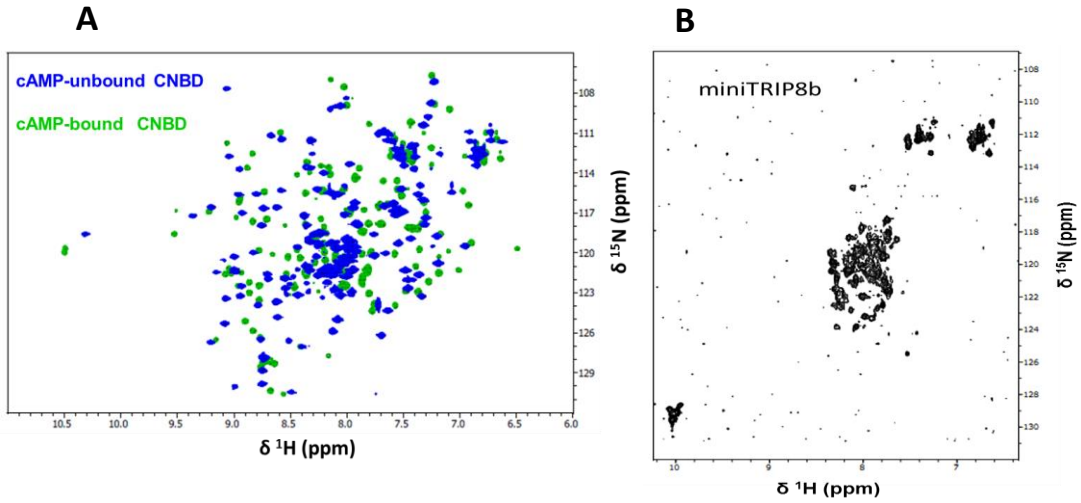

Fig. 10: Comparative analysis of folding of miniTRIP8b and CNBD.
Left: [^{1}H, ^{15}N] HSQC spectra of CNBD in the cAMP-unbound (blue) and cAMP-bound (red) form. Right: [^{1}H, ^{15}N] HSQC spectrum of miniTRIP8b. All spectra were acquired in 150 mM KCl, 20 mM phosphate buffer, pH 7.0, at 298K, in a 600 MHz spectrometer equipped with a cryoprobe. The spectra were acquired in 150 mM KCl, 20 mM phosphate buffer, pH 7.0, at 298K, in a 600 MHz spectrometer equipped with a cryoprobe.

This feature of the miniTRIP8b spectrum is presumably due to intrinsic disorder of this polypeptide. Indeed, parallel *in silico* analysis predicts that the N-terminus is α-helically folded, and the C-terminus is unstructured (Fig. 11A). This structural prediction was confirmed by Circular Dichroism (CD) spectroscopy by comparing the CD spectrum of miniTRIP8b with the CD spectrum of a mutant lacking the C-terminal part (hereafter "microTRIP8b"). As shown in Fig. 11B, CD spectrum of miniTRIP8b confirms the presence of the α-helical folding as well as the unfolded region, as the typical α-helix shape of a CD spectrum is partially affected by the unfolded component. On the contrary, microTRIP8b spectrum is no longer affected by the contribution of an unfolded element (Fig. 11B), confirming that the C-terminal portion of miniTRIP8b is indeed unfolded. To further validate the location of the α-helical element in the microTRIP8b sequence, CD spectra of miniTRIP8b and microTRIP8b were normalized to their respective number of residues. Fig. 11C shows the normalized CD spectra, in which the α-helical content is calculated per residue, leading to directly compare the amount of secondary structures in the two polypeptides. As expected, the α-helical content in microTRIP8b

spectrum is increased compared to miniTRIP8b spectrum, proving that the α-helical element is indeed located in microTRIP8b. We further characterized the properties of the tertiary structure of microTRIP8b, in particular asking whether the predicted α-helices display residue-residue contacts. To this end, we performed a thermal denaturation curve of microTRIP8b, increasing temperature from 5°C to 80°C and measuring CD absorption at 222 nm, wavelength that reflects changes in α-helical content. As shown in Fig. 11D the measured values fit a linear curve, which is an indication of the absence of allosteric cooperativeness in the unfolding, and thus no residue-residue interactions. This feature can be due to either the absence of interactions between the predicted α-helices, or the presence of a unique α-helix encompassing all of them. To clarify the role of the C-terminal unstructured region of miniTRIP8b in the binding to CNBD, we repeated the NMR titration using microTRIP8b. Superimposition of the two [^{1}H, ^{15}N] HSQC of CNBD corresponding to the last point of the titration (mini or microTRIP8b/CNBD molar ratio of 2) identified no differences in the chemical shift perturbation due to miniTRIP8b and microTRIP8b presence (Fig. 12). Therefore, we can argue that the portion of miniTRIP8b relevant for the interaction is its N-terminal part (microTRIP8b sequence). To unambiguously validate that microTRIP8b includes all the relevant residues that are needed for full effect, we tested the effect of this fragment on the full-length HCN2 channel. The perfusion of the channel with microTRIP8b gave rise to similar effects to the ones obtained with miniTRIP8b (Fig. 13) [26]. Given that microTRIP8b is the relevant portion of TRIP8b for antagonizing the cAMP effect, and does not contain a remarkable unfolded region, which may explain the low quality data of miniTRIP8b NMR spectra, further NMR analysis will be performed on microTRIP8b in order to test its feasibility for the NMR methodology. Notably, as for miniTRIP8b, microTRIP8b-CNBD complex is also susceptible to precipitation at the high concentrations required for the NMR experiments. Thus, the instability of the complex is not due to the unfolded region of miniTRIP8b, but appears to be an intrinsic property of mini/microTRIP8b-CNBD complex.

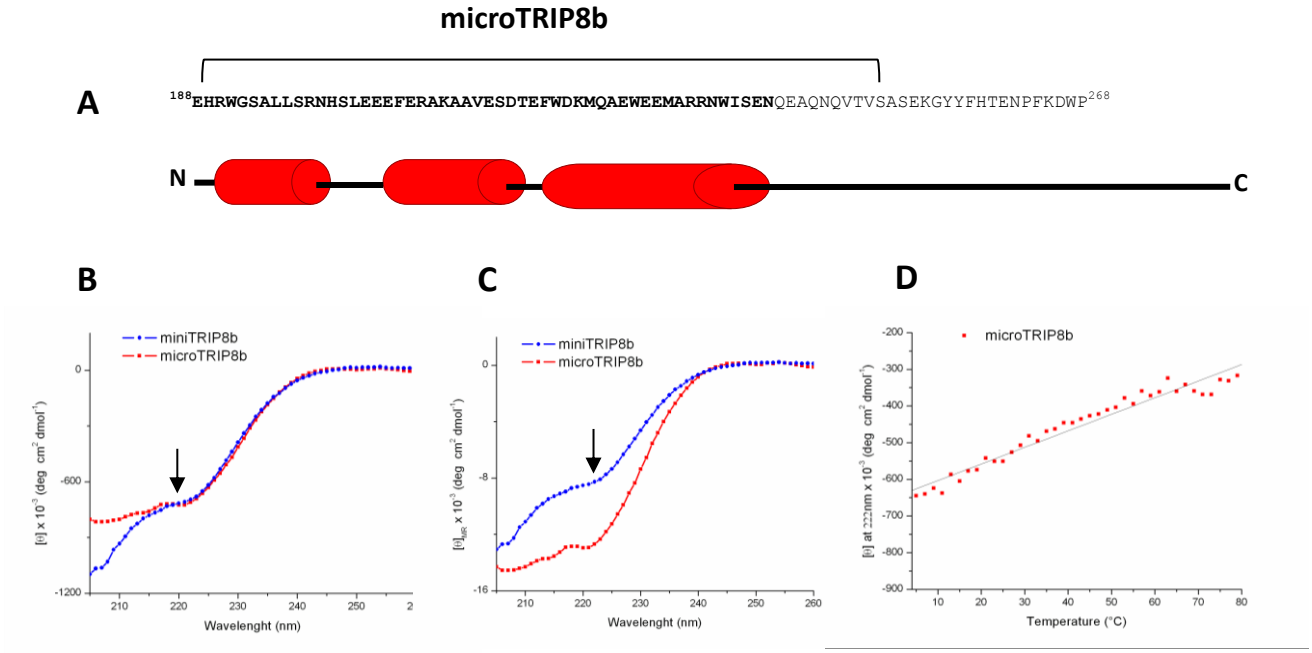

Fig. 11: Structural characterization of mini/microTRIP8b.

A, Amino acid sequence of human mini/microTRIP8b fragment. Below the sequence a schematic cartoon represents the secondary structure consensus prediction calculated by the following servers: nnPREDICT, PREDICTPROTEIN, JUFO, CFSSP. Red cylinders represent α-helices, while black lines represent unstructured regions. B, CD spectra of miniTRIP8b (red line) and microTRIP8b (blue line) in the far-UV region. C, CD spectra shown in panel B represented as Mean Residue Ellipticity, which reports the molar ellipticity for individual protein residues instead of the whole protein molecules. Arrows point the value of far UV-CD measured at 222nm. D, Analysis of the thermal denaturation of microTRIP8b observed by the far UV-CD at 222 nm.

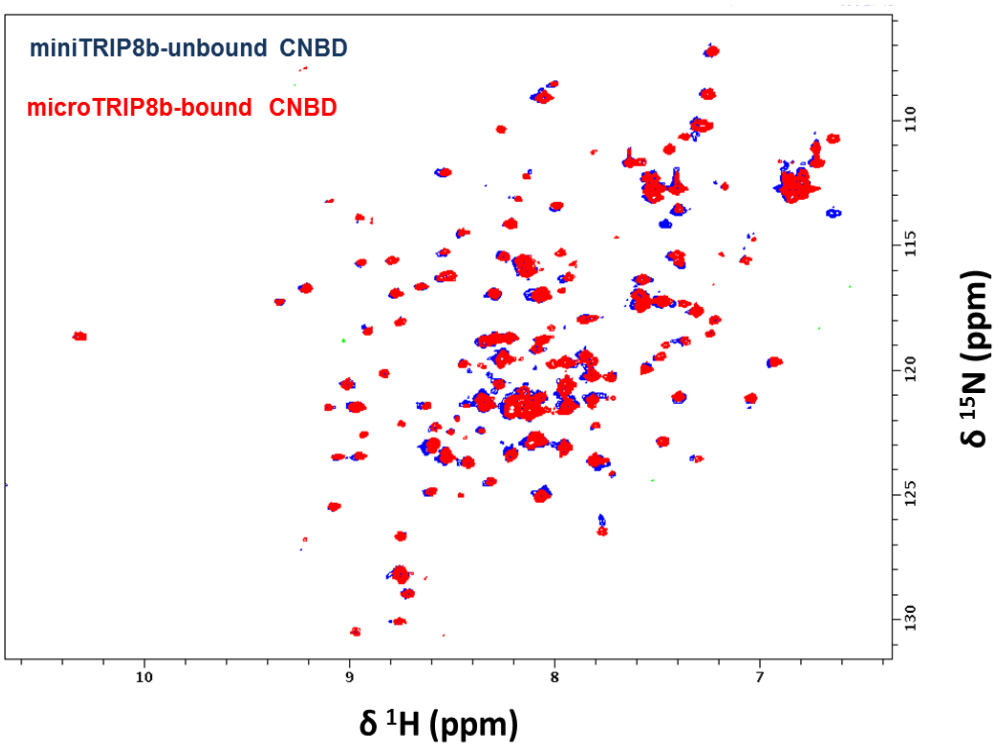

Fig. 12: mini and microTRIP8b bind to the same residues of CNBD.
Superimposition of [^{1}H, ^{15}N] HSQC spectra of cAMP-unbound CNBD in the miniTRIP8b-bound (blue) and microTRIP8b-bound (red) form. The spectra were acquired in 150 mM KCl, 20 mM phosphate buffer, pH 7.0, at 298K, in a 600 MHz spectrometer equipped with a cryoprobe.

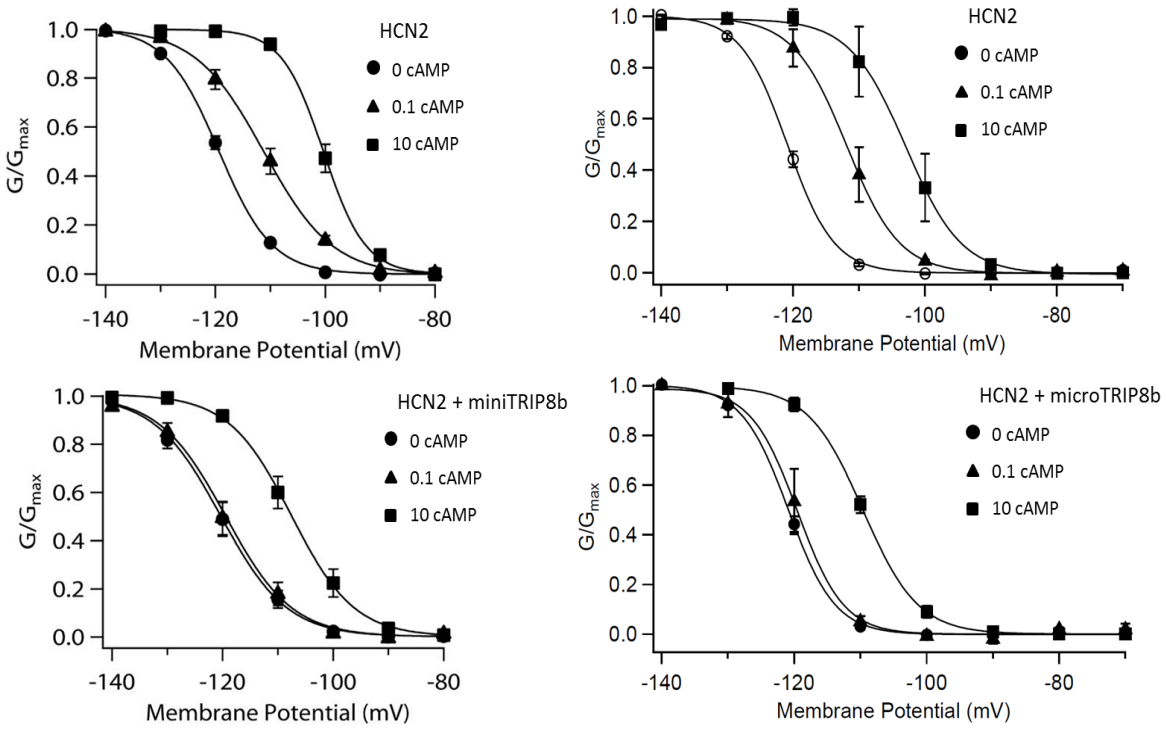

Fig. 13: mini and microTRIP8b display the same antagonistic action on the cAMP-dependent HCN channel voltage gating.

Left, Normalized G-V relationship for HCN2 channel tail currents in 0, 0.1, or 10 µM cAMP (up) and normalized G-V relationship for HCN2 channel tail currents in the presence of 4 µM miniTRIP8b plus 0 ($V_{1/2}$ = -120.5 mV), 0.1 ($V_{1/2}$ = -119 mV), or 10 µM cAMP ($V_{1/2}$ = -110.1 mV) (down) [26]. Right, Normalized G-V relationship for HCN2 channel tail currents in 0, 0.1, or 10 µM cAMP (up) and normalized G-V relationship for HCN2 channel tail currents in the presence of 4 µM microTRIP8b plus 0 ($V_{1/2}$ = -121.1 mV), 0.1 ($V_{1/2}$ = -119.5 mV), or 10 µM cAMP ($V_{1/2}$ = -109.5 mV) (down). Measurements and analysis of the data were performed as described in reference 26.

3.6 Biochemical confirmation of TRIP8b binding site

Using NMR titration analysis, we identified two regions of the cAMP-unbound form of CNBD affected by mini/microTRIP8b addition: the N-bundle loop and the C-helix/stretch (Fig. 9). In order to validate our NMR results, we biochemically tested the relevance, for the complex formation, of the two elements forming the TRIP8b binding site. First of all, we tested the C-helix/stretch. Given that HCN1, HCN2 and HCN4 have a total sequence identity in the N-bundle loop and the C helix/stretch, we performed a binding assay under native conditions by expressing wild-type TRIP8b in *Xenopus* oocytes, together with truncated HCN1 missing CNBD ($HCN1_{1-472}$, canonical nomenclature [31, 32]) or only the C-helix/stretch ($HCN1_{1-565}$). These channels constructs were previously shown to be functional [18]. As shown in Fig. 14, the truncation of the CNBD ($HCN1_{1-472}$), as well as the removal of the C-helix/stretch ($HCN1_{1-565}$), completely abolish TRIP8b binding. Therefore, these findings already demonstrate that the C-helix/stretch is essential for TRIP8b binding even in the presence of the N-bundle loop. We can postulate that the N-bundle loop, though involved in binding, is not sufficient to stabilize the interaction with TRIP8b. As the C-helix/stretch is necessary for TRIP8b binding, we analyzed further this region in order to restrict the area that is essential for the interaction with TRIP8b. To this end, we have used an *in vitro* assay co-expressing miniTRIP8b with CNBD mutants lacking the C-helix/stretch, or truncated at different points of the C-helix/stretch. In particular, the eighteen residues forming the C-helix were divided in three groups, as well as the nine residues forming the stretch after the C-helix. The complex formation was tested by means of a strep-tactin affinity purification. In agreement with our previous finding (Fig. 14), the removal of the C-helix/stretch impairs the complex formation (Fig. 15) confirming its importance in the interaction with TRIP8b. The inability to bind miniTRIP8b is specifically due to the lack of the C-helix/stretch, rather than a problem associated to a general loss of structure, since the mutant protein retains the regular fold as the wild-type. (Fig. 16). The progressive increment of the C-helix does not rescues the binding with miniTRIP8b and even its full presence confers only a minimal binding under these conditions (Fig. 15). Unexpectedly, the interaction with miniTRIP8b is fully restored with the CNBD mutant containing the first three residues of the stretch following the C-helix (GKK, residues 664-666) (Fig. 15). This finding clearly underlines the relevance, on the complex formation, of the small unstructured stretch following the C-helix and in particular the GKK sequence. This finding is in agreement with the NMR titration, which shows that chemical shift of HN backbone signal of G_{664}, the first residue belonging to

the nine of the stretch, is strongly affected by mini/microTRIP8b addition (Fig. 9A). On the entire sequence GKKNSILLH (residues 664-672) of the stretch, the last three residues are not affected by mini/microTRIP8b presence (Fig. 9A), therefore they are not involved in the binding with TRIP8b. For the remaining six residues (GKKNSI), the biochemical assay highlights the relevance of the GKK sequence for the binding (Fig. 15), but does not exclude the contribution of the NSI tripeptide sequence. Given the fact that the chemical shift of HN signal of I_{669} is strongly affected by the presence of mini/microTRIP8b (Fig. 9A), a conclusive study of the relative contribution for the binding of the residues forming GKKNSI sequence will require further site-directed mutational analysis tested by means of a quantitative approach for the study of protein-protein interaction.

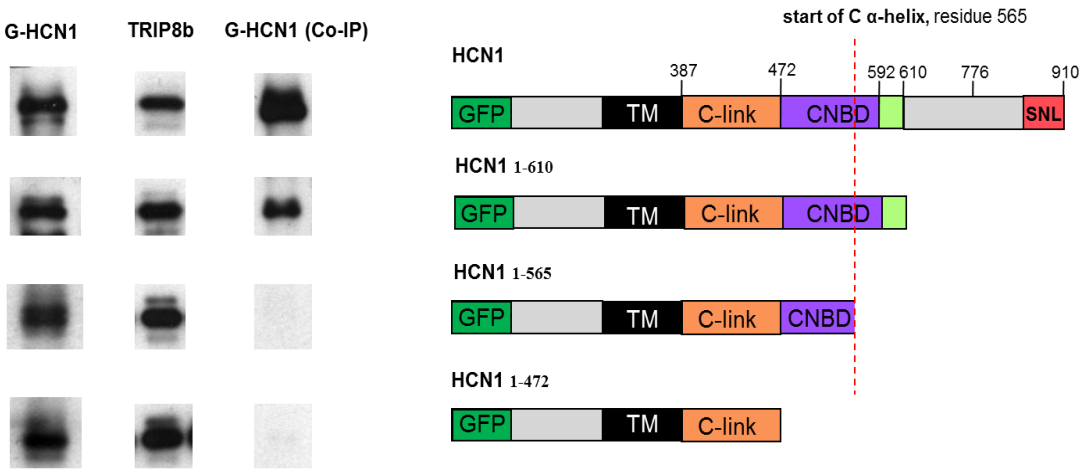

Fig. 14: Contribution on the C-helix and the small following fragment for the binding to TRIP8b. The interaction of HCN1, its deletion mutants, and the chimera membrane proteins with wild type TRIP8b was assessed by co-immunuprecipitation from Xenopus oocyte extracts. In the icons on the right are represented HCN1 channel domains and amino acid positions (GFP in green; transmembrane domain in black; C-linker in orange; CNBD in purple; small unstructured fragment immediately after the Lid α-helix in light green, C-terminal SNL tripeptide in red, N and C-terminal regions in gray). Left and middle columns shows Western blots using respectively anti-GFP and anti-TRIP8b antibody as input signals. Right column shows the amount of target proteins co-immunoprecipitated with anti-TRIP8b antibody (Western blot using anti-GFP antibody). Individual bands were cut from the intact gel pictures and aligned to allow direct comparison of intensities for wild-type and mutants, having different molecular

weight. It is to note that exposure times are directly comparable down each column, but not along each row.). Results obtained by Dr. Bina Santoro using the procedure described in reference 25.

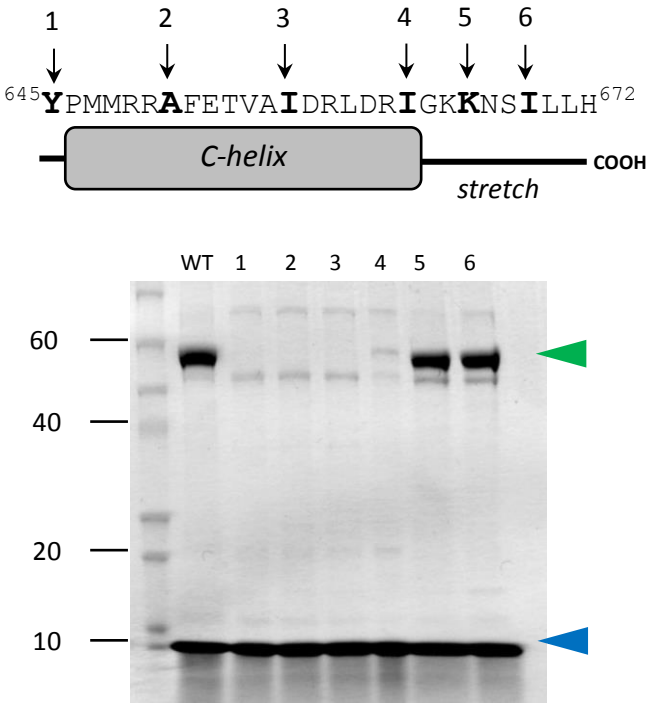

Fig. 15: Contribution of the C-helix/stretch on the binding to TRIP8b.
Bacterial lysates from cells co-expressing Strep-miniTRIP8b (Blue arrowhead) and CNBD wild-type and mutants (Green arrowhead) were loaded onto a Strep-tactin affinity column for Strep-tag purification. Samples corresponding to the eluate fractions were analyzed by Coomassie Blue staining following SDS-PAGE separation. Numbers indicate molecular weight markers (kDa), loaded in the first lane. The C-helix/stretch was removed, or truncated introducing a stop codon after the following residues: Y_{645} (1), A_{651} (2), I_{657} (3), I_{663} (4), K_{666} (5), I_{669} (6). Y_{645} and I_{663} correspond respectively to the first and last aminoacid of the C α-helix.

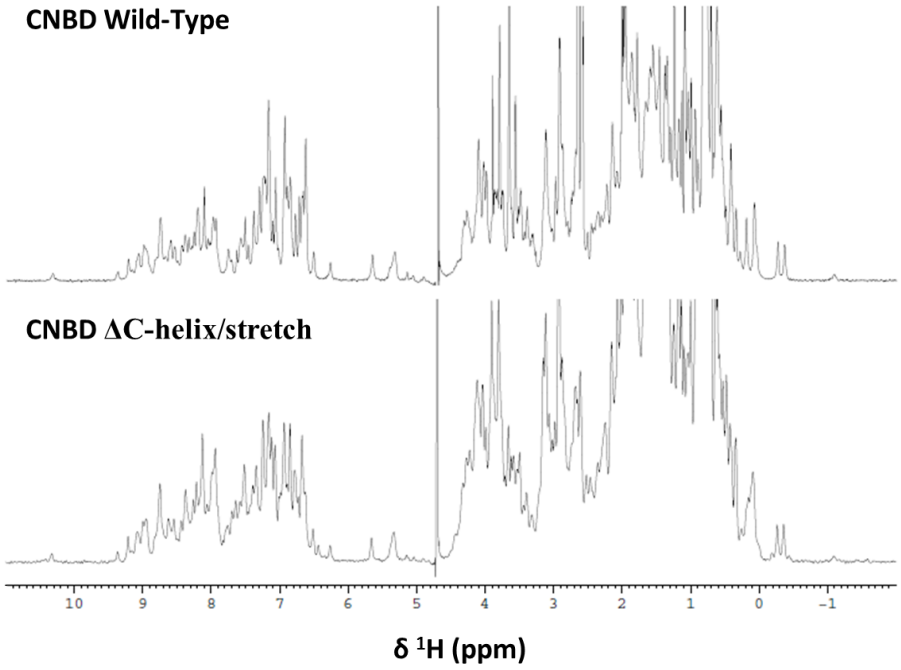

Fig. 16: Structural Comparison of CNBD wild-type and ⊿C-helix/stretch.
^{1}H-monodimensional spectra of CNBD wild-type (up) and mutant ⊿C-helix/stretch (down).

4 DISCUSSION AND FUTURE PROSPECTS

In this study we propose a molecular mechanism, based on NMR structural data, accounting for the mutual allosteric antagonism of cAMP and TRIP8b, which regulates HCN channel activity. Recently, our electrophysiological results showed that the mutual antagonistic effects of cAMP and TRIP8b can be explained by an allosteric mechanism [26]. Thus, structural information on CNBD accounting for the transition due to cAMP binding, as well as the identification of the TRIP8b binding site on CNBD are crucial to validate the allosteric model.

4.1 cAMP-induced structural rearrangements in HCN CNBD

We show here, for the first time, a structural model of the human HCN2 CNBD in the cAMP-unbound form generated by CS-ROSETTA, which now allows us to identify all conformational transitions occurring upon ligand binding. By the comparison of the unbound and bound structures we highlighted that HCN CNBD behaves in line with the universally conserved mechanism of CNBDs [30]. In our opinion, this mechanism justifies the inclusion of the last two helices of the C-linker among the N-terminal helical bundle, which we recommend for all future descriptions of the HCN CNBD, as well as CNBD-containing channel family. The cAMP-unbound structure clearly highlights that the N-terminal helical bundle plays a key role in the cAMP regulation of channel opening. Given that the N-terminal helical bundle undergoes a large reorientation upon cAMP binding and connects the CNBD with the C-linker, we argue that this is the element by which CNBD affects the rearrangement of the C-linker, though the precise movements of the C-linker, as well as how they affect the pore module remain unclear. Moreover, both CS-ROSETTA structure and dynamics data provide direct structural evidence that the second half of the C-helix is flexible and less ordered in the absence of cAMP. Thus, the cAMP-unbound structure confirms the stabilization of the F' and C-helix upon cAMP binding, that had been indirectly suggested using transition metal ion FRET [58, 59]. A previous cAMP-free CNBD X-ray structure, containing bromide ions in contact to the PBC, shows an overall conformation very similar to the cAMP-bound form, because bromide-induced PBC rearrangements propagate to the helical components, forcing CNBD to a cAMP-bound like

conformation [58]. Notably, in this structure the C-terminal half of C-helix is not resolved, indicating that in the absence of ligand this region is less ordered and indeed cAMP binding directly promotes structural stabilization of the C-helix. For this reason, we suggest that the C-helix stabilization following ligand interaction constitutes a mechanism of regulation of cAMP-affinity among the CNBD-containing proteins. Arginine 659, the key residue for the binding to cAMP, localizes in the flexible region of the C-helix. Thus, in HCN the capture of the ligand onto the CNBD requires the stabilization of a dynamic element, a process that can affect the affinity of the protein for cyclic nucleotides. This is in agreement with the fact that the affinity of HCN CNBD for cAMP is about 15 times lower than MloK1 CNBD, which presents a rigid C-helix in the cAMP-unbound form [60]. Evolutionarily linked to HCN channels, the voltage-dependent potassium channel (KCNH) family shares a cyclic nucleotide binding homologous domain (CNBHD), in which the C-helix is partially unstructured [33, 61, 62]. Although KCNH have lost the cyclic nucleotide regulation, and therefore their C-helices have a different function, the absence of a defined secondary structure in the second half of the C-helix appears to be a conserved feature of the eukaryote family of CNBD-containing channels.

4.2 The binding site of TRIP8b on CNBD

In this work we have identified the TRIP8b binding site on HCN CNBD. Our results definitely prove that TRIP8b and cAMP do not compete for the same binding region and provides a strong structural support to the allosteric antagonistic model recently proposed [26]. The NMR titration identified two regions of CNBD that are equally affected upon mini/microTRIP8b addition: the N-bundle loop and the C-helix/stretch. Using deletion mutants, both in the full length HCN channel and in the isolated CNBD protein, we provided biochemical evidence that the C-helix/stretch is necessary for the interaction of CNBD with TRIP8b. Moreover, we highlighted the importance of the unstructured stretch following the C-helix for the binding event. In particular, we showed that the GKK sequence of the stretch is necessary for complex formation. Interestingly, microTRIP8b includes the acidic stretch of residues (EEEFE) that have been shown to be essential for the binding [26], suggesting the involvement of an electrostatic interaction between CNBD and TRIP8b. The relevance of the stretch sequence following the C-helix in the regulation of channel activity appears to be evolutionarily conserved in the eukaryote family of CNBD-containing channels, since KCNH channels show an intrinsic

mechanism of regulation that involved the stretch following the C-helix [33, 61, 62]. Though our biochemical analysis does not attribute a direct role to the N-bundle loop in the complex formation, the NMR titration clearly showed that this sequence is strongly affected by mini/microTRIP8b as much as the C-helix/stretch. Moreover, the N-bundle loop and the C-helix/stretch are in close proximity in the CNBD tertiary structure (both in the cAMP-unbound and bound forms) and in the quaternary structure are exposed to the solvent. These data strongly suggest that the N-bundle loop and the C-helix/stretch generate the CNBD binding area of TRIP8b. This new structural information will allow a full understanding of this important molecular complex, leading to a better understaning of the molecular bases of neurological disorders originated by CNBD mutations and possibly the design of drugs able to modulate HCN channel-mediated cognitive processes.

4.3 Molecular model of the binary cAMP-TRIP8b regulatory system of HCN channels

It is known that the cAMP-induced conformational changes in the CNBD are determinant in shifting the equilibrium of the closed-open transition of the channel towards the open state [18, 20, 59]. Here, we demonstrate that, both the N-bundle loop, which is part of the N-terminal helical bundle, and the C-helix constitute the elements of CNBD that undergo the largest structural rearrangement in the cAMP-unbound/bound transition of CNBD. Thus, we can argue that TRIP8b allosterically antagonizes the effect of cAMP by blocking both the N-terminal helical bundle and the C-helix in the conformation they adopt in the cAMP-unbound state. This molecular model of interaction between TRIP8b and CNBD can easily explain the mutual antagonistic effect of TRIP8b and cAMP that we proposed [26]. The stabilization of the CNBD in its cAMP-unbound conformation shifts the closed-open transition of the channel toward the closed one: exactly the opposite versus of the effect caused by the cyclic nucleotide. In our model, the binding of TRIP8b to the CNBD does not block the entry of the cyclic nucleotide in the cavity of the β-roll, but interacts with the C-helix, preventing its movement. Thus, CNBD bound to TRIP8b has a decrease in affinity for cAMP, as recently estimated from electrophysiological results [26]. Moreover, here we showed that N-terminal helical bundle is a crucial element for the regulation of channel opening. Therefore, in the

proposed model TRIP8b causes the stabilization of the closed state of the channel blocking the C-linker in its resting conformation via the stabilization of the cAMP-unbound conformation of the N-terminal helical bundle. Since HCN channels are involved in a wide number of cognitive processes, understanding the molecular mechanism of regulation of this family of channels is critically important. Thus, our work offers an important contribute to the understanding of the binary cAMP-TRIP8b regulatory system of HCN channels, a powerful topic as it pertains to the physiological processes and diseases associated with dysfunction in I_h conductance in neurons.

REFERENCES

1. Robinson R. B., Siegelbaum S. A., " hyperpolarization-activated cation currents: From Molecules to Physiological Function", *Annu. Rev. Physiol.,* vol. 65, pp. 453-480, 2003;
2. Brown H.F., DiFrancesco D., Noble S.J., "How does adrenaline accelerate the heart?", *Nature,* vol 280, pp. 235–36, 1979;
3. Halliwell J.V., Adams P.R., "Voltage-clamp analysis of muscarinic excitation in hippocampal neurons", *Brain Res.,* vol. 250, pp. 71–92, 1982;
4. Yanagihara K., Irisawa H., "Inward current activated during hyperpolarization in the rabbit sinoatrial node cell", *Pflugers Arch.,* vol. 385, pp. 11–19, 1980;
5. Biel M., Wahl-Schott C., Michalakis S., Zong X., "Hyperpolarization-Activated Cation Channels: From Genes to Function", *Physiol Rev,* vol. 89, pp. 847–885, 2009;
6. Nolan M.F., Dudman J.T., Dodson P.D., Santoro B., "HCN1 channels control resting and active integrative properties of stellate cells from layer II of the entorhinal cortex",

   J Neurosci, vol. 27, pp. 12440–12451, 2007;
7. Magee J.C., "Dendritic Ih normalizes temporal summation in hippocampal CA1 neurons", *Nat. Neurosci.,* vol. 2, pp. 508–14, 1999;
8. teriade M., McSCormick D.A, Sejnowski T.J., "Thalamocortical oscillations in the sleeping and aroused brain" *Science,* vol. 262, pp. 679–685, 1993;
9. DiFrancesco D., "Pacemaker mechanisms in cardiac tissue", *Annu. Rev. Physiol.,* vol. 55, pp. 455–72, 1993;
10. Luthi A., McCormick D.A., "H-current: properties of a neuronal and network pacemaker", *Neuron,* vol. 21, pp. 9–12, 1998;
11. Maccaferri G., McBain C.J., "The hyperpolarization-activated current (Ih) and its contribution to pacemaker activity in rat CA1 hippocampal stratum oriens-alveus interneurons", *J. Physiol.,* vol. 497(Pt.1), pp. 119–30, 1996;
12. Ludwig A., Zong X., Jeglitsch M., Hofmann F., Biel M., "A family of hyperpolarization-activated mammalian cation channels" *Nature,* vol. 393, pp. 587–91, 1998;
13. Santoro B., Tibbs G.R., "The HCN gene family: molecular basis of the hyperpolarization-activated pacemaker channels", *Ann. NY Acad. Sci.,* vol. 868, pp. 741–64, 1999;
14. Altomare C., Terragni B., Brioschi C., Milanesi R., Pagliuca C., Viscomi C., Moroni A., Baruscotti M., DiFrancesco D., "Heteromeric HCN1-HCN4 channels: a comparison with native pacemaker channels from the rabbit sinoatrial node", *J Physiol,* vol. 549, pp. 347–359, 2003;

15. Santoro B., Chen S., Luthi A., Pavlidis P., Shumyatsky G.P., et al. “Molecular and functional heterogeneity of hyperpolarization-activated pacemaker channels in the mouse CNS”, *J. Neurosci.,* Vol. 20, pp. 5264–75, 2000;

16. Moosmang S., Stieber J., Zong X., Biel M., Hofmann F., Ludwig A., “Cellular expression and functional characterization of four hyperpolarization-activated pacemaker channels in cardiac and neuronal tissues”, *Eur. J. Biochem.,* vol. 268, pp. 1646–52, 2001;

17. Shi W., Wymore R., Yu H., Wu J., Wymore R.T., et al. “Distribution and prevalence of hyperpolarization-activated cation channel (HCN) mRNA expression in cardiac tissues”, *Circ. Res.,* vol. 85, pp. E1–6, 1999;

18. Wainger B.J., DeGennaro M., Santoro B., Siegelbaum S.A., Tibbs G.R, “Molecular mechanism of cAMP modulation of HCN pacemaker channels”, *Nature,* vol. 411(6839), pp. 805-809, 2001;

19. Craven K.B, Zagotta W.N., “CNG and HCN channels: Two Peas, One Pod”, *Annu. Rev. Physiol.*, vol. 68, pp. 375–401, 2006;

20. Chen S., Wang J., Zhou L., George M.S,Siegelbaum S.A., “Voltage Sensor Movement and cAMP Binding Allosterically Regulate an Inherently Voltage-independent Closed−Open Transition in HCN Channels”, *J. Gen. Physiol*. vol. 129 (2), pp. 175–188, 2007;

21. Santoro B., Piskorowski R.A., Pian P., Hu L., Liu H., Siegelbaum S.A., “TRIP8b splice variants form a family of auxiliary subunits that regulate gating and trafficking of HCN channels in the brain”, *Neuron,* vol. 62, pp. 802-813, 2009;

22. Zolles G., Wenzel D., Bildl W., Schulte U., Hofmann A., Muller C.S., Thumfart J.O., Vlachos A., Deller T., Pfeifer A., Fleischmann B.K., Roeper J., Fakler B., Klocker N., “Association with the auxiliary subunit PEX5R/Trip8b controls responsiveness of HCN channels to cAMP and adrenergic stimulation”, *Neuron,* vol. 62, pp. 814-825, 2009;

23. Lewis A.L., Schwartz E., Chan C.S., Noam Y., Shin M., Wadman W.J., Surmeier D.J., Baram T.Z., Macdonald R.L., Chetkovich D.M., “alternatively spliced isoforms of TRIP8b differentially control h channel trafficking and function”, *J. Neurosci.,* vol. 29(19), pp. 6250–6265, 2009;

24. Bankston J.R., Camp S.S., DiMaio F., Lewis A.S., Chetkovich D.M., Zagotta W.N., “Structure and stoichiometry of an accessory subunit TRIP8b interaction with hyperpolarization activated cyclic nucleotide-gated channels”, *PNAS,* vol. 109(20), pp. 7899-904, 2012;

25. Santoro B., Hu L., Liu H., Saponaro A., Pian P., Piskorowski R.A., Moroni A., Siegelbaum S.A., “TRIP8b Regulates HCN1 Channel Trafficking and Gating through Two Distinct C-Terminal Interaction Sites”, *J. Neurosci.,* vol. 31(11), pp. 4074-86, 2011;

26. Hu L., Santoro B., Saponaro A., Liu H., Moroni A., Siegelbaum S.A., “binding of the auxiliary subunit TRIP8b to HCN channels shifts the mode of action of cAMP”, *J. Gen. Physiol,* vol. 142(6), pp. 599-612, 2013;

27. Han Y., Noam Y., Lewis A.S., Gallagher J.J., Wadman W.J., Baram T.Z., Chetkovich D.M., “trafficking and gating of hyperpolarization-activated cyclic nucleotide-gated channels are

regulated by interaction with tetratricopeptide repeat-containing rab8b-interacting protein (TRIP8b) and cyclic AMP at distinct sites", *J Biol Chem.,* vol. 286(23), pp. 20823–20834, 2011;

28. Schünke S., Stoldt M., Lecher J., Kaupp U.B., Willbold D., "Structural insights into conformational changes of a cyclic nucleotide-binding domain in solution from Mesorhizobium loti K1 channel", *PNAS*, vol. 108(15), pp. 6121–6126, 2011;
29. Wu J., Brown S.,Xuong N.,. Taylor S.S., "RIα subunit of PKA: A cAMP-free structure reveals a hydrophobic capping mechanism for docking cAMP into Site B", *Structure*, vol. 12, pp. 1057–1065, 2004;
30. Rehmann H., Wittinghofer A., Bos J.L., "Capturing cyclic nucleotides in action: snapshots from crystallographic studies", *Nature Reviews,* vol. 8(1), pp. 63-73, 2007;
31. Lolicato M., Nardini M., Gazzarrini S., Möller S., Bertinetti D., Herberg F.W., Bolognesi M., Martin H., Fasolini M., Bertrand J.A., Arrigoni A., Thiel G, Moroni A., "tetramerization dynamics of C-terminal domain underlies isoform-specific cAMP gating in hyperpolarization-activated cyclic nucleotide-gated channels", *J BiolChem.,* vol. 286(52), pp. 44811-20, 2012;
32. Zagotta W.N., Olivier N.B., Black K.D., Young E.C., Olson R., Gouaux E., "Structural basis for modulation and agonist specificity of HCN pacemaker channels", *Nature,* vol. 425, pp. 200-205, 2003;
33. Marques-Carvalho M.J., Sahoo N., Muskett F.W., Vieira-Pires R.S., Gabant G., Cadene M., Schonherr R., Morais-Cabral J.H., "Structural, biochemical, and functional characterization of the cyclic nucleotide binding homology domain from the mouse eag1 potassium channel", *J.Mol.Biol.*, vol. 423, pp.34-46, 2012;
34. Titus D. J., Furones C., Kang Y., Atkins C. M., "age-dependent alterations in cAMP signaling contribute to synaptic plasticity deficits following traumatic brain injury", *Neuroscience*, vol. 231, pp. 182–194, 2013;
35. Ramos B., Stark D., Verduzco L., van Dyck C.H., Arnsten A.F.T., "Alpha-2A-Adrenoceptor stimulation improves prefrontal cortical regulation of behavior through inhibition of cAMP signaling in aging animals", *Learn. Mem.*, vol. 13, pp. 770–776, 2006;
36. Klamer D., Palsson E., Fejgin K., Zhang J., Engel J.A., Svensson L., "Activation of a nitric-oxide-sensitive cAMP pathway with phencyclidine: elevated hippocampal cAMP levels are temporally associated with deficits in prepulse inhibition", *Psychopharmacology (Berl)*, vol. 179, pp. 479–488, 2005;
37. Nolan M.F., Malleret G.I., Dudman J.T., Buhl D.L., Santoro B., Gibbs E., Vronskaya S., Buzsàki G., Siegelbaum S.A., Kandel E.R., Morozov A., "A Behavioral Role for Dendritic Integration: HCN1 Channels Constrain Spatial Memory and Plasticity at Inputs to Distal Dendrites of CA1 Pyramidal Neurons", Cell, vol. 119, pp. 719–732, 2004;
38. Noam Y., Bernard C., Baram T.Z., "Towards an integrated view of HCN channel role in epilepsy", *Current Opinion in Neurobiology*, vol. 21, pp. 873–879, 2011;

39. Paspalas C.D., Wang M, Arnsten A.F.T., “Constellation of HCN channels and cAMP regulating proteins in dendritic spines of the primate prefrontal cortex: potential substrate for working memory deficits in Schizophrenia”, *Cerebral Cortex*, vol. 23, pp. 1643–1654, 2013;

40. Saito Y., Inoue T., Zhu G., Kimura N., Okada M., Nishimura M., Kimura N., Murayama S., Kaneko S., Shigemoto R., Imoto K., Suzuki T., “Hyperpolarization-activated cyclic nucleotide gated channels: a potential molecular link between epileptic seizures and Aβ generation in Alzheimer’s disease”, *Molecular Neurodegeneration,* vol. 7, pp. 50, 2012;

41. Wang M., Ramos B.P., Paspalas C.D, Shu Y., Simen A., Duque A., Vijayraghavan S., Brennan A., Dudley A., Nou E., Mazer J.A., McCormick D.A., Arnsten A.F.T., “α2A-Adrenoceptors strengthen working memory networks by inhibiting cAMP-HCN channel signaling in Prefrontal Cortex”, *Cell*, vol. 129, pp. 397–410, 2007;

42. Lewis A.S., Vaidya S.P., Blaiss C.A., Liu Z., Stoub T.R., Brager D.H., Chen X., Bender R.A., Estep C.M., Popov A.B., Kang C.E., Van Veldhoven P.P., Bayliss D.A., Nicholson D.A., Powell C.M., Johnston D., Chetkovich D.M., “Deletion of the hyperpolarization-activated cyclic nucleotide gated channel auxiliary subunit TRIP8b impairs hippocampal Ih localization and function and promotes antidepressant behavior in mice”, *J. Neurosci.*, vol. 31(20), pp. 7424-40, 2011;

43. Brager D.H., Lewis A.S., Chetkovich D.M., Johnston D., “Short- and long-term plasticity in CA1 neurons from mice lacking h-channel auxiliary subunit TRIP8b”, *J. Neurophysiol.,* vol. 110(10), pp. 2350-7, 2013;

44. Marcelin B., Liu Z., Chen Y., Lewis A.S., Becker A., McClelland S., Chetkovich D.M., Migliore M., BaramT.Z., EsclapezM., BernardC.,“Dorsoventral differences in intrinsic properties in devel oping CA1 pyramidal cells”, *J. Neurosci.*, vol. 32(11), pp. 3736-47. 2012;

45. Heys J.G., Hasselmo M.E., “Neuromodulation of I(h) in layer II medial entorhinal cortex stellate cells: a voltage-clamp study”, *J. Neurosci.*, vol. 32(26), pp. 9066-72, 2012;

46. Chow S.S., Van Petegem F., Accili E.A., “Energetics of cyclic AMP binding to HCN channel C terminus reveal negative cooperativity”, *J. Biol Chem.*, vol. 287(1), pp. 600-6, 2011;

47. Wider G., “Structure determination of biological macromolecules in solution using nuclear magnetic resonance spectroscopy”, *Biotechniques.*, vol. 29(6), pp. 1278-82, 2000;

48. Wishart D.S., Sykes B.D., Richards F.M.., “Relationship between nuclear magnetic resonance chemical shift and protein secondary structure”, *J. Mol. Biol.*, vol. 222, pp. 311–333, 1991;

49. Wagner G., Pardi A., Wuthrich K., “Hydrogen-bond length and H-1-NMR chemical-shifts in proteins”, *J. Am. Chem. Soc.*, vol. 105, pp. 5948–5949, 1983;

50. Case D.A., “Calibration of ring-current effects in proteins and nucleic acids.”, *J. Biomol. NMR*, vol. 6, pp. 341–346, 1995;

51. Shen Y., Lange O., Delaglio F., Rossi P., Aramini J.M., Liu G., Eletsky A., Wu Y., Singarapu K.K., Lemak A., Ignatchenko A., Arrowsmith C.H., Szyperski T., Montelione G.T., Baker D., Bax

A., "Consistent blind protein structure generation from NMR chemical shift data", *PNAS*, vol. 105(12), pp. 4685-90, 2009;

52. Lange O.F, Baker D., "Resolution-adapted recombination of structural features significantly improves sampling in restraint-guided structure calculation", *Proteins*, vol. 80(3), pp. 884-95, 2012;

53. Raman S., Lange O.F., Rossi P., Tyka M., Wang X., Aramini J., Liu G., Ramelot T.A., Eletsky A., Szyperski T., Kennedy M.A., Prestegard J., Montelione G.T., Baker D., "NMR structure determination for larger proteins using backbone-only data", *Science*, vol. 327(5968), pp. 1014-8, 2010;

54. Kay L.E., Torchia D.A., Bax A., "Backbone dynamics of proteins as studied by 15N inverse detected heteronuclear NMR spectroscopy: application to staphylococcal nuclease", *Biochemistry*, vol. 28(23), pp. 8972-9, 1989;

55. Zuiderweg E.R., "Mapping protein-protein interactions in solution by NMR spectroscopy", *Biochemistry*, vol. 41(1), pp. 1-7, 2002;

56. Williamson R.A., Carr M.D., Frenkiel T.A., Feeney J., Freedman R.B., "Mapping the binding site for matrix metalloproteinase on the N-terminal domain of the tissue inhibitor of metalloproteinases-2 by NMR chemical shift perturbation", *Biochemistry,* vol. *36,* pp. 13882-13889, 1997;

57. Balbach J., Forge V., Lau W.S., van Nuland N.A., Brew K., Dobson C.M., "protein folding monitored at individual residues during a two-dimensional NMR experiment", *Science*, vol. 274(5290), pp. 1161-1163, 1996;

58. Taraska J.W., Puljung M.C., Olivier N.B., Flynn G.E., Zagotta W.N., "Mapping the structure and conformational movements of proteins with transition metal ion FRET", *Nat. Methods*, vol. 6(7), pp. 532-7, 2009;

59. Puljung M.C., Zagotta W.N., "A secondary structural transition in the C-helix promotes gating of cyclic nucleotide-regulated ion channels", *J. Biol. Chem.*, vol. 288(18), pp. 12944-56, 2013;

60. Cukkemane A., Grüter B., Novak K., Gensch T., Bönigk W., Gerharz T., Kaupp U.B., Seifert R., "Subunits act independently in a cyclic nucleotide-activated K^+ channel", *EMBO Rep.*, vol. 8(8), pp. 749-55, 2007;

61. Brelidze T.I., Carlson A.E., Sankaran B., Zagotta W.N., "Structure of the carboxy-terminal region of a KCNH channel", *Nature*, vol. 481(7382), pp. 530-3, 2012;

62. Brelidze T.I., Gianulis E.C., DiMaio F., Trudeau M.C., Zagotta W.N., "Structure of the C-terminal region of an ERG channel and functional implications", *PNAS*, vol. 110(28), pp. 11648-53, 2013;

63. Wiseman T., Williston S., Brandts J.F., Lin L.N., "Rapid measurement of binding constants and heats of binding using a new titration calorimeter", *Anal. Biochem.*, vol. 179(1), pp. 131-7, 1989;

64. Ferentz A.E., Wagner G., “NMR spectroscopy: a multifaceted approach to macromolecular structure”, *Q. Rev. Biophys*, vol. 33(1), pp. 29-65 2000;

65. Neuhaus D., Vanmierlo C. P. M., “Measurement of heteronuclear NOE enhancements in biological macromolecules: a convenient pulse sequence for use with aqueous solutions”, *J. Magn. Reson.*, vol. 100, pp. 221–228, 1992;

66. Vranken W.F., Boucher W., Stevens T.J., Fogh R.H., Pajon A., Llinas M., Ulrich E.L., Markley J.L., Ionides J., Laue E.D., “The CCPN data model for NMR spectroscopy: development of a software pipeline”, *Proteins*, vol. 59(4), pp. 687-96, 2005;

67. R. Keller, “The Computer Aided Resonance Assignment Tutorial”, *CANTINA Verlag*, 2004;

68. Garrett D. S., Seok Y. J., Peterkofsky A., Clore G. M., Gronenborn A. M., “Identification by NMR of the binding surface for the histidine-containing phosphocarrier protein HPr on the N-terminal domain of enzyme I of the Escherichia coli phosphotransferase system”, *Biochemistry*, vol. 36, pp. 4393-4398, 1997.

PART II

Cellular/Molecular

TRIP8b Regulates HCN1 Channel Trafficking and Gating through Two Distinct C-Terminal Interaction Sites

Bina Santoro,[1] Lei Hu,[1] Haiying Liu,[3] Andrea Saponaro,[4] Phillip Pian,[1] Rebecca A. Piskorowski,[1] Anna Moroni,[4] and Steven A. Siegelbaum[1,2,3]

Departments of [1]Neuroscience and [2]Pharmacology, [3]Howard Hughes Medical Institute, Columbia University, New York, New York 10032, and [4]Department of Biology and Consiglio Nazionale delle Ricerche-Istituto di Biofisica, University of Milan, 20133 Milano, Italy

Hyperpolarization-activated cyclic nucleotide-regulated (HCN) channels in the brain associate with their auxiliary subunit TRIP8b (also known as PEX5R), a cytoplasmic protein expressed as a family of alternatively spliced isoforms. Recent *in vitro* and *in vivo* studies have shown that association of TRIP8b with HCN subunits both inhibits channel opening and alters channel membrane trafficking, with some splice variants increasing and others decreasing channel surface expression. Here, we address the structural bases of the regulatory interactions between mouse TRIP8b and HCN1. We find that HCN1 and TRIP8b interact at two distinct sites: an upstream site where the C-linker/cyclic nucleotide-binding domain of HCN1 interacts with an 80 aa domain in the conserved central core of TRIP8b; and a downstream site where the C-terminal SNL (Ser-Asn-Leu) tripeptide of the channel interacts with the tetratricopeptide repeat domain of TRIP8b. These two interaction sites play distinct functional roles in the effects of TRIP8b on HCN1 trafficking and gating. Binding at the upstream site is both necessary and sufficient for TRIP8b to inhibit channel opening. It is also sufficient to mediate the trafficking effects of those TRIP8b isoforms that downregulate channel surface expression, in combination with the trafficking motifs present in the N-terminal region of TRIP8b. In contrast, binding at the downstream interaction site serves to stabilize the C-terminal domain of TRIP8b, allowing for optimal interaction between HCN1 and TRIP8b as well as for proper assembly of the molecular complexes that mediate the effects of TRIP8b on HCN1 channel trafficking.

Introduction

The function and expression of many ion channels are regulated by subunits that do not contribute to the channel pore, but stably associate with pore-forming subunits. Recent studies provide strong evidence that the cytoplasmic tetratricopeptide repeat-containing Rab8b interacting protein TRIP8b (also known as PEX5R) is a regulatory subunit of the hyperpolarization-activated cyclic nucleotide-regulated (HCN) channels in the brain (Santoro et al., 2004, 2009: Zolles et al., 2009; Lewis et al., 2009). TRIP8b undergoes extensive alternative splicing at its N terminus. All splice forms inhibit HCN channel activation by antagonizing the ability of cyclic nucleotides to facilitate channel opening (Santoro et al., 2009; Zolles et al., 2009). In contrast, different splice variants produce diverse effects on HCN channel membrane trafficking (Lewis et al., 2009; Santoro et al., 2009).

TRIP8b isoforms contain a large constant domain (exons 5–16) preceded by a variable region at which exons 1a or 1b combine with subsets of exons 2–4. The C-terminal half of TRIP8b (exons 9–16) comprises an ~350 aa tetratricopeptide repeat (TPR) protein-binding domain with 57% identity to the PEX5 peroxisome receptor TPR domain. In contrast, TRIP8b and PEX5 have no sequence similarity in their initial N-terminal ~250 aa, consistent with their divergent functions. TRIP8b(1a-4) and TRIP8b(1a-2–4) (the naming convention lists the alternatively spliced exons) cause a fourfold to sixfold increase in surface expression of HCN1 channels when coexpressed in *Xenopus* oocytes. In contrast, TRIP8b(1a) decreases HCN1 surface expression by 10-fold, and both TRIP8b(1b-2) and TRIP8b(1b-2–4) virtually eliminate channel surface expression (>50-fold decrease) (Santoro et al., 2009). The decrease in surface expression requires N-terminal consensus sites for adaptor protein (AP) complex binding in exons 2 and 5 that likely promote clathrin-dependent channel endocytosis (Santoro et al., 2004, 2009; Popova et al., 2008; Petrenko et al., 2010).

Our laboratory initially found that the TRIP8b TPR domain interacts with the SNL (Ser-Asn-Leu) tripeptide at the C terminus of HCN1, −2, and −4 (Santoro et al., 2004), which we refer to as the "downstream" interaction site. More recently, Lewis et al. (2009) identified a second "upstream" interaction site at which the C-linker region and contiguous cyclic nucleotide-binding domain (CNBD) of HCN1 binds to an internal sequence in the conserved middle region of TRIP8b. Here we map in finer detail the boundaries of the two physical interaction sites between HCN1 and TRIP8b, and define the roles of these interactions in protein binding, channel trafficking, and channel gating. We find that the upstream interaction site is necessary and sufficient to

Received Oct. 27, 2010; revised Dec. 17, 2010; accepted Jan. 9, 2011.

This work was partially supported by National Institutes of Health Grant NS36658 (S.A.S.), a Fellowship from the Italian Academy for Advanced Studies in America (B.S.), and a Research Grant from the Epilepsy Foundation (B.S.), as well as Award F32NS064732 from National Institute of Neurological Disorders and Stroke (R.A.P.). We thank Alexander Kushnir for his contributions during the development of this study, Lei Zhou and Yuhang Chen for help with homology modeling and figure construction, and John Riley for excellent technical assistance. We are also indebted to Justine Barry for her advice and critical reading of the manuscript.

Correspondence should be addressed to Steven A. Siegelbaum, Departments of Neuroscience and Pharmacology, Howard Hughes Medical Institute, Columbia University, 1051 Riverside Drive, New York, NY 10032. E-mail: sas8@columbia.edu.

DOI:10.1523/JNEUROSCI.5707-10.2011

 0270-6474/11/314074-13$15.00/0

enable TRIP8b to downregulate channel surface expression and inhibit channel activation. In contrast, the downstream interaction site stabilizes the C-terminal domain of TRIP8b, allowing for optimal interaction between HCN1 and TRIP8b. In addition, an intact TPR domain is required for the effect of certain TRIP8b splice forms to enhance HCN1 channel surface expression. Finally, we identify an 80 aa fragment within the core of TRIP8b that is sufficient to inhibit the action of cyclic nucleotides to facilitate HCN1 channel opening.

Materials and Methods

Plasmids and heterologous expression in Xenopus *oocytes.* All constructs were cloned in pGHE or pGH19 vectors, linearized, and transcribed into cRNA using T7 polymerase (MessageMachine, Ambion) as described previously (Santoro et al., 2004, 2009). cDNA clones encoding HCN1 and TRIP8b both corresponded to the *Mus musculus* sequence. Site-directed mutagenesis was performed using either the QuickChange Mutagenesis kit (Stratagene) or PCR cloning. The enhanced green fluorescent protein (GFP) tag (derived from vector pEGFP-C1, Clontech) was always inserted at the N-terminal end of the target protein (HCN1 or TRIP8b, wild-type or mutant) (Santoro et al., 2004), with the exception of the CD8 fusion construct, where the GFP sequence was inserted between the CD8 transmembrane domain and the $HCN1_{776–910}$ domain (CD8-GFP-$HCN1_{776–910}$). Mutant HCN1 constructs are as described previously (Wainger et al., 2001; Santoro et al., 2004), with $HCN1_{\Delta SNL}$ comprising residues $HCN1_{1–907}$, $HCN1_{\Delta CX}$ comprising residues $HCN1_{1–610}$, and $HCN1_{\Delta CNBD}$ comprising residues $HCN1_{1–472}$. Specific residue numbers for corresponding mutations introduced in the background of the three TRIP8b splice variants are as follows: $TRIP8b_{\Delta NX}$, which lacks most of the initial N-terminal region that is divergent from PEX5, corresponds to TRIP8b(1b-2)$_{204–615}$ [identical to TRIP8b(1a-4)$_{191–602}$ or TRIP8b(1a)$_{156–567}$]; $TRIP8b_{\Delta Nter}$, a larger N-terminal deletion extending into the PEX5 homology domain, corresponds to TRIP8b(1b-2)$_{272–615}$ [identical to TRIP8b(1a-4)$_{259–602}$ or TRIP8b(1a)$_{224–567}$]; $TRIP8b_{\Delta Cter}$, the complementary fragment to $TRIP8b_{\Delta Nter}$ (see also supplemental Fig. 1, available at www.jneurosci.org as supplemental material), corresponds to TRIP8b(1b-2)$_{1–271}$, TRIP8b(1a-4)$_{1–258}$, and TRIP8b(1a)$_{1–223}$; $TRIP8b_{\Delta TPR}$, which lacks all but the first two helices of the C-terminal TPR domain, corresponds to TRIP8b(1b-2)$_{1–346}$, TRIP8b(1a-4)$_{1–333}$, and TRIP8b(1a)$_{1–298}$; the minimal TRIP8b fragment ($TRIP8b_{mini}$), which consists of an 81 aa stretch immediately upstream of the TPR domain, corresponds to TRIP8b(1b-2)$_{236–316}$ [identical to TRIP8b(1a-4)$_{223–303}$ or TRIP8b(1a)$_{188–268}$]; $TRIP8b_{\Delta int}$, in which a 22 aa region in the conserved core of TRIP8b is internally deleted, corresponds to TRIP8b(1b-2)$_{\Delta 250–271}$, TRIP8b(1a-4)$_{\Delta 237–258}$, and TRIP8b(1a)$_{\Delta 202–223}$; and $TRIP8b_{NK,}$ in which a conserved asparagine in the TPR domain is mutated to lysine, corresponds to TRIP8b(1b-2)$_{N501K}$, TRIP8b(1a-4)$_{N488K}$, and TRIP8b(1a)$_{N453K}$. Oocytes were injected with 50 nl of cRNA solution each, at a concentration of 0.1–1.0 $\mu g/\mu l$ for HCN1 channel constructs (as specified in figure legends) and 0.2 $\mu g/\mu l$ for TRIP8b constructs and GFP (or as specified in figure legends). In each given set of experiments, we always used a constant ratio of HCN1 cRNA to TRIP8b or GFP cRNA.

Coimmunoprecipitation and Western blots. Oocytes were screened for GFP expression by live confocal microscopy 3 d after cRNA injection. Positive oocytes were collected, briefly rinsed in Barth's Saline (Millipore Bioscience Research Reagents), and homogenized in ice-cold lysis buffer (150 mM NaCl, 10 mM Tris-Cl pH 7.4, 1 mM EGTA, 2 mM EDTA, 1% Triton) with protease inhibitors (Complete Mini, Roche) using a glass Teflon homogenizer, at a constant ratio of 12 oocytes per 300 μl of buffer. The homogenate was spun twice for 5 min at 12,000 × *g* (4°C), and the second supernatant was used for Western blot analysis of protein expression levels (input) or coimmunoprecipitation. For coimmunoprecipitation, 30 μl of extract was mixed with 120 μl of coimmunoprecipitation buffer (150 mM NaCl, 10 mM Tris), precleared for 1 h at 4°C, and then incubated overnight at 4°C with 15 μl of Protein-A-Sepharose beads (GE Healthcare) bound to anti-GFP antibody (Abcam 290; 1.5 μl of for each sample) or anti-TRIP8b antibody (rabbit polyclonal 794, 2 μl of serum for each sample) (Santoro et al., 2009). Beads were washed three times with TBST (150 mM NaCl, 10 mM Tris-Cl pH 7.4, 0.1% Triton) and proteins eluted in Laemmli sample buffer. Proteins were resolved by 8% SDS-PAGE, transferred to a polyvinylidene difluoride membrane (PolyScreen, PerkinElmer) in CAPS buffer (10 mM CAPS, pH 11, 10% methanol) and Western blot analysis performed as described previously (Santoro et al., 2009). Primary antibody dilutions were as follows: anti-HCN1 (rat monoclonal 7C3, generous gift from Frank Müller, Forschungszentrum Jülich, Jülich, Germany) 1:500; anti-TRIP8b (rabbit polyclonal 794) (Santoro et al., 2009) 1:5000; and anti-GFP (Abcam 290) 1:5000. HRP-anti-rat conjugate (Jackson ImmunoResearch) or HRP-anti-rabbit conjugate (Cell Signaling Technology) were used as secondary antibodies. The protein bands were visualized by chemiluminescence using SuperSignal reagent (Pierce).

Yeast two-hybrid assay. Assays were performed using the Grow'N'Glow Two-Hybrid kit (Bio 101) (Santoro et al., 2004) and yeast strain EGY48. Bait constructs representing the indicated HCN1 channel domains were cloned into vector pEG202, and prey constructs representing the indicated TRIP8b domains (or mutants thereof) were cloned in vector pJG4–5. Channel domains representing successive deletions of the six (A′–F′) helixes that comprise the HCN1 C-linker region (a highly conserved 84 aa region, residues 387–471, connecting the channel transmembrane domain to the 120 aa CNBD) are as follows: CNBD alone, $HCN1_{472–592}$; E′–F′ C-linker helixes plus the CNBD, $HCN1_{453–592}$; C′–F′ C-linker helixes plus the CNBD, $HCN1_{429–592}$; and A′–F′ C-linker helixes plus the CNBD, $HCN1_{387–592}$. The construct representing the C-terminal domain of HCN1 is as described previously (Santoro et al., 2004) and comprises residues $HCN1_{776–910}$. The C-linker/CNBD region construct (see Fig. 4*B*,*C*) comprises residues $HCN1_{390–610}$ (same C-terminal ending as $HCN1_{\Delta CX}$). Note that all TRIP8b constructs used for the yeast two-hybrid assay comprise the constant domain of TRIP8b only (exons 5–16); that is, they exclude all N-terminal alternatively spliced exons. To facilitate referencing, however, numbering in Figure 4 is based on full-length TRIP8b(1b-2). Bait and prey plasmids were cotransformed with reporter plasmid pGNG1, and cells were plated onto glucose-containing medium. Transformants were restreaked (in triplicate) on galactose$^+$/Leu$^-$ selective medium and screened for positive GFP expression under a UV light following 3–5 d of growth.

Affinity purification of protein complexes from bacterial lysates. A cDNA fragment encoding residues 470–672 of hHCN2 (Ludwig et al., 1999) was cloned into a modified pET-24b vector (generous gift from Dan Minor, University of California, San Francisco, San Francisco, CA) downstream of a double His_6-maltose binding protein (MBP) tag, while cDNA fragments corresponding to residues 236–316 ($TRIP8b_{mini}$) and 272–615 ($TRIP8b_{\Delta Nter}$) of TRIP8b(1b-2) were cloned into vector pET-52b (Novagen) downstream of a Strep(II) tag sequence. Plasmids were cotransformed into *Escherichia coli* BL21 Rosetta strain (Novagen), under double ampicillin and kanamycin selection. Cells were grown at 37°C in Luria broth to 0.6 OD_{600} and induced with 0.4 mM isopropyl-1-thioβ-D-galactopyranoside. After 3 h, cells were collected by centrifugation, resuspended in ice-cold lysis buffer (150 mM NaCl, 100 mM Tris-Cl pH 8, 1 mM EDTA, 1 mM β-mercaptoethanol, 5 μg/ml leupeptin, 1 μg/ml pepstatin, 100 μM phenylmethylsulphonyl chloride) with the addition of 10 μg/ml DNase and 0.25 mg/ml lysozyme, sonicated on ice 12 × 20 s, and the lysate was cleared by centrifugation for 30 min at 20,000 × *g*. Proteins were purified by affinity chromatography using StrepTrap HP columns (GE Healthcare), according to the manufacturer's instructions, and eluted in 500 mM NaCl, 30 mM HEPES pH 7.5, 10% glycerol, plus 2.5 mM desthiobiotin. All purification steps were performed at 4°C and monitored using the ÄKTApurifier UPC 10 fast protein liquid chromatography system (GE Healthcare). Samples were analyzed by SDS-PAGE using a NuPAGE (Novex) Bis-Tris 4–12% gel, in MES buffer (Invitrogen).

Electrophysiology. Two-microelectrode voltage-clamp recordings were obtained 3 d after cRNA injection, using a Warner Instruments OC-725C amplifier. Data were digitized and acquired with an ITC-16 interface (Instrutech), filtered at 1 kHz and sampled at 2 kHz, and analyzed using Pulse software (HEKA). Microelectrodes filled with 3 M KCl had resistances of 0.5–2.0 MΩ. Oocytes were bathed in extracellular solution containing the following (in mM): 94 NaCl, 4 KCl, 10 HEPES, and 2 $MgCl_2$, pH 7.5. Three-second voltage steps were applied from a holding

potential of −30 mV to a range of test potentials between −15 and −125 mV in 10 mV decrements, followed by a depolarizing step to 0 mV. Peak tail-current amplitudes were measured at 0 mV after the decay of the capacitive transient, and tail-current current–voltage curves fitted using the Boltzmann equation, $I(V) = A1 + A2/\{1 + \exp[(V - V_{1/2})/s]\}$, in which A1 is the offset caused by holding current, A2 is the maximal tail current amplitude, V is the test pulse voltage, $V_{1/2}$ is the midpoint voltage of activation, and s is the slope factor (in mV). All recordings were obtained at room temperature (22–24°C).

Results

Structural mapping

Previous studies have identified upstream and downstream HCN1/TRIP8b interaction sites largely based on the binding activity of isolated protein fragments (Santoro et al., 2004; Lewis et al., 2009). Here we have addressed the relative contribution of the two putative interaction domains to binding under more physiological conditions by performing a series of coimmunoprecipitation experiments with wild-type and mutant TRIP8b and HCN1 proteins coexpressed in *Xenopus* oocytes from injected cRNAs. In addition to expressing the channel in its native membrane context, this approach allowed us to titrate the amount of HCN1 and TRIP8b protein in each cell to ensure that wild-type and mutant proteins were expressed at similar levels, thus allowing their binding activity to be compared in a semiquantitative manner. Further, we tagged the N terminus of wild-type and mutant constructs with GFP so that, in addition to monitoring expression levels, all experiments could be performed using the same antibody, independent of the position of the deletion being studied.

In a first set of experiments, we compared the binding of different HCN1 deletion mutants with full-length, wild-type TRIP8b (Fig. 1). Consistent with previous results, truncation of the C-terminal SNL tripeptide of HCN1 strongly reduced, but did not abolish, channel binding to TRIP8b. Binding activity was still retained in a larger HCN1 C-terminal truncation in which the CNBD was intact but all downstream 300 aa were deleted ($HCN1_{\Delta CX}$, containing residues 1–610) (Wainger et al., 2001). However, an even larger truncation in which both the CNBD and downstream C-terminal amino acids were deleted ($HCN1_{\Delta CNBD}$, containing residues 1–472) (Wainger et al., 2001) essentially abolished TRIP8b binding. These findings suggest that the CNBD is an essential component of the upstream interaction site, and that the N terminus, trans-

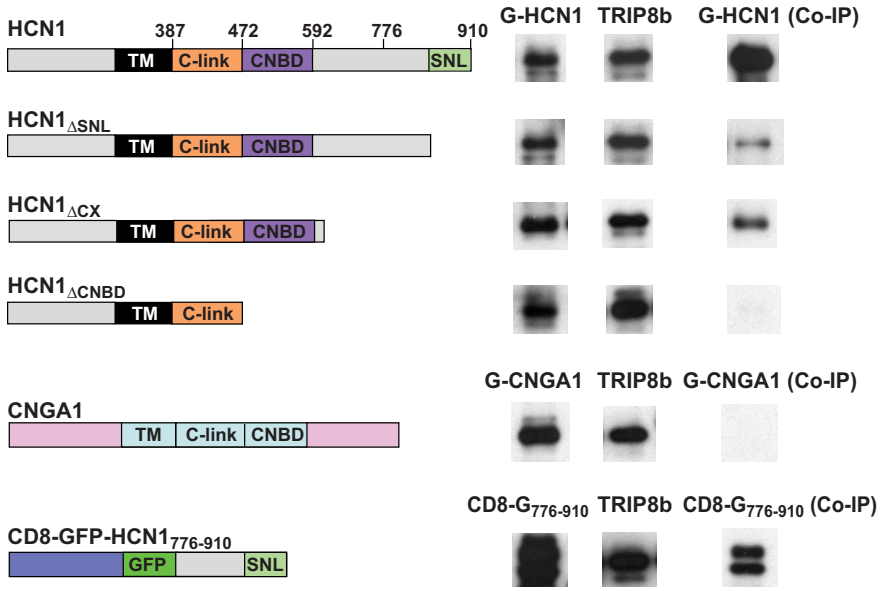

Figure 1. Contribution of HCN1 upstream and downstream binding sites to the interaction with TRIP8b. Western blots show binding of HCN1, its deletion mutants, and other membrane proteins to wild-type TRIP8b(1b-2) assessed by coimmunoprecipitation from *Xenopus* oocyte extracts. Oocytes were coinjected with TRIP8b cRNA (0.2 μg/μl) and cRNAs (at indicated concentration) of various constructs, all tagged with GFP: GFP-HCN1 (1.0 μg/μl), GFP-$HCN1_{\Delta SNL}$ (1.0 μg/μl), GFP-$HCN1_{\Delta CX}$ (0.1 μg/μl), GFP-$HCN1_{\Delta CNBD}$ (0.1 μg/μl), GFP-CNGA1 (0.5 μg/μl), and CD8-GFP-$HCN1_{776-910}$ (0.5 μg/μl). The left column shows Western blot using GFP antibody as measure of input signal. The middle column shows the TRIP8b input signal using an anti-TRIP8b antibody. The right column shows the amount of target protein coimmunoprecipitated with TRIP8b antibody (Western blot using GFP antibody). Note that exposure times are directly comparable down each column, but not along each row. The two bands in the CD8-GFP-$HCN1_{776-910}$ samples likely represent the unglycosylated (lower) and glycosylated (upper) forms of the CD8 receptor moiety (Pascale et al., 1992). Individual bands have been cut from intact gel pictures and aligned to allow direct comparison of intensities for wild-type and mutant constructs with differing molecular weights. Relevant HCN1 channel domains and amino acid positions are indicated in the icons on the left (black, transmembrane domain; orange, C-linker region; purple, cyclic nucleotide binding domain; light green, C-terminal SNL tripeptide).

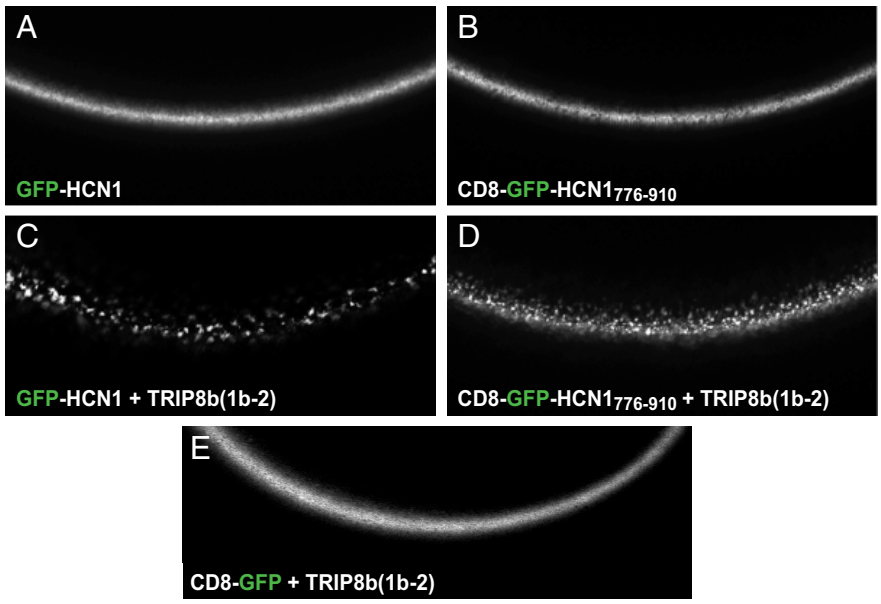

Figure 2. Functional assay of the interaction between TRIP8b(1b-2) and the HCN1 extreme C terminus in live cells. ***A–D***, Live confocal imaging of *Xenopus* oocytes injected with cRNA encoding either a GFP-HCN1 (***A***) or a CD8-GFP-$HCN1_{776-910}$ fusion protein alone (***B***), or in combination with TRIP8b(1b-2) (***C***, ***D***). A redistribution of the GFP fluorescence into distinct puncta is visible in both cases, indicating the ability of TRIP8b(1b-2) to alter the localization of both fusion proteins. ***E***, Coexpression of TRIP8b(1b-2) with a CD8-GFP fusion protein lacking the C-terminal domain of HCN1 does not show such redistribution, indicating that the action of TRIP8b(1b-2) is specifically dependent on its binding to the target $HCN1_{776-910}$ sequence.

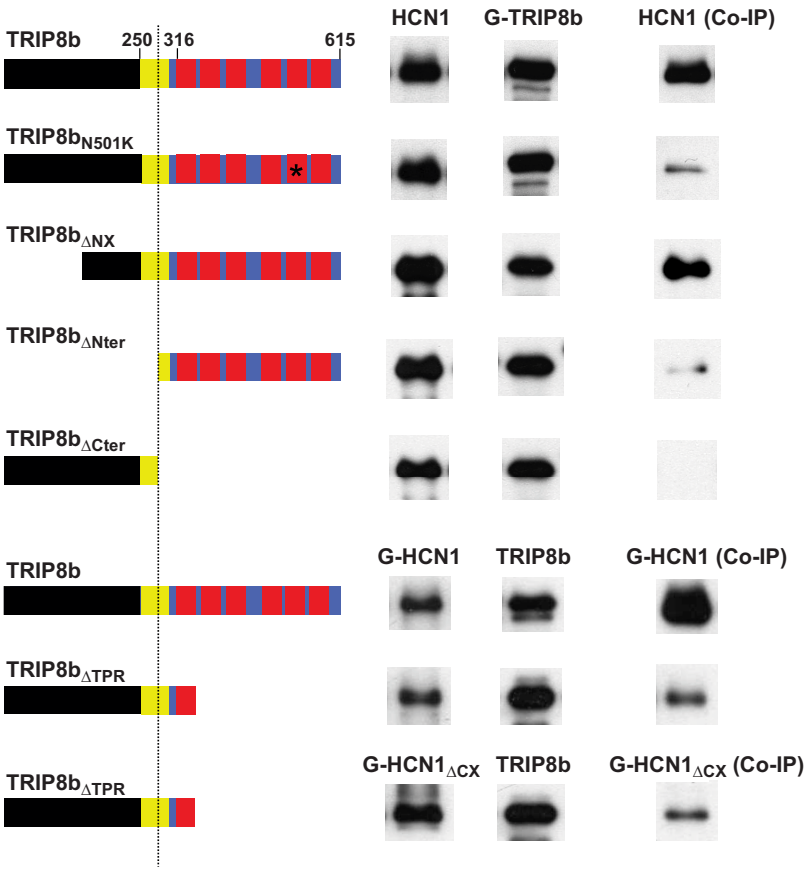

Figure 3. Contribution of TRIP8b upstream and downstream binding sites to the interaction with HCN1. Western blots show binding of a set of TRIP8b(1b-2) mutants to wild-type HCN1 assessed by coimmunoprecipitation from *Xenopus* oocyte extracts, as in Figure 1. Oocytes were coinjected with cRNA encoding HCN1 (0.5 μg/μl), GFP-HCN1 (1.0 μg/μl), or GFP-HCN1$_{\Delta CX}$ (0.1 μg/μl), as indicated, and cRNA for TRIP8b N-terminally tagged with GFP (GFP-TRIP8b; 0.2 μg/μl, first five rows) or untagged TRIP8b (0.2 μg/μl, last three rows). Left column, HCN1 input signal (Western blot using HCN1 antibody for first five rows or GFP antibody for last three rows). Middle column, TRIP8b input signal (Western blot using GFP antibody for first five rows or TRIP8b antibody for last three rows). Right column, amount of HCN1 coimmunoprecipitated with TRIP8b (immunoprecipitation performed using anti-GFP for first five rows or anti-TRIP8b antibody for last three rows). As in Figure 1, exposure times are directly comparable down each column, but not along each row. Individual bands have been cut from intact gel pictures and aligned to allow direct comparison of intensities for wild-type and mutant constructs with differing molecular weights. Relevant protein domains and amino acid positions are indicated in the icons on the left. The black color denotes the N-terminal region that is unique to TRIP8b. The blue color denotes the region of TRIP8b that is homologous to PEX5, with the red squares representing the tetratricopeptide repeats. The yellow square represents a highly conserved core region, homologous to the corresponding region of PEX5, immediately preceding the TPR repeats (see supplemental Fig. 1, available at www.jneurosci.org as supplemental material). The vertical dotted line marks the position of residue 272 in isoform TRIP8b(1b-2), corresponding to residue 259 in isoform TRIP8b(1a-4).

membrane domain, and C-linker region of the channel are not, by themselves, sufficient to support significant HCN1/TRIP8b interaction.

Given the high degree of conservation between the CNBD of HCN channels and that of cyclic nucleotide-gated (CNG) channels, we asked whether these close relatives might also display TRIP8b binding activity. However, when assayed in the same conditions, no binding was observed between the CNGA1 channel and TRIP8b, demonstrating the specificity of the HCN/TRIP8b interaction (Fig. 1). Finally, we asked whether interaction at the downstream SNL/TPR site was sufficient for protein binding in native conditions. To address this question, we attached the extreme C-terminal 134 aa of HCN1 (residues 776–910) to the C terminus of a fusion protein in which the single-pass membrane protein CD8 was fused at its C terminus to GFP (CD8-GFP-HCN1$_{776–910}$). Coimmunoprecipitation experiments showed that TRIP8b was able to bind efficiently to the HCN1 C terminus in the context of this minimal membrane protein (Fig. 1). When TRIP8b(1b-2) is coexpressed with HCN channels, in either *Xenopus* oocytes or HEK293 cells, the channel protein relocalizes to intracellular puncta (Fig. 2*A*,*C*) (Santoro et al., 2004, 2009). Interestingly, coexpression in oocytes of TRIP8b(1b-2) with CD8-GFP-HCN1$_{776–910}$ similarly resulted in the formation of distinct puncta (Fig. 2*B*,*D*). The redistribution of CD8-GFP-HCN1$_{776–910}$ into puncta confirms that TRIP8b(1b-2) is able to interact functionally with the HCN1 extreme C terminus, as the formation of the puncta was clearly dependent on the presence of the HCN1$_{776–910}$ fragment (Fig. 2*E*).

In a complementary set of experiments, we compared the binding of different TRIP8b mutants, in the background of isoform TRIP8b(1b-2), to full-length wild-type HCN1 (Fig. 3). We first sought to selectively disrupt the interaction between HCN1 and TRIP8b(1b-2) by introducing a point mutation in a conserved TPR residue, N501K, which greatly diminishes the binding of the PEX5 TPR domain to the C-terminal SKL (Ser-Lys-Leu) tripeptide in PEX5 target proteins (Gatto et al., 2000). In the crystal structure of the PEX5/target peptide complex, the side-chain amide group of this asparagine forms a direct hydrogen bond with the C-terminal carboxylate of the SKL peptide. As expected, TRIP8b(1b-2)$_{N501K}$ binding to HCN1 was strongly reduced, although not abolished, similar to what we observed upon deletion of the HCN1 SNL tripeptide (compare Figs. 1, 3). This suggests that the interaction between the TRIP8b TPR domain and the HCN channel SNL sequence is similar to the interaction of PEX5 with its SKL-containing targets. Furthermore, this result indicates that an intact TPR domain is not required for an interaction between HCN1 and TRIP8b at the upstream CNBD/core binding site in native conditions.

We next examined whether the N-terminal region of TRIP8b, which is not homologous with PEX5, plays any role in HCN1 binding. We first deleted the initial 203 aa of TRIP8b(1b-2), which eliminates all alternatively spliced exons as well as the consensus motifs required for the putative binding of TRIP8b to intracellular trafficking factors (Santoro et al., 2009; Petrenko et al., 2010). This TRIP8b(1b-2) N-terminal deletion mutant (TRIP8b$_{\Delta NX}$) still strongly binds to HCN1, indicating that the extreme N terminus of TRIP8b is not necessary for channel binding. However, a larger N-terminal deletion mutant lacking the first 271 residues (TRIP8b$_{\Delta Nter}$), a deletion that extends into the initial segment of the homology region between TRIP8b and PEX5 but leaves the TPR domain intact, exhibited a significant

reduction in binding activity (Fig. 3). This finding is consistent with previous observations suggesting that the TRIP8b$_{\Delta Nter}$ fragment binds to the HCN channel extreme C terminus, but not to the C-linker/CNBD region (Lewis et al., 2009). It further suggests that the contribution of the upstream interaction site to TRIP8b/HCN channel binding in native conditions is substantial and comparable to that of the downstream TPR/SNL interaction site. The portion of the homology region removed in TRIP8b$_{\Delta Nter}$ is not sufficient to confer HCN binding activity, as the complementary N-terminal fragment (TRIP8b$_{\Delta Cter}$) failed to coimmunoprecipitate HCN1 (Fig. 3). However, a larger N-terminal fragment that includes the first tetratricopeptide repeat of TRIP8b (TRIP8b$_{\Delta TPR}$) did efficiently bind both wild-type HCN1 as well as the HCN1 extreme C-terminal truncation mutant (HCN1$_{\Delta CX}$), presumably due to its efficient interaction with the CNBD of the channel at the upstream binding site (Fig. 3).

To localize further the sequences required for interaction at the upstream and downstream binding sites, we used the yeast two-hybrid system to assay the binding activities of a series of HCN1 and TRIP8b constructs (Fig. 4). First, we explored the relative importance of the HCN1 120 aa CNBD and 80 aa C-linker region that connects the transmembrane domain of the channel to the CNBD (Fig. 4*A*). Although a construct expressing the CNBD alone produced large amounts of protein in yeast, as assessed by Western blot analysis (data not shown), it failed to bind to TRIP8b. We therefore explored CNBD constructs that included variable lengths of the C-linker region, which consists of six α helixes (A′–F′) (Zagotta et al., 2003). We found that the minimal construct that bound to TRIP8b comprised the CNBD plus the two immediate upstream E′–F′ helixes. Given that a channel truncation mutant that contains an intact C-linker but lacks the CNBD was not able to bind to TRIP8b (Fig. 1, HCN1$_{\Delta CNBD}$), the E′-F′ helix pair probably does not directly interact with TRIP8b but rather enables the proper folding of the CNBD. Indeed, in the HCN2 crystal structure the E′-F′ helix pair directly contacts the CNBD, whereas the A′-D′ helixes do not (Zagotta et al., 2003).

Next, we dissected the regions of TRIP8b involved in the upstream interaction with the HCN1 C-linker/CNBD domain and the downstream interaction with the C-terminal SNL tripeptide (HCN1$_{776-910}$) (Fig. 4*B*). We found that a highly conserved ~80 aa TRIP8b fragment extending from position 236 to position 316 in TRIP8b(1b-2), located just upstream of the first tetratricopeptide repeat (see supplemental Fig. 1, available at www.jneurosci.org as supplemental material), was sufficient to bind to the C-linker/CNBD of HCN1. In contrast, this minimal TRIP8b fragment (TRIP8b$_{mini}$) failed to interact with the HCN1 extreme C terminus, confirming that the 80 aa core region of TRIP8b interacts with HCN1 only at the upstream site. Conversely, a TRIP8b(1b-2) internal deletion mutant lacking 22 aa within the middle of the core region (TRIP8b$_{\Delta int}$, which is missing amino acids 250–271) (supplemental Fig. 1, available at www.jneurosci.org as supplemental material) lost the ability to bind to the upstream C-linker/CNBD site of HCN1 but retained the capacity to interact with the downstream SNL site of the channel. Thus, sequences within TRIP8b$_{mini}$ are both necessary and sufficient to interact with the HCN1 C-linker/CNBD site, as assayed through the yeast two-hybrid screen.

To rule out potential artifacts of the yeast two-hybrid assay, we sought to confirm the interaction between the TRIP8b$_{mini}$ fragment and the HCN C-linker/CNBD region by direct biochemical analysis. To this end, we coexpressed in *E. coli* the HCN2 C-linker/CNBD region (Zagotta et al., 2003) tagged with a double His$_6$-MBP sequence, together with Strep-tagged TRIP8b fragments corresponding to either TRIP8b$_{mini}$ or TRIP8b$_{\Delta Nter}$. As shown in Figure 5, the

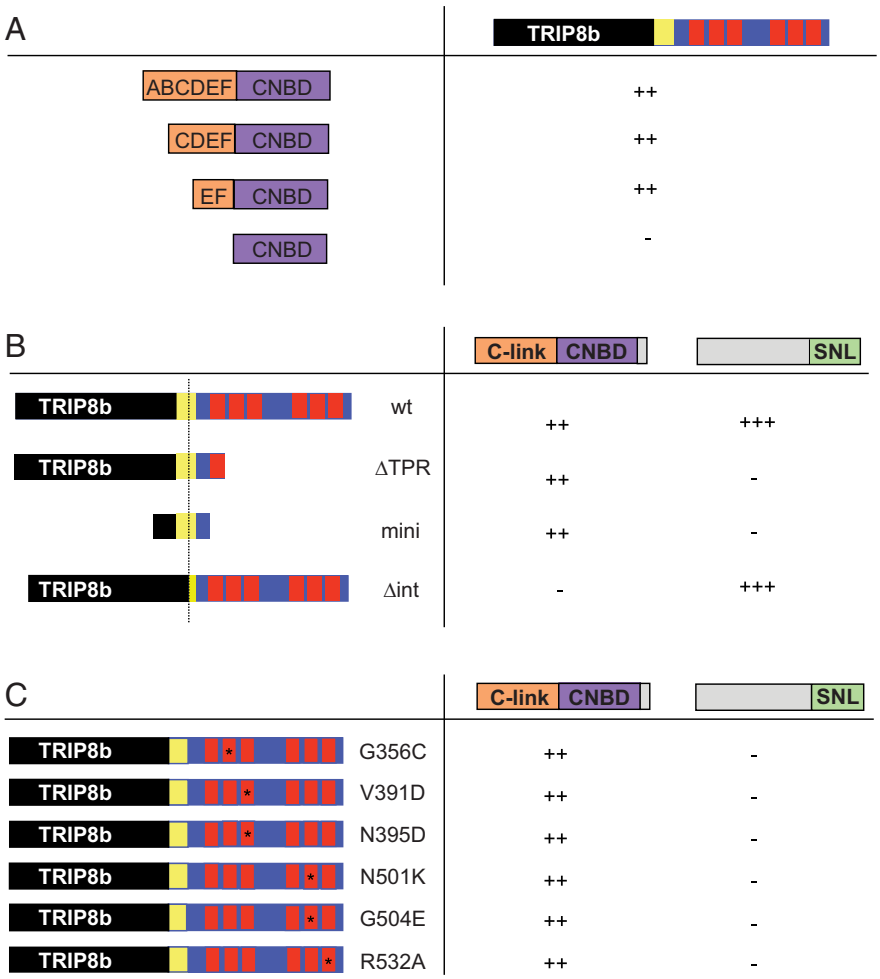

Figure 4. Minimal HCN1 and TRIP8b domains required for binding at the upstream and downstream interaction sites. The binding activity of a set of HCN1 and TRIP8b fragments was assessed using the yeast two-hybrid assay. Activity was detected by transactivation of a GFP reporter gene. ++, Strong fluorescence; +++, very strong fluorescence; −, no detectable fluorescence. ***A***, Binding of TRIP8b to HCN1 C-linker and CNBD region. The TRIP8b construct (see Materials and Methods) failed to interact with the CNBD alone, but showed strong binding to the CNBD plus two (E and F), four (C–F) or all six C-linker α helixes (A–F). ***B***, Binding of different TRIP8b wild-type and mutant constructs to the HCN1 C-linker/CNBD region (HCN1$_{390-611}$) or extreme C-terminal 134 aa region, including the SNL tripeptide (HCN1$_{776-910}$). ***C***, Binding of TRIP8b bearing different TPR domain point mutations to HCN1 C-linker/CNBD or extreme C-terminus regions (as in ***B***). All TPR mutants prevented interaction with the extreme C terminus of HCN1 but did not alter binding to the C-linker/CNBD fragment. TRIP8b numbering is based on isoform TRIP8b(1b-2), as used in Figure 3 (see Materials and Methods).

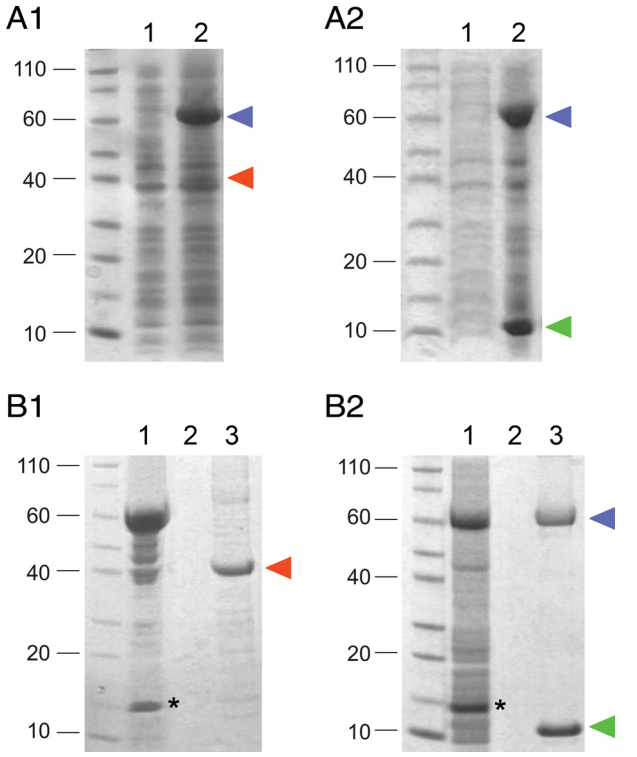

Figure 5. Association of TRIP8b$_{mini}$ and HCN2$_{470-672}$ fragments in bacterial lysates. ***A1***, ***A2***, Co-expression of the MBP-tagged HCN2 C-linker/CNBD region (HCN2$_{470-672}$) with either Strep-tagged TRIP8b$_{\Delta Nter}$ (***A1***) or TRIP8b$_{mini}$ (***A2***) in *E. coli* cells. Coomassie staining following SDS/PAGE shows uninduced bacterial lysate (1) and IPTG-induced bacterial lysate (2). In each case, an amount corresponding to 100 μl of bacterial culture was loaded per lane. Blue arrowhead marks position of MBP-HCN2 band, red arrowhead Strep-TRIP8b$_{\Delta Nter}$ and green arrowhead Strep-TRIP8b$_{mini}$. ***B1***, ***B2***, Bacterial lysates from cells coexpressing MBP-HCN2 and Strep-TRIP8b$_{\Delta Nter}$ (***B1***) or MBP-HCN2 and Strep-TRIP8b$_{mini}$ (***B2***) were loaded onto a Strep-Tactin column for Strep-tag purification. Equivalent samples were analyzed by Coomassie staining following SDS-PAGE separation, at the following stages: flow-through (1), last wash (2), eluate (3). The MBP-HCN2 fragment is found in the eluate along with the purified Strep-TRIP8b$_{mini}$ fragment, indicating the formation of a stable complex between the two proteins, but not with the purified Strep-TRIP8b$_{\Delta Nter}$ fragment which lacks the conserved core region required for upstream site interaction. Labeling as in ***A***. Asterisks mark the band corresponding to the lysozyme protein, which is added during the lysis stage. Molecular weight marker positions are indicated to the left of each panel.

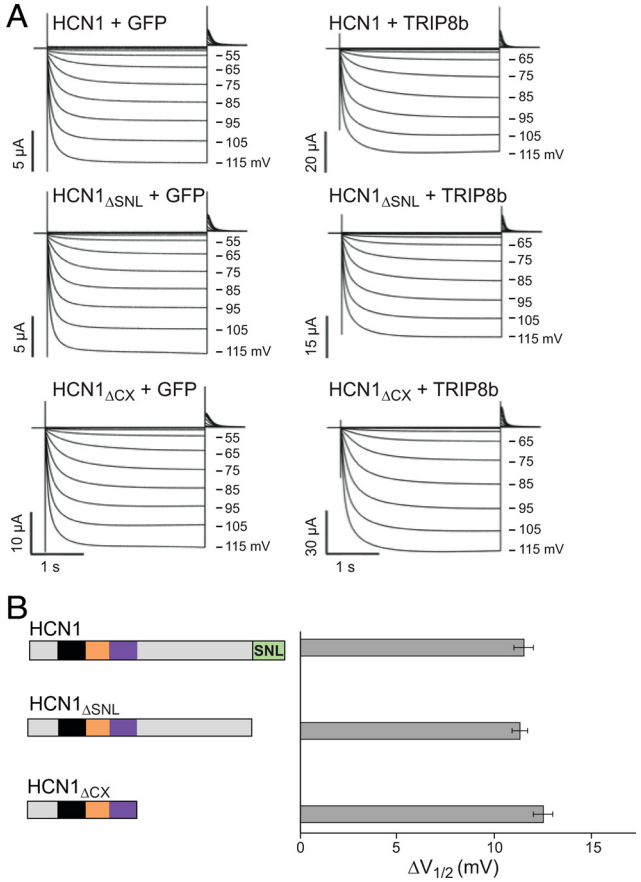

Figure 6. TRIP8b inhibition of HCN1 opening is not affected by deletion of HCN1 extreme C terminus. TRIP8b(1a-4) (0.2 μg/μl) or GFP as a baseline control (0.2 μg/μl) were coinjected in *Xenopus* oocytes with wild-type HCN1 (0.5 μg/μl), HCN1$_{\Delta SNL}$ (0.5 μg/μl), or HCN1$_{\Delta CX}$ (0.1 μg/μl). ***A***, Two-microelectrode voltage-clamp current traces elicited from a holding potential of −30 mV to a range of test potentials between −15 and −115 mV in 10 mV decrements (as indicated), followed by a depolarizing step to 0 mV. Note that TRIP8b coexpression slows the rate of current activation and shifts opening to more negative potentials. ***B***, Population data showing effect of TRIP8b to shift voltage at which channels are half activated ($V_{1/2}$). $\Delta V_{1/2}$ was calculated by subtracting $V_{1/2}$ values obtained when each HCN1 construct was coexpressed with GFP from corresponding $V_{1/2}$ values when same HCN1 constructs were coexpressed with TRIP8b(1a-4). Note that $V_{1/2}$ values used for subtraction were always obtained from the same batch of oocytes to minimize variability. Error bars show SEM. Mean $\Delta V_{1/2}$ values ± SEM (n = number of observations) are as follows: HCN1, 11.5 ± 0.5 mV (n = 26, GFP; n = 26, TRIP8b); HCN1$_{\Delta SNL}$, 11.3 ± 0.4 mV (n = 21, GFP; n = 21, TRIP8b); HCN1$_{\Delta CX}$, 12.5 ± 0.5 mV (n = 28, GFP; n = 28, TRIP8b).

HCN2 C-linker/CNBD fragment was efficiently copurified following passage over a Strep-tactin affinity column of the bacterial lysate containing TRIP8b$_{mini}$ but not TRIP8b$_{\Delta Nter}$. These results confirm that the binding of the HCN C-linker/CNBD region to TRIP8b$_{mini}$ is direct and specific, and that removal of the initial segment of the TRIP8b/PEX5 homology domain (as in TRIP8b$_{\Delta Nter}$) completely abolishes interaction at the upstream site (Lewis et al., 2009).

Finally, we extended our analysis of the interaction between the TRIP8b TPR domain and HCN1 by using the yeast two-hybrid system to screen the ability of a range of TPR point mutations, which have been found to disrupt the interaction between PEX5 and its SKL-containing targets (Gatto et al., 2000; Klein et al., 2001), to alter the binding of TRIP8b to the HCN1 C-linker/CNBD or extreme C terminus (Fig. 4*C*). In addition to N501K, three mutations designed to disrupt specific contact sites between the TPR domain and the SNL tripeptide (V391D, N395D, R532A) abolished binding to HCN1$_{776-910}$. Furthermore, two mutations designed to disrupt the formation of specific α-helixes within the tetratricopeptide repeats (G356C, G504E) also abolished binding to HCN1$_{776-910}$, strongly suggesting that the interaction between the TRIP8b TPR domain and the HCN channel SNL tripeptide is very similar to the PEX5/SKL interaction. Strikingly, none of the point mutations in the TPR domain altered the binding of TRIP8b to the HCN1 C-linker/CNBD region (Fig. 4*C*), providing strong evidence that the upstream and downstream interaction domains are independent sites of binding.

Role of upstream and downstream interaction sites in the regulation of HCN1 gating and trafficking by TRIP8b

How do the upstream and downstream interaction sites contribute to the actions of TRIP8b to regulate HCN1 trafficking and gating? To address this question, we examined the functional effects of the mutations characterized in the above interaction studies. HCN1 hyperpolarization-activated currents were measured by two-microelectrode voltage-clamp from *Xenopus* oocytes coexpressing wild-type or mutant TRIP8b with wild-type or mutant HCN1 cRNAs, under the same conditions used for biochemical analysis. Normally, coexpression of wild-type TRIP8b with wild-type HCN1 in *Xenopus* oocytes shifts the voltage-dependent activa-

tion of HCN1 channels to more negative potentials by 10–15 mV (Santoro et al., 2009). This negative shift is caused by TRIP8b antagonizing the facilitatory effect on HCN1 opening that is exerted by the basal levels of cAMP present in the oocyte (Chen et al., 2001b). We therefore assayed the activity of wild-type and mutant TRIP8b (following coexpression with wild-type or mutant HCN1 channels) by testing their effects on the HCN1 midpoint voltage of activation ($V_{1/2}$), a measure of the voltage dependence of channel gating, and on the HCN1 maximal tail-current amplitude (I_{max}) following strong hyperpolarizations, a measure of channel surface expression (Santoro et al., 2004, 2009).

Regulation of HCN1 channel gating by TRIP8b depends selectively on the upstream CNBD/core interaction site

To assess the gating phenotypes of HCN1 or TRIP8b mutations, we focused on TRIP8b(1a-4) as this is the most abundant isoform expressed in the brain and strongly enhances HCN1 surface expression (Santoro et al., 2009), ensuring the presence of large, measurable hyperpolarization-activated currents. We first analyzed the effects of coexpressing wild-type TRIP8b(1a-4) with two HCN1 C-terminal deletions that retain some TRIP8b binding activity (Fig. 1), $HCN1_{\Delta SNL}$ and $HCN1_{\Delta CX}$. As illustrated in Figure 6, neither of these deletions affected the ability of TRIP8b(1a-4) to shift the channel $V_{1/2}$ to more negative potentials. Thus, TRIP8b binding to HCN1 at the upstream CNBD interaction site must be sufficient to inhibit gating.

Next, we analyzed the effects of a series of mutations in TRIP8b on its ability to alter the gating of wild-type HCN1 (Fig. 7) [see Materials and Methods for exact positions of mutations in TRIP8b(1a-4)]. Deletion of the extreme N-terminal domain of TRIP8b ($TRIP8b_{\Delta NX}$), which contains sequences important for the regulation of channel trafficking but does not contribute to HCN1 binding (Fig. 3), had no effect on the ability of the protein to induce a negative shift in the $V_{1/2}$ of HCN1. In contrast, the larger N-terminal deletion extending into the 80 aa TRIP8b core domain ($TRIP8b_{\Delta Nter}$) completely blocked the capacity of the mutant protein to alter HCN1 gating. This result is consistent with a previous report that the same TRIP8b fragment failed to alter the facilitatory effect of cAMP on gating of HCN2 in inside-out patches (Zolles et al., 2009).

As $TRIP8b_{\Delta Nterm}$ can bind efficiently to HCN1 at the downstream SNL/TPR interaction site but cannot bind to HCN channels at the upstream C-linker/CNBD site (Figs. 3, 5) (Lewis et al., 2009), the upstream interaction must be necessary for the TRIP8b-dependent inhibition of HCN1 channel opening. We directly tested this idea by examining the ability of the 22 aa core deletion mutant, $TRIP8b_{\Delta int}$ [deleting residues 237–258 of TRIP8b(1a-4)], to inhibit HCN1 gating as this mutant protein binds to the downstream but not upstream HCN1 interaction site (Fig. 4*B*). Indeed, the internal deletion abolished the ability of TRIP8b(1a-4) to inhibit HCN1 gating (Fig. 7), confirming the importance of the upstream CNBD/core interaction in regulating channel opening. Conversely, selective disruption of the downstream interaction site, either by introducing the

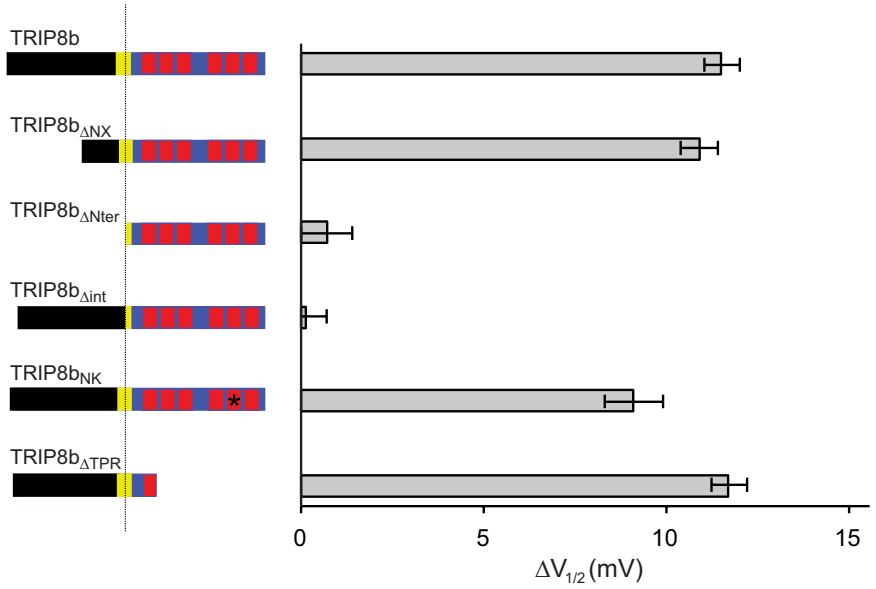

Figure 7. Effect of various TRIP8b(1a-4) mutants on the gating of wild-type HCN1. *Xenopus* oocytes were injected with cRNA encoding wild-type or mutant TRIP8b(1a-4) (0.2 $\mu g/\mu l$) or GFP as a baseline control (0.2 $\mu g/\mu l$), together with cRNA encoding wild-type HCN1 (0.5 $\mu g/\mu l$). Population data show the difference between the $V_{1/2}$ observed when HCN1 was coexpressed with GFP and the $V_{1/2}$ when HCN1 was coexpressed with indicated TRIP8b construct, with data points matched by batch of oocytes as described for Figure 6. Specific residue numbers for mutations introduced in the background of isoform TRIP8b(1a-4) are provided in Materials and Methods. Mean $\Delta V_{1/2}$ values ± SEM (*n*) are as follows: TRIP8b, 11.5 ± 0.5 mV ($n = 26$, GFP; $n = 26$, TRIP8b); $TRIP8b_{\Delta NX}$, 10.9 ± 0.5 mV ($n = 30$, GFP; $n = 30$, $TRIP8b_{\Delta NX}$); $TRIP8b_{\Delta Nter}$, 0.7 ± 0.7 mV ($n = 11$, GFP; $n = 11$, $TRIP8b_{\Delta Nter}$); $TRIP8b_{\Delta int}$, 0.1 ± 0.6 mV ($n = 16$, GFP; $n = 16$, $TRIP8b_{\Delta int}$); $TRIP8b_{NK}$, 9.1 ± 0.8 mV ($n = 12$, GFP; $n = 12$, $TRIP8b_{NK}$); $TRIP8b_{\Delta TPR}$, 11.7 ± 0.5 mV ($n = 18$, GFP; $n = 18$, $TRIP8b_{\Delta TPR}$).

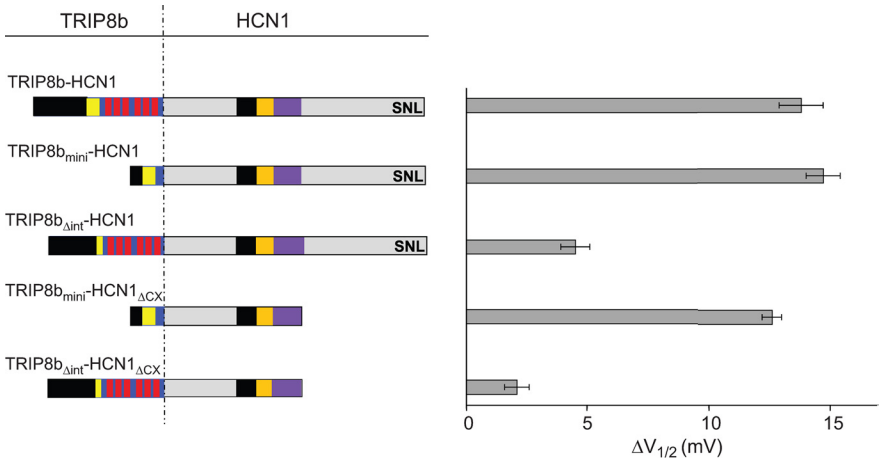

Figure 8. Characterization of a minimal TRIP8b domain that inhibits HCN1 gating using TRIP8b-HCN1 fusion proteins. Shift in $\Delta V_{1/2}$ produced when wild-type or mutant TRIP8b(1a-4) was fused to the N terminus of HCN1. $\Delta V_{1/2}$ values obtained relative to $V_{1/2}$ of GFP-HCN1 fusion construct. All constructs expressed using cRNA injections in *Xenopus* oocytes (HCN1 fusions, 0.5 $\mu g/\mu l$; $HCN1_{\Delta CX}$ fusions, 0.2 $\mu g/\mu l$). Population data show the difference between the $V_{1/2}$ obtained when HCN1 was fused to GFP and the $V_{1/2}$ when HCN1 was fused to indicated TRIP8b construct. All data points were matched by batch of oocytes, as above. Mean $\Delta V_{1/2}$ values ± SEM (*n*) are as follows: TRIP8b-HCN1, 13.8 ± 0.9 mV ($n = 14$, GFP-HCN1; $n = 14$, 1a4-HCN1); $TRIP8b_{mini}$-HCN1, 14.7 ± 0.7 mV ($n = 14$, GFP-HCN1; $n = 14$, mini-HCN1); $TRIP8b_{\Delta int}$-HCN1, 4.5 ± 0.6 mV ($n = 12$, GFP-HCN1; $n = 12$, Δint-HCN1); $TRIP8b_{mini}$-$HCN1_{\Delta CX}$, 12.6 ± 0.4 mV ($n = 14$, GFP-$HCN1_{\Delta CX}$; $n = 14$, mini-$HCN1_{\Delta CX}$); $TRIP8b_{\Delta int}$-$HCN1_{\Delta CX}$, 2.1 ± 0.5 mV ($n = 14$, GFP-$HCN1_{\Delta CX}$; $n = 14$, Δint-$HCN1_{\Delta CX}$).

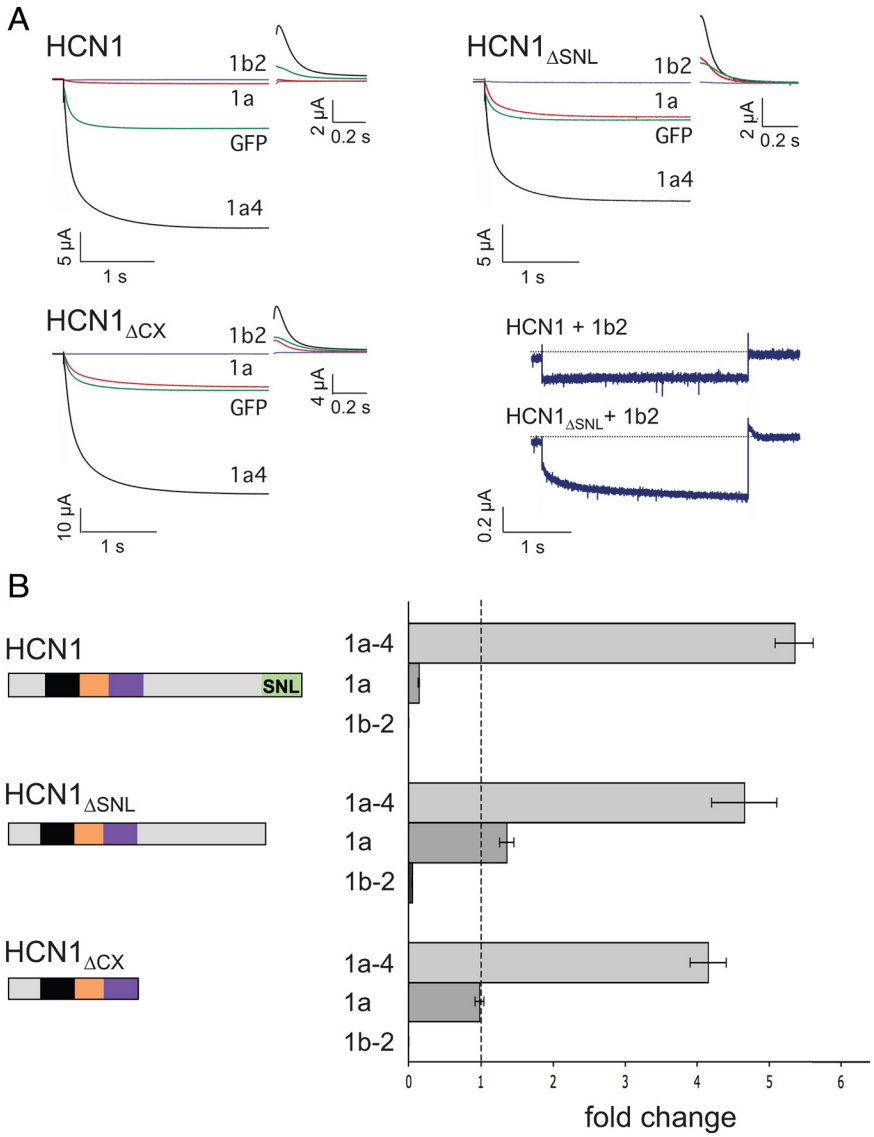

Figure 9. HCN1 C-terminal deletions differentially alter the ability of three TRIP8b isoforms to regulate HCN1 surface expression. *Xenopus* oocytes were injected with cRNA encoding wild-type HCN1 (0.5 μg/μl), $HCN1_{\Delta SNL}$ (0.5 μg/μl) or $HCN1_{\Delta CX}$ (0.1 μg/μl) together with cRNA encoding one of the indicated TRIP8b splice variants (0.2 μg/μl) or GFP (0.2 μg/μl) to provide a baseline control. Recordings were performed 3 d after injection; two-microelectrode voltage-clamp current traces obtained as in Figure 6. ***A***, Sample current traces elicited from a holding potential of −30 mV to a test potential of −105 mV shown for HCN1, $HCN1_{\Delta SNL}$, or $HCN1_{\Delta CX}$ (as indicated) coexpressed with GFP (green traces), TRIP8b(1a-4) (black traces), TRIP8b(1a) (red traces), or TRIP8b(1b-2) (blue traces). Tail current traces are shown at an expanded scale. Lower right, Current traces obtained at the −105 mV test potential upon coexpression of TRIP8b(1b-2) with HCN1 or $HCN1_{\Delta SNL}$. ***B***, Maximal tail current amplitude (I_{max}) for HCN1 constructs coexpressed with a given TRIP8b isoform normalized by maximal tail current amplitude when the same channel construct was coexpressed with GFP. As in Figure 6, data points were matched by batch of oocytes. Error bars show SEM. Mean normalized I_{max} values ± SEM (*n*) are as follows: HCN1 + TRIP8b(1a-4), 5.35 ± 0.27 ($n = 67$, GFP; $n = 70$, 1a-4); HCN1 + TRIP8b(1a), 0.14 ± 0.01 ($n = 56$, GFP; $n = 60$, 1a); HCN1 + TRIP8b(1b-2), undetectable current ($n = 34$, GFP; $n = 27$, 1b-2); $HCN1_{\Delta SNL}$ + TRIP8b(1a-4), 4.65 ± 0.45 ($n = 15$, GFP; $n = 14$, 1a-4); $HCN1_{\Delta SNL}$ + TRIP8b(1a), 1.36 ± 0.1 ($n = 15$, GFP; $n = 15$, 1a); $HCN1_{\Delta SNL}$ + TRIP8b(1b-2), 0.05 ± 0.005 ($n = 15$, GFP; $n = 15$, 1b-2); $HCN1_{\Delta CX}$ + TRIP8b(1a-4), 4.15 ± 0.25 ($n = 17$, GFP; $n = 16$, 1a-4); $HCN1_{\Delta CX}$ + TRIP8b(1a), 0.98 ± 0.06 ($n = 17$, GFP; $n = 17$, 1a); $HCN1_{\Delta CX}$ + TRIP8b(1b-2), undetectable current ($n = 13$, GFP; $n = 13$, 1b-2).

N to K mutation in the TRIP8b(1a-4) TPR domain or by ablating the TPR domain in the $TRIP8b(1a\text{-}4)_{\Delta TPR}$ construct, had essentially no effect on the ability of TRIP8b to inhibit HCN1 activation (Fig. 7).

Next, we asked whether the interaction between HCN1 and the 80 aa core region of TRIP8b is sufficient to regulate channel opening. To obtain equimolar expression of this relatively small protein fragment and HCN1 subunits in *Xenopus* oocytes, we fused $TRIP8b_{mini}$ to the N terminus of HCN1 ($TRIP8b_{mini}$-HCN1). We then compared the voltage dependence of the resulting fusion protein channel with that of two other fusion constructs we previously characterized: GFP-HCN1, which gates identically to wild-type HCN1, and TRIP8b(1a-4)-HCN1, which shows a negative shift in its $V_{1/2}$ identical to the shift seen when TRIP8b(1a-4) is coexpressed with HCN1 as independent proteins (Santoro et al., 2009). As an additional control, we fused the TRIP8b(1a-4) internal deletion mutant lacking the central 22 aa of the core domain to the N terminus of HCN1 ($TRIP8b_{\Delta int}$-HCN1).

When fused to HCN1, the 80 aa $TRIP8b_{mini}$ fragment was as effective as full-length TRIP8b(1a-4) in shifting the midpoint of channel activation to more negative potentials (Fig. 8). Conversely, the $TRIP8b_{\Delta int}$ internal deletion mutant caused only a minor shift in $V_{1/2}$ when fused to the N terminus of HCN1. Moreover, $TRIP8b_{mini}$ also produced a full negative shift in $V_{1/2}$ when fused to the N terminus of the $HCN1_{\Delta CX}$ truncation mutant, consistent with the view that the TRIP8b core does not interact with the downstream HCN1 binding site, and that the extreme C terminus of the channel does not contribute to the effects of TRIP8b on gating. Using cell-free inside-out patches, we further found that a $TRIP8b_{mini}$-HCN2 fusion protein showed a reduced voltage shift in response to cAMP, but no change in voltage-dependent gating in the absence of cAMP relative to a GFP-HCN2 fusion protein or HCN2 alone (supplemental Fig. 2, available at www.jneurosci.org as supplemental material). These effects are similar to those seen when full-length TRIP8b(1a-4) is fused to HCN2 or when TRIP8b(1a-4) and HCN2 are coexpressed as independent proteins (Zolles et al., 2009). These findings thus provide strong evidence that an interaction between the 80 aa $TRIP8b_{mini}$ core with the HCN channel upstream C-linker/CNBD site is necessary and sufficient for the regulatory effect that TRIP8b exerts on cyclic nucleotide gating.

Upstream and downstream interaction sites differentially participate in the regulation of HCN1 channel trafficking by TRIP8b

As the upstream interaction site is both necessary and sufficient for the action of TRIP8b to inhibit HCN1 gating, we asked whether the downstream interaction site might be important in the control of HCN1 trafficking. To explore this possibility, we examined the effects of mutations in HCN1 or in three selected TRIP8b splice variants—TRIP8b (1a-4), TRIP8b(1a), and TRIP8b(1b-2). As mentioned above, these isoforms exert distinct effects on HCN1 trafficking: TRIP8b(1a-4) strongly increases HCN1 surface expression; TRIP8b(1a) produces a ~10-fold decrease of HCN1 surface ex-

pression in *Xenopus* oocytes (Santoro et al., 2009) but enhances HCN1 expression in a mammalian cell line (Lewis et al., 2009); and TRIP8b(1b-2) essentially abolishes surface expression in both oocytes and mammalian cells (>50-fold decrease) by promoting channel endocytosis (Santoro et al., 2004, 2009; Lewis et al., 2009). Although both TRIP8b(1a) and TRIP8b(1b-2) decrease surface expression of HCN1 in *Xenopus* oocytes, the two splice variants depend on distinct trafficking sequence motifs, suggesting the possibility that their effects rely on distinct mechanisms. Thus, the effect of TRIP8b(1a) to downregulate HCN1 requires a dileucine-based trafficking motif in exon 5 whereas channel downregulation with TRIP8b(1b-2) depends on a tyrosine-based trafficking motif in exon 2 (Santoro et al., 2009).

We first examined the ability of the three wild-type TRIP8b isoforms to regulate the trafficking of the $HCN1_{\Delta SNL}$ truncation mutant characterized above that lacks the downstream interaction site. Deletion of the SNL tripeptide caused a selective impairment in the downregulation of HCN1 surface expression by either TRIP8b(1a) or TRIP8b(1b-2). Surprisingly, the truncation had no effect on the upregulation of channel surface expression with TRIP8b(1a-4) (Fig. 9). We also found a quantitative difference in the effect of the SNL truncation on channel downregulation with TRIP8b(1a) versus TRIP8b(1b-2). Whereas the SNL deletion only partially inhibited channel downregulation with TRIP8b(1b-2), it fully blocked the effect of TRIP8b(1a) to decrease HCN1 expression. Thus, the downstream SNL interaction site of HCN1 appears selectively required for the effect of TRIP8b isoforms to downregulate HCN1 surface expression. In contrast, binding at the downstream site has little role in the effect of the TRIP8b(1a-4) isoform to upregulate HCN1 surface expression or to inhibit HCN1 gating (Figs. 6, 8).

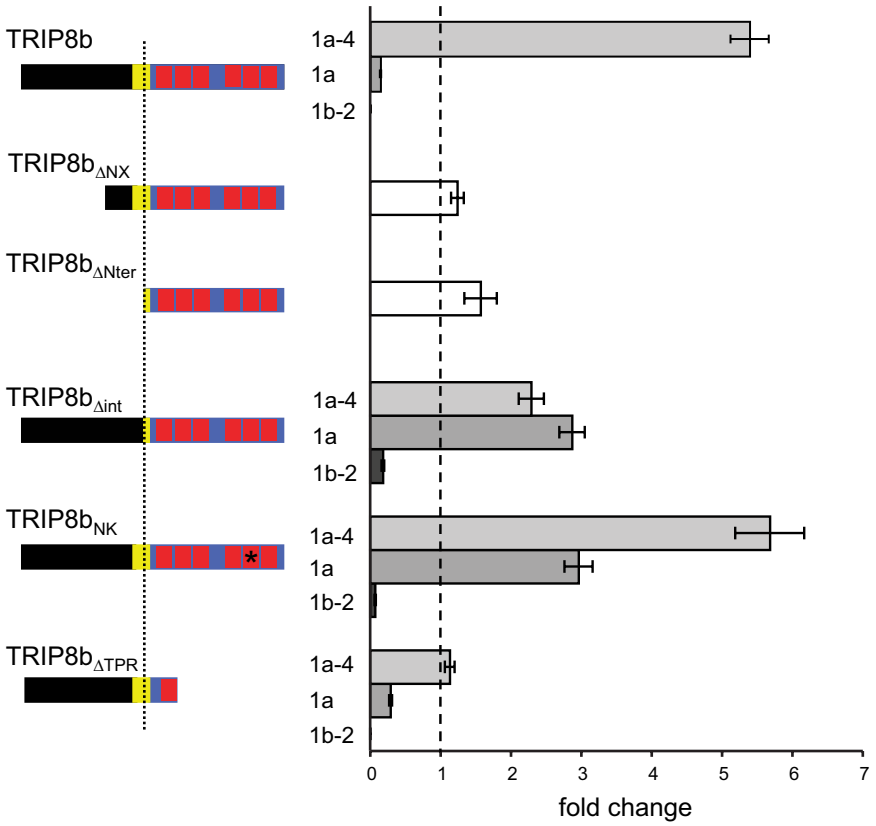

Figure 10. Both downstream and upstream interaction sites in TRIP8b contribute to regulation of HCN1 trafficking by the three TRIP8b isoforms. Population data showing maximal tail current amplitudes (I_{max}) upon coexpression of wild-type HCN1 with the indicated mutant TRIP8b isoform, normalized to the baseline current value determined following coexpression of HCN1 with GFP control, with data points matched by batch of oocytes. As the N-terminal deletion mutants are identical for all three TRIP8b isoforms, only one set of data is shown for each mutant. Specific residue numbers for mutations introduced in the background of each isoform are provided in Materials and Methods. Mean normalized I_{max} values ± SEM (n) are as follows: HCN1 + TRIP8b(1a-4), 5.35 ± 0.27 ($n = 67$, GFP; $n = 70$, 1a-4); HCN1 + TRIP8b(1a), 0.14 ± 0.01 ($n = 56$, GFP; $n = 60$, 1a); HCN1 + TRIP8b(1b-2), undetectable current ($n = 34$, GFP; $n = 27$, 1b-2); HCN1 + TRIP8b$_{\Delta NX}$, 1.24 ± 0.09 ($n = 30$, GFP; $n = 30$, ΔNX); HCN1 + TRIP8b$_{\Delta Nter}$, 1.57 ± 0.23 ($n = 11$, GFP; $n = 11$, ΔNter); HCN1 + TRIP8b(1a-4)$_{\Delta int}$, 2.29 ± 0.18 ($n = 19$, GFP; $n = 23$, 1a-4$_{\Delta int}$); HCN1 + TRIP8b(1a)$_{\Delta int}$, 2.87 ± 0.18 ($n = 19$, GFP; $n = 23$, 1a$_{\Delta int}$); HCN1 + TRIP8b(1b-2)$_{\Delta int}$, 0.18 ± 0.02 ($n = 19$, GFP; $n = 23$, 1b-2$_{\Delta int}$); HCN1 + TRIP8b(1a-4)$_{NK}$, 5.68 ± 0.49 ($n = 12$, GFP; $n = 12$, 1a-4$_{NK}$); HCN1 + TRIP8b(1a)$_{NK}$, 2.96 ± 0.2 ($n = 19$, GFP; $n = 23$, 1a$_{NK}$); HCN1 + TRIP8b(1b-2)$_{NK}$, 0.07 ± 0.01 ($n = 15$, GFP; $n = 15$, 1b-2$_{NK}$); HCN1 + TRIP8b(1a-4)$_{\Delta TPR}$, 1.13 ± 0.07 ($n = 18$, GFP; $n = 18$, 1a-4$_{\Delta TPR}$); HCN1 + TRIP8b(1a)$_{\Delta TPR}$, 0.29 ± 0.02 ($n = 18$, GFP; $n = 18$, 1a$_{\Delta TPR}$); HCN1 + TRIP8b(1b-2)$_{\Delta TPR}$, undetectable current ($n = 15$, GFP; $n = 10$, 1b-2$_{\Delta TPR}$). One-way ANOVA was used to determine that all experimental groups, except for TRIP8b$_{\Delta NX}$, TRIP8b$_{\Delta Nter}$, and TRIP8b(1a-4)$_{\Delta TPR}$, significantly differ from the GFP baseline control group ($p < 0.01$, Tukey's multiple-comparison test).

Truncation of the entire extreme C terminus of HCN1 distal to the CNBD ($HCN1_{\Delta CX}$) also fully blocked the capacity of TRIP8b(1a) to decrease channel surface expression with no effect on the enhancement of channel surface expression with TRIP8b(1a-4), similar to the effects seen above with the SNL deletion (Fig. 9). However, the effects of $HCN1_{\Delta SNL}$ and $HCN1_{\Delta CX}$ diverged when tested against TRIP8b(1b-2); surprisingly, truncation of the entire HCN1 extreme C terminus restored the capacity of TRIP8b(1b-2) to fully abolish channel surface expression. This result reinforces the idea that TRIP8b(1a) and TRIP8b(1b-2) are likely to downregulate surface expression through distinct mechanisms (Santoro et al., 2009). Moreover, it suggests that the extreme C-terminus of HCN1, when not bound to the TPR domain of TRIP8b, may exert an inhibitory effect on the ability of TRIP8b to promote channel endocytosis.

Next, we analyzed the effects of mutations in each of the three TRIP8b isoforms on their ability to regulate the trafficking of wild-type HCN1 channels. Neither of the two N-terminal deletion mutants (TRIP8b$_{\Delta NX}$ and TRIP8b$_{\Delta Nter}$) exerted any regulatory effect on the surface expression of HCN1 (Fig. 10), consistent with the presence of key trafficking consensus sequences in the deleted regions (Santoro et al., 2009; Petrenko et al., 2010).

As our results show that the downstream SNL interaction site in HCN1 is important in the downregulation of channel surface expression by TRIP8b isoforms, we performed complementary experiments to probe the importance of the downstream interaction site in TRIP8b by introducing the equivalent of the N501K point mutation in the TPR domains of the three TRIP8b splice variants. The resulting phenotypes closely mirrored the effects seen with the HCN1 SNL truncation (compare Figs. 9, 10). Thus, the N to K mutation significantly inhibited the ability of both TRIP8b(1a) and TRIP8b(1b-2) to downregulate HCN1 surface expression, but had little effect on the ability of TRIP8b(1a-4) to

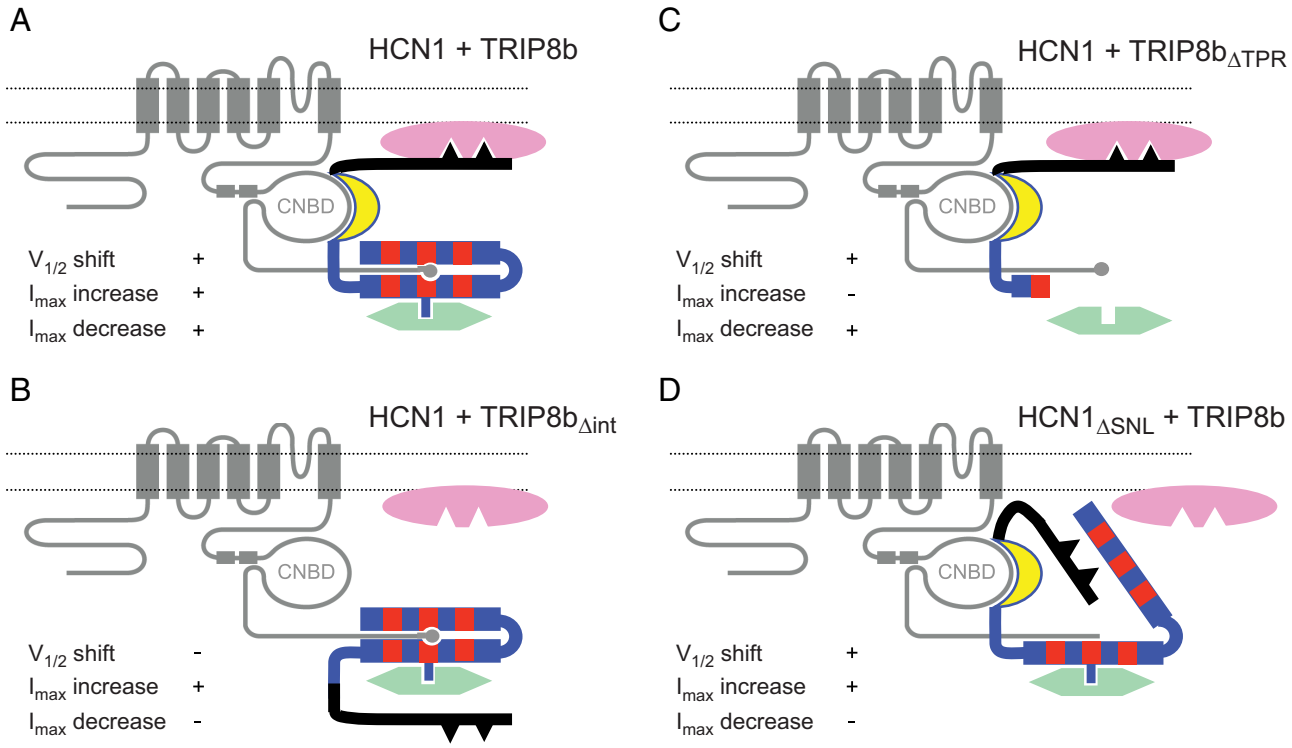

Figure 11. Schematic representation of HCN1/TRIP8b interactions in the presence of intracellular trafficking factors. ***A***, Summary of interactions between HCN1, TRIP8b, and trafficking proteins. The HCN1 channel protein is represented in gray, with C-linker helices E′ and F′ indicated by rectangles, and the C-terminal SNL sequence indicated by a circle. The TRIP8b protein is color coded as in previous figures (black, unique N-terminal region; yellow, highly conserved core domain; blue, region of homology to PEX5 with TPR repeats indicated in red). Dileucine- or tyrosine-based AP binding motifs are present in the N-terminal domain of TRIP8b, indicated by black triangles. AP complex proteins (AP-1 or AP-2) are represented in pink, positioned closely to the plasma membrane (Bonifacino and Traub, 2003), and bind to the N terminus of TRIP8b. An additional trafficking factor (potentially Rab8b), indicated in green, is shown to interact with the C-terminal TPR region of TRIP8b. Note that both of these interacting elements are hypothetical. Gating and trafficking phenotypes are indicated in each panel for their respective mutants. ***B***, Deletion of a critical sequence within the conserved core domain of TRIP8b (Δint) results in a loss of the ability to modulate channel gating and to downregulate channel expression. A hypothetical displacement of the TRIP8b N-terminal domain is shown to impede the binding of AP complex proteins, but not of factors involved in the upregulation of HCN1 surface expression. ***C***, Deletion of the portion of the TPR domain following the first tetratricopeptide repeat (ΔTPR) leads to a loss in the ability of TRIP8b to upregulate surface expression. We speculate that this is because required factors are unable to bind the protein's C-terminal domain. Efficient interaction at the upstream CNBD/core binding site and between the N terminus of TRIP8b and AP complex proteins would still allow for the regulation of channel gating and endocytosis. ***D***, Deletion of the HCN1 channel's C-terminal SNL tripeptide ($HCN1_{\Delta SNL}$) or the N to K point mutation in the TPR domain ($TRIP8b_{NK}$) results in a loss of the ability of TRIP8b to downregulate surface expression. We speculate that failure to interact at the downstream SNL/TPR binding site leads to a displacement of the C-terminal half of the TPR domain, which prevents the access of AP complex proteins to their target sequences in the TRIP8b N terminus. Interaction at the upstream CNBD/core site and with factors bound to the TPR domain that upregulate channel surface expression would not be impaired, resulting in normal gating and I_{max} increase phenotypes.

upregulate channel surface expression. In fact, the TRIP8b(1a) mutant now caused a significant increase in HCN1 surface expression, similar to what we previously observed upon mutation of N-terminal trafficking consensus site in this isoform (Santoro et al., 2009).

Having established that the upstream interaction site is critical for the regulation of HCN1 channel gating by TRIP8b (Figs. 7, 8), we wondered whether it might also play a role in the control of HCN1 trafficking. We tested this hypothesis by coexpressing HCN1 with internal deletion mutants of each of the three TRIP8b isoforms lacking the central 22 aa of the core domain ($TRIP8b_{\Delta int}$). As shown in Figure 10, disruption of the upstream interaction site clearly altered the ability of all three TRIP8b isoforms to modulate channel surface expression. Indeed, the effects of the internal deletion resembled the effects of the HCN1 SNL truncation and TRIP8b N to K mutations described above, with a significant loss of the ability of TRIP8b(1a) and TRIP8b(1b-2) to downregulate HCN1 surface expression. The ability of TRIP8b(1a-4) to enhance channel surface expression was also somewhat reduced, though still present (Fig. 10). Thus, disruption of TRIP8b/HCN1 binding at either the upstream or downstream interaction sites greatly reduces the ability of TRIP8b isoforms to downregulate HCN1 surface expression but has a limited effect on the ability of TRIP8b isoforms to enhance surface expression.

As the TPR point mutations disrupt the ability of TRIP8b(1a) and TRIP8b(1b-2) to downregulate HCN1 surface expression, we expected to observe a similar phenotype when we deleted the TPR domain of these isoforms ($TRIP8b_{\Delta TPR}$). Surprisingly, both of these truncated TRIP8b isoforms efficiently downregulated HCN1 surface expression, very similar to the effects of the wild-type isoforms (Fig. 10). This observation is consistent with the fact that the $TRIP8b_{\Delta TPR}$ truncation mutant can efficiently bind to HCN1 at its C-linker/CNBD interaction site, and exert a normal inhibitory effect on channel gating (Figs. 3, 7). Moreover, it indicates that the presence of an unbound TPR domain can impair the ability of TRIP8b to downregulate HCN1 surface expression (see Discussion) (Fig. 11), similar to the inhibitory effect seen above with the unbound extreme C-terminus of HCN1 (Fig. 9). Of interest, deletion of the TPR domain of TRIP8b(1a-4) completely blocked the capacity of this isoform to enhance HCN1 surface expression [$TRIP8b(1a\text{-}4)_{\Delta TPR}$] in contrast to the lack of effect of the TPR N to

K point mutation on channel upregulation (Fig. 10). This suggests that, in addition to binding to HCN1 at the downstream interaction site, the TPR domain may serve to recruit specific factors important for the enhancement of channel trafficking to the surface membrane.

Discussion

Here we have mapped distinct upstream and downstream sites of interaction between HCN1 and TRIP8b, and defined the differential roles of these sites in the functional effects of three different TRIP8b splice variants on channel trafficking and cyclic nucleotide gating. The interactions between wild-type HCN1 and TRIP8b are summarized in schematic form in Figure 11, which also provides a more speculative model to explain certain phenotypes of HCN1 and TRIP8b mutants.

Structural findings

Using biochemical and molecular biological approaches, we confirmed the presence of upstream and downstream interaction sites on HCN1 and TRIP8b (Lewis et al., 2009), and refined the localization of the interaction surfaces (Fig. 11*A*). We found that the upstream interaction involves binding of the CNBD and last two helixes of the C-linker region of HCN1 (E′–F′/CNBD) to an 80 aa conserved core region of TRIP8b [TRIP8b$_{mini}$, residues 236–316 in TRIP8b(1b-2)], immediately upstream of the TPR domain. At the downstream site, the C-terminal SNL tripeptide of the channel interacts with the TPR domain of TRIP8b, similar to the interaction of the PEX5 TPR domain with its SKL-containing targets (Gatto et al., 2000).

Using coimmunoprecipitation assays from *Xenopus* oocytes, we further determined that, in native conditions, both interaction sites contribute to the stability of the TRIP8b/HCN1 complex. Interestingly, the crystal structure of PEX5 in complex with the sterol carrier protein 2 (SCP2) similarly reveals a second interaction site outside the TPR domain's contact with the C-terminal AKL sequence of SCP2 (Stanley et al., 2006). The binding affinity of full-length SCP2 for PEX5 is 5- to 10-fold higher than the affinity of its C-terminal PTS1 peptide (PGNAKL), suggesting a substantial contribution of the secondary interface to overall binding. An analogous situation is found in the PEX5/alanine:glyoxylate aminotransferase complex, where an ancillary targeting domain is present ~60 aa upstream of the C-terminal PTS1 peptide (Huber et al., 2005) (see also PDB accession 3IMZ for solved crystal structure of the complex). Indeed, it has been suggested that bipartite target binding by a second topologically distinct interaction site could be a general feature of target recognition by the PEX5 receptor (Stanley et al., 2006). Given the close evolutionary relationship between the two proteins, a similar strategy may have been adopted by TRIP8b for the recognition of its HCN channel target.

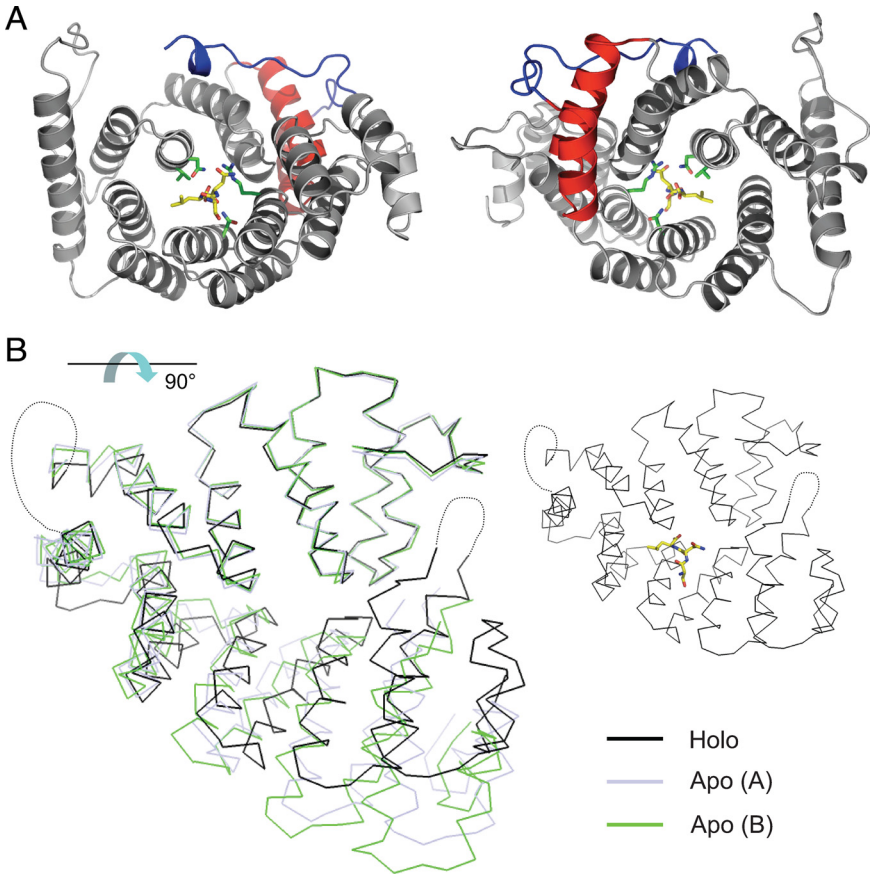

Figure 12. Homology model of the TRIP8b tetratricopeptide repeat domain in bound and unbound form. ***A***, Top view (left) and bottom view (right) of homology model of TRIP8b TPR domain in complex with the HCN channel C-terminal tripeptide (−SNL, yellow stick figure representation) based on PEX5 structure. The side chains of four TRIP8b amino acid residues predicted to make critical contacts with the target peptide are shown in green stick figure representations (V391, N395, N501, R532) (Fig. 4*C*). Note that the N-terminal two helices, corresponding to the first tetratricopeptide repeat (TPR1, in red) do not contact the SNL target peptide. These helices are preserved in TRIP8b$_{\Delta TPR}$ (only the gray portion of the TPR domain is deleted in this construct). The N-terminal end of the structure is colored in blue, and corresponds to the C-terminal tail of the TRIP8b$_{mini}$ construct (no structural information is available N-terminal to this point). ***B***, Homology models of different conformations assumed by the TPR domain of TRIP8b upon binding or unbinding of the SNL target peptide. The holo (bound) structure (black) is superimposed on two alternative conformations assumed by the apo (unbound) structure (light blue and green). Note that the C-terminal TPR segments rotate away from the N-terminal TPR segments, with the two halves of the TPR domain behaving as near-rigid bodies (Stanley et al., 2007). Models were constructed using the program MODELLER based on Protein Data Bank accessions 1FCH, 2C0M, and 2J9Q. Molecular figures were generated using PyMOL (DeLano, 2002). The view of the structure in ***B*** is rotated ~90° with respect to the view shown in ***A***, as indicated by the arrow. For orientation purposes, the holo structure is reproduced on the right, showing the position of the −SNL peptide. Structure in ***A*** corresponds to residues 297–615 of TRIP8b(1b-2), and structures in ***B*** to residues 304–615 (see supplemental Fig. 3, available at www.jneurosci.org as supplemental material). The loop between TPR3 and TPR4 (Gatto et al., 2000), as well as the loop between TPR7 and the C-terminal three-helical bundle (7C loop) (Stanley et al., 2006), have been substituted by a dotted line, as these elements are not resolved in the PEX5 structures.

Functional findings

Our studies indicate that the two TRIP8b/HCN1 interaction sites play distinct functional roles in the effects of the different TRIP8b isoforms to inhibit channel gating compared with the effects of these isoforms to upregulate versus downregulate channel trafficking. Interaction at the upstream site between the channel CNBD and the conserved 80 aa core of TRIP8b is both necessary and sufficient to mediate the inhibitory effects of TRIP8b on HCN1 channel opening. Specifically, the ability of full-length TRIP8b to shift the channel $V_{1/2}$ to more negative potentials is fully reproduced by TRIP8b$_{mini}$ and is unaffected by deletion of the TRIP8b TPR domain or extreme C terminus of the channel.

The structural bases for the effects of the three TRIP8b isoforms on trafficking are complex. Interaction at the upstream site is necessary ($TRIP8b_{\Delta int}$) (Fig. 11*B*) and also sufficient ($TRIP8b_{\Delta TPR}$) (Fig. 11*C*) for TRIP8b(1a) or TRIP8b(1b-2) to downregulate HCN1 surface expression, as long as the trafficking motifs in the N-terminal region of TRIP8b are present. Interaction at the downstream site between the TPR domain of TRIP8b and the SNL tripeptide of HCN1 is not strictly required for the downregulation of HCN1 surface expression with TRIP8b(1a) or TRIP8b(1b-2), given that normal downregulation is observed in the absence of the TRIP8b TPR domain (though see discussion below). In contrast, deletion of the TPR domain fully blocks the ability of TRIP8b(1a-4) to upregulate HCN1 surface expression ($TRIP8b_{\Delta TPR}$) (Fig. 11*C*). This effect cannot be explained by the simple loss of binding at the downstream interaction site because channel upregulation by TRIP8b(1a-4) is unaffected in the $TRIP8b_{NK}$ and $HCN1_{\Delta SNL}$ mutants, which both have disrupted downstream binding (Fig. 11*D*). Rather, we suggest that the TPR region may recruit some cytoplasmic trafficking factor independent of the TPR domain's role in binding to the SNL site of HCN1 (e.g., Rab8b) (Chen et al., 2001a; Fransen et al., 2008). To upregulate HCN1 surface expression, the recruitment of such a factor must act in combination with sequences present in the N-terminal region of TRIP8b, as upregulation is not observed when this region is deleted ($TRIP8b_{\Delta NX}$ and $TRIP8b_{\Delta Nter}$).

One surprising result is that relatively small perturbations in the downstream binding site of either HCN1 (e.g., $HCN1_{\Delta SNL}$) or TRIP8b (e.g., $TRIP8b_{NK}$) are more effective in disrupting the downregulation of channel surface expression than are larger truncations of either the C-terminal TPR domain of TRIP8b ($TRIP8b_{\Delta TPR}$) or the extreme C terminus of HCN1 ($HCN1_{\Delta CX}$). We hypothesize that the unbound TPR domain of TRIP8b may exert an inhibitory effect to prevent the assembly of macromolecular complexes involved in channel trafficking at the N terminus of TRIP8b (Fig. 11*D*). This implies that the normal interaction of HCN1 and TRIP8b at the downstream binding site may induce a conformational change in the TPR domain that allows for assembly of the trafficking complex.

The idea that the downstream interaction of the HCN1 SNL tripeptide with TRIP8b triggers a conformational change in the TPR domain is consistent with x-ray crystal structures of the PEX5 TPR region when bound and unbound to its cargo target peptide. Such studies reveal that cargo binding causes the TPR region to undergo a conformational change from a more open to a more closed structure (Stanley et al., 2006, 2007). Based on the high degree of amino acid similarity between the TPR regions of PEX5 and TRIP8b (see supplemental Fig. 3, available at www.jneurosci.org as supplemental material), we generated a structural homology model for TRIP8b with its SNL peptide bound or absent (Fig. 12). In the model, unbinding of the cargo peptide causes the C-terminal half of the TRIP8b TPR domain to swing away from the N-terminal half, which remains relatively immobile (Fig. 12*B*), similar to the PEX5 results. Thus, the downstream TPR/SNL interaction site might primarily act to stabilize the C-terminal structure of TRIP8b. A displaced TPR domain could interfere with clathrin-mediated endocytosis of the HCN1/TRIP8b complex; deletion of the C-terminal portion of the TPR domain would remove this inhibitory effect, rescuing the ability of TRIP8b to mediate HCN channel endocytosis.

Given that the conserved core region of TRIP8b is contiguous with the TPR domain, a similar scenario may explain how an internal deletion in the upstream site ($TRIP8b_{\Delta int}$) interferes with the downregulation of HCN1 surface expression. Loss of the upstream interaction may lead to the improper positioning of the N-terminal domain of TRIP8b, preventing it from interacting with its normal protein trafficking partners (Fig. 11*B*). Alternatively, the upstream site could help anchor the SNL/TPR complex to the rest of the channel to prevent it from interfering with the assembly of protein complexes required for membrane trafficking.

Physiological consequences of the bipartite TRIP8b-HCN1 interaction

Our findings that mutations that perturb the downstream interaction between TRIP8b and HCN1 differentially alter the functional consequences of residual binding at the upstream site have interesting implications for the dynamic regulation of the TRIP8b/HCN1 interaction *in vivo*. For example, our results with $HCN1_{\Delta SNL}$ suggest that a post-translational modification that weakens the downstream interaction might prevent downregulation of channel expression with TRIP8b(1a) without changing the upregulation of channel expression with TRIP8b(1a-4) (Fig. 9) or the effect of either isoform to regulate cyclic nucleotide-mediated channel gating (Fig. 6).

Given this potential for regulation, it is of interest that two proteomic screens of phosphopeptides from mouse brain synapses identified *in vivo* phosphorylation sites within TRIP8b (Trinidad et al., 2006; Munton et al., 2007). One such phosphorylation site, located in the loop between TPR3 and TPR4, is poised to regulate the downstream interaction between TRIP8b and HCN1. A second phosphorylation site, located in the conserved core region ($TRIP8b_{mini}$), could potentially affect binding at the upstream site and thus disrupt the gating and trafficking effects of all TRIP8b isoforms (Fig. 10). Differential phosphorylation may also explain why TRIP8b(1a) downregulates HCN1 surface expression in *Xenopus* oocytes (Santoro et al., 2009), whereas it upregulates HCN1 in a mammalian cell line (Lewis et al., 2009).

As the proper assembly of trafficking complexes appears to depend on the specific conformation of TRIP8b N-terminal and C-terminal domains, might the large cytoplasmic N-terminal and C-terminal domains of the HCN channels play a similar regulatory function? Indeed, we find that whereas the extreme N and C termini of HCN1 (outside of the SNL sequence) do not directly bind TRIP8b, these domains appear to modulate the functional association between HCN1 and TRIP8b. Thus, the decreased ability of TRIP8b(1b-2) to abolish HCN1 surface expression seen with truncation of the SNL tripeptide of the channel is rescued upon truncation of the entire nonconserved C terminus of HCN1 (Fig. 9). Moreover, deletion of the extreme N terminus of HCN1 strongly enhances the ability of TRIP8b(1a) to downregulate channel surface expression (A. Kushnir and B. Santoro, unpublished observation). Given that the extreme N and C termini of the four HCN channel isoforms diverge in length and sequence, the association of TRIP8b with different channel isoforms could result in different functional phenotypes. Indeed, whereas TRIP8b(1a-4) strongly increases HCN1 surface expression (Lewis et al., 2009; Santoro et al., 2009), this isoform decreases the surface expression of HCN2 (Zolles et al., 2009) (L. Hu, unpublished observation). Such variations could add a further layer of complexity and versatility to the regulatory roles played by the HCN channel TRIP8b auxiliary subunit within the nervous system.

References

Bonifacino JS, Traub LM (2003) Signals for sorting of transmembrane proteins to endosomes and lysosomes. Annu Rev Biochem 72:395–447.

Chen S, Liang MC, Chia JN, Ngsee JK, Ting AE (2001a) Rab8b and its interacting partner TRIP8b are involved in regulated secretion in AtT20 cells. J Biol Chem 276:13209–13216.

Chen S, Wang J, Siegelbaum SA (2001b) Properties of hyperpolarization-activated pacemaker current defined by coassembly of HCN1 and HCN2 subunits and basal modulation by cyclic nucleotide. J Gen Physiol 117:491–504.

DeLano WL (2002) The PyMOL molecular graphics system. Available at http://www.pymol.org. DeLano Scientific.

Fransen M, Amery L, Hartig A, Brees C, Rabijns A, Mannaerts GP, Van Veldhoven PP (2008) Comparison of the PTS1- and Rab8b-binding properties of Pex5p and Pex5Rp/TRIP8b. Biochim Biophys Acta 1783:864–873.

Gatto GJ Jr, Geisbrecht BV, Gould SJ, Berg JM (2000) Peroxisomal targeting signal-1 recognition by the TPR domains of human PEX5. Nat Struct Biol 7:1091–1095.

Huber PA, Birdsey GM, Lumb MJ, Prowse DT, Perkins TJ, Knight DR, Danpure CJ (2005) Peroxisomal import of human alanine:glyoxylate aminotransferase requires ancillary targeting information remote from its C terminus. J Biol Chem 280:27111–27120.

Klein AT, Barnett P, Bottger G, Konings D, Tabak HF, Distel B (2001) Recognition of peroxisomal targeting signal type 1 by the import receptor Pex5p. J Biol Chem 276:15034–15041.

Lewis AS, Schwartz E, Chan CS, Noam Y, Shin M, Wadman WJ, Surmeier DJ, Baram TZ, Macdonald RL, Chetkovich DM (2009) Alternatively spliced isoforms of TRIP8b differentially control h channel trafficking and function. J Neurosci 29:6250–6265.

Ludwig A, Zong X, Stieber J, Hullin R, Hofmann F, Biel M (1999) Two pacemaker channels from human heart with profoundly different activation kinetics. EMBO J 18:2323–2329.

Munton RP, Tweedie-Cullen R, Livingstone-Zatchej M, Weinandy F, Waidelich M, Longo D, Gehrig P, Potthast F, Rutishauser D, Gerrits B, Panse C, Schlapbach R, Mansuy IM (2007) Qualitative and quantitative analyses of protein phosphorylation in naive and stimulated mouse synaptosomal preparations. Mol Cell Proteomics 6:283–293.

Pascale MC, Malagolini N, Serafini-Cessi F, Migliaccio G, Leone A, Bonatti S (1992) Biosynthesis and oligosaccharide structure of human CD8 glycoprotein expressed in a rat epithelial cell line. J Biol Chem 267:9940–9947.

Petrenko AG, Popova NV, Deyev IE (2010) Association of brain-specific adapter protein TRIP8b with clathrin. Soc Neusci Abstr 36:41.10.

Popova NV, Plotnikov AN, Ziganshin RKh, Deyev IE, Petrenko AG (2008) Analysis of proteins interacting with TRIP8b adapter. Biochemistry (Moscow) 73:644–651.

Santoro B, Wainger BJ, Siegelbaum SA (2004) Regulation of HCN channel surface expression by a novel C-terminal protein-protein interaction. J Neurosci 24:10750–10762.

Santoro B, Piskorowski RA, Pian P, Hu L, Liu H, Siegelbaum SA (2009) TRIP8b splice variants form a family of auxiliary subunits that regulate gating and trafficking of HCN channels in the brain. Neuron 62:802–813.

Stanley WA, Filipp FV, Kursula P, Schüller N, Erdmann R, Schliebs W, Sattler M, Wilmanns M (2006) Recognition of a functional peroxisome type 1 target by the dynamic import receptor pex5p. Mol Cell 24:653–663.

Stanley WA, Pursiainen NV, Garman EF, Juffer AH, Wilmanns M, Kursula P (2007) A previously unobserved conformation for the human Pex5p receptor suggests roles for intrinsic flexibility and rigid domain motions in ligand binding. BMC Struct Biol 7:24.

Trinidad JC, Specht CG, Thalhammer A, Schoepfer R, Burlingame AL (2006) Comprehensive identification of phosphorylation sites in postsynaptic density preparations. Mol Cell Proteomics 5:914–922.

Wainger BJ, DeGennaro M, Santoro B, Siegelbaum SA, Tibbs GR (2001) Molecular mechanism of cAMP modulation of HCN pacemaker channels. Nature 411:805–810.

Zagotta WN, Olivier NB, Black KD, Young EC, Olson R, Gouaux E (2003) Structural basis for modulation and agonist specificity of HCN pacemaker channels. Nature 425:200–205.

Zolles G, Wenzel D, Bildl W, Schulte U, Hofmann A, Müller CS, Thumfart JO, Vlachos A, Deller T, Pfeifer A, Fleischmann BK, Roeper J, Fakler B, Klöcker N (2009) Association with the auxiliary subunit PEX5R/Trip8b controls responsiveness of HCN channels to cAMP and adrenergic stimulation. Neuron 62:814–825.

Published November 25, 2013

Binding of the auxiliary subunit TRIP8b to HCN channels shifts the mode of action of cAMP

Lei Hu,[1] Bina Santoro,[1] Andrea Saponaro,[4] Haiying Liu,[3] Anna Moroni,[4,5] and Steven Siegelbaum,[1,2,3]

[1]Department of Neuroscience, [2]Department of Pharmacology, and [3]Howard Hughes Medical Institute, Columbia University, New York, NY 10032

[4]Department of Biosciences and [5]National Research Council (CNR) Biophysics Institute (IBF), University of Milan, 20133 Milan, Italy

Hyperpolarization-activated cyclic nucleotide–regulated cation (HCN) channels generate the hyperpolarization-activated cation current Ih present in many neurons. These channels are directly regulated by the binding of cAMP, which both shifts the voltage dependence of HCN channel opening to more positive potentials and increases maximal Ih at extreme negative voltages where voltage gating is complete. Here we report that the HCN channel brain-specific auxiliary subunit TRIP8b produces opposing actions on these two effects of cAMP. In the first action, TRIP8b inhibits the effect of cAMP to shift voltage gating, decreasing both the sensitivity of the channel to cAMP ($K_{1/2}$) and the efficacy of cAMP (maximal voltage shift); conversely, cAMP binding inhibits these actions of TRIP8b. These mutually antagonistic actions are well described by a cyclic allosteric mechanism in which TRIP8b binding reduces the affinity of the channel for cAMP, with the affinity of the open state for cAMP being reduced to a greater extent than the cAMP affinity of the closed state. In a second apparently independent action, TRIP8b enhances the action of cAMP to increase maximal Ih. This latter effect cannot be explained by the cyclic allosteric model but results from a previously uncharacterized action of TRIP8b to reduce maximal current through the channel in the absence of cAMP. Because the binding of cAMP also antagonizes this second effect of TRIP8b, application of cAMP produces a larger increase in maximal Ih in the presence of TRIP8b than in its absence. These findings may provide a mechanistic explanation for the wide variability in the effects of modulatory transmitters on the voltage gating and maximal amplitude of Ih reported for different neurons in the brain.

INTRODUCTION

The electrical activity of the nervous system depends on the precise tuning of the electrophysiological properties of neurons through various mechanisms. The interaction of auxiliary subunits of voltage-gated channels with their pore-forming α-subunits provides one powerful means of regulating neural function by controlling channel expression and gating (Arikkath and Campbell, 2003; Vacher and Trimmer, 2011). The actions of neurotransmitters to modulate voltage-gated channel function through various second messenger signaling pathways provide another means for the more dynamic control of neural firing properties. We now find that the cAMP-dependent modulation of hyperpolarization-activated cyclic nucleotide–regulated cation (HCN) channels undergoes a surprising form of regulation by the brain-specific auxiliary HCN channel subunit TRIP8b (Santoro et al., 2004).

HCN channels are composed of four pore-forming α-subunits encoded by members of a small gene family (HCN1–4) that is part of the larger voltage-gated channel superfamily (Robinson and Siegelbaum, 2003; Biel et al., 2009). Unlike most voltage-gated channels, the HCN channels are nonselective cation channels that are activated by membrane hyperpolarization, resulting in the hyperpolarization-activated cation current, Ih. The binding of cAMP to the highly conserved HCN cytoplasmic C-terminal cyclic nucleotide–binding domain (CNBD) enhances channel opening by shifting the voltage dependence of HCN channel gating to more positive potentials (DiFrancesco and Tortora, 1991; Wainger et al., 2001). This effect is sometimes associated with an increase in the maximal current through the population of HCN channels (I_{max}) at strongly hyperpolarized voltages (Craven and Zagotta, 2004; Shin et al., 2004). These results are consistent with a model in which channel opening consists of a voltage-dependent activation step coupled to a voltage-independent opening step: cAMP binding enhances channel opening and shifts the voltage dependence of gating to more positive potentials by stabilizing the closed to open transition of the channel (Zhou and Siegelbaum, 2007).

Correspondence to Steven Siegelbaum: sas8@columbia.edu

Abbreviations used in this paper: CNBD, cyclic nucleotide–binding domain; HCN, hyperpolarization-activated cyclic nucleotide–regulated cation; TPR, tetratricopeptide repeat.

The Rockefeller University Press $30.00
J. Gen. Physiol. Vol. 142 No. 6 599–612
www.jgp.org/cgi/doi/10.1085/jgp.201311013

Supplemental Material can be found at:
http://jgp.rupress.org/content/suppl/2013/11/20/jgp.201311013.DC1.html

Published November 25, 2013

One puzzling aspect of the actions of modulatory transmitters on Ih is that the relative extent by which they alter maximal Ih or shift the voltage dependence of channel gating can vary widely among different classes of neurons. In most neurons, neurotransmitters act through second messenger cascades primarily to shift the voltage dependence of Ih gating; in some cells, however, transmitters produce substantial changes in maximal Ih elicited by voltage steps to extreme negative potentials where voltage gating has reached completion, with or without an accompanying shift in voltage gating (Bobker and Williams, 1989; McCormick and Williamson, 1991; Kiehn and Harris-Warrick, 1992; Larkman and Kelly, 1992; Erickson et al., 1993; Gasparini and DiFrancesco, 1999; Bickmeyer et al., 2002; Schweitzer et al., 2003; Frère and Lüthi, 2004; Battefeld et al., 2010; Heys and Hasselmo, 2012).

Here we report that the binding of TRIP8b to the HCN2 α-subunit differentially alters the two major actions of cAMP on HCN channel function. TRIP8b, the major auxiliary subunit of HCN channels in the brain, controls HCN channel membrane trafficking, dendritic localization, and cAMP-dependent voltage gating (Santoro et al., 2004, 2009, 2011; Lewis et al., 2009; Zolles et al., 2009; Han et al., 2011; Piskorowski et al., 2011). TRIP8b undergoes extensive alternative splicing at its N terminus, generating at least 10 splice variants expressed in the brain that produce diverse effects to either enhance or suppress channel plasma membrane expression. However, all isoforms exert an identical action to inhibit the ability of cAMP to shift HCN channel opening to more positive potentials (Santoro et al., 2009; Zolles et al., 2009), an effect which has been mapped to a specific interaction site. TRIP8b interacts with HCN channels at two distinct sites: an upstream site in which a conserved central core region of TRIP8b binds to the HCN CNBD and a downstream site in which the C-terminal tetratricopeptide repeat (TPR) domain of TRIP8b interacts with the Ser-Asn-Leu (SNL) tripeptide at the C terminus of the channel (Lewis et al., 2009; Han et al., 2011; Santoro et al., 2011). It is the interaction of the central core domain of TRIP8b with the CNBD that is responsible for the effect of the auxiliary subunit to antagonize the action of cAMP (Santoro et al., 2011).

The precise mechanism by which TRIP8b binding reduces the response to cAMP is controversial. In a biochemical study, Han et al. (2011) have suggested that TRIP8b directly antagonizes the binding of cAMP by a competitive interaction with the ligand-binding site of the CNBD. In contrast Zolles et al. (2009), using an electrophysiological approach, reported that TRIP8b reduces the maximal voltage shift in response to saturating concentrations of cAMP, ΔV_{max}, an effect incompatible with direct competition. No study to date has addressed whether TRIP8b binding alters the ability of cAMP to enhance maximal HCN channel current.

Here we have investigated the effects of TRIP8b on HCN channel function using both TRIP8b-HCN2 fusion proteins and direct application of the TRIP8b core region to HCN2 channels in inside-out patches. Our results indicate that TRIP8b acts through an allosteric mechanism to decrease the affinity of the channel for cAMP. Moreover, we report a previously uncharacterized action of TRIP8b to reduce maximal current through the channel in the absence of cAMP. By reversing this action of TRIP8b, cAMP produces an increase in maximal current significantly greater than that seen in the absence of the auxiliary subunit. Thus, TRIP8b exerts opposing influences on the two major actions of cAMP on HCN channel function. The auxiliary subunit reduces the effect of cAMP to shift the voltage dependence of channel gating but enhances the action of cAMP to increase maximal current. These effects have important implications for the physiological actions of cAMP to alter neuronal excitability.

MATERIALS AND METHODS

Constructs and expression

All constructs were cloned in pGHE or pGH19 vectors, linearized, and transcribed into cRNA using T7 polymerase (MessageMachine; Ambion) as described previously (Santoro et al., 2004, 2009). cDNA clones encoding HCN2 and TRIP8b both correspond to the *Mus musculus* sequence. GFP, TRIP8b, and $TRIP8b_{core}$ fused to HCN2 channels were created as described previously (Santoro et al., 2011). Site-directed mutagenesis was performed using either the QuikChange Mutagenesis kit (Agilent Technologies) or PCR cloning. *Xenopus laevis* oocytes were injected with 30–50 nl cRNA solutions at a concentration of 0.5–1 μg/μl.

Biochemical binding assays

The yeast two-hybrid assay and coimmunoprecipitation techniques used here were described in detail in a previous publication (Santoro et al., 2011). In brief, yeast two-hybrid assays were performed using the Grow'N'Glow Two-Hybrid kit (Bio 101) and yeast strain EGY48. Bait constructs representing the indicated HCN1 channel domains were cloned into vector pEG202, and prey constructs representing the indicated TRIP8b domains (or mutants thereof) were cloned in vector pJG4-5. Bait and prey plasmids were cotransformed with reporter plasmid pGNG1, and cells were plated onto glucose-containing medium. Transformants were restreaked (in triplicate) on $galactose^{+}/Leu^{-}$ selective medium and screened for positive GFP expression under a UV light after 3–5 d of growth. For coimmunoprecipitation, *Xenopus* oocytes were injected with 50 nl of cRNA solution each, at a concentration of 1.0 μg/μl for HCN1 channel constructs and 0.2 μg/μl for TRIP8b or GFP-TRIP8b fusion constructs. Oocytes were collected 3 d after injection, and protein extracts were prepared in ice-cold lysis buffer, followed by coimmunoprecipitation and Western blot analysis as described previously (Santoro et al., 2011). Primary antibodies used were anti-HCN1 (rat monoclonal 7C3; gift of F. Müller [Institute of Complex Systems, Jülich, Germany] and U.B. Kaupp [Center of Advanced European Studies and Research, Bonn, Germany]), anti-TRIP8b (rabbit polyclonal 794; Santoro et al., 2009), and anti-GFP (290; Abcam). HRP-anti–rat conjugate (Jackson ImmunoResearch Laboratories, Inc.) or HRP-anti–rabbit conjugate (Cell Signaling Technology) was used as

Published November 25, 2013

a secondary antibody. The protein bands were visualized by chemiluminescence using SuperSignal reagent (Thermo Fisher Scientific).

Affinity purification of TRIP8b$_{core}$ peptide

A cDNA fragment encoding residues 223–303 (TRIP8b$_{core}$) of TRIP8b (1a-4) was cloned into vector pET52b (EMD Millipore) downstream of a Strep (II) tag sequence. The plasmid was transformed into *Escherichia coli* BL21 Rosetta strain (EMD Millipore) under ampicillin selection. Cells were grown at 37°C in Luria broth to 0.6 OD_{600} and induced with 0.4 mM isopropyl-1-thio-D-galactopyranoside. After 3 h, cells were collected by centrifugation, resuspended in ice-cold lysis buffer (150 mM NaCl, 100 mM Tris-Cl, pH 8, 1 mM EDTA, 1 mM β-mercaptoethanol, 5 mg/ml leupeptin, 1 mg/ml pepstatin, and 100 µM phenylmethylsulfonyl fluoride) with the addition of 10 µg/ml DNase and 0.25 mg/ml lysozyme, and sonicated on ice 12 times for 20 s, and the lysate was cleared by centrifugation for 30 min at 20,000 *g*. Protein was purified by affinity chromatography using StrepTrap HP columns (GE Healthcare) according to the manufacturer's instructions and eluted in 150 mM KCl, 30 mM HEPES, pH 7.4, and 10% wt/vol glycerol plus 2.5 mM desthiobiotin. All purification steps were performed at 4°C and monitored using the ÄKTApurifier UPC 10 fast protein liquid chromatography system (GE Healthcare). The eluted protein was then loaded into HiLoad 16/60 Superdex 200 prep grade size exclusion column (GE Healthcare), which was equilibrated with 150 mM KCl, 30 mM HEPES, pH 7.4, and 10% wt/vol glycerol, and the protein purity was confirmed by SDS-PAGE.

Inside-out patch recordings and data analysis

Macroscopic currents were recorded from excised patches 2–3 d after cRNA injection using an EPC-9 amplifier and PULSE acquisition software (HEKA). Patch pipettes had resistances around 1 MΩ after fire polishing. External (pipette) solutions contained (mM): 96 KCl, 1 NaCl, 1 $MgCl_2$, 1.8 $CaCl_2$, and 10 HEPES, pH 7.4 (titrated with 50% KOH). Internal (bath) solutions contained (mM): 96 KCl, 1 NaCl, 10 HEPES, and 5 EGTA, pH 7.4. 3-s voltage steps were applied from a holding potential of −30 mV to a range of test potentials between −70 and −140 mV in 10-mV decrements, followed by a depolarizing step to −40 mV to measure tail currents. All recordings were obtained at room temperature (22–24°C). Peak tail current amplitudes were measured at either 0 mV for two electrode voltage clamp or −40 mV for patch clamp recordings after the decay of the capacitive transient, and tail current–voltage curves were fitted using the Boltzmann equation $I(V) = A_1 + A_2/\{1 + \exp[(V - V_{1/2})/s]\}$, in which A_1 is the offset caused by holding current, A_2 is the maximal tail current amplitude, V is the test pulse voltage, $V_{1/2}$ is the midpoint voltage of activation, and *s* is the slope factor (in mV). Because the 3-s long pulse was not sufficient to reach steady-state activation levels at less negative voltage steps, these represent isochronal activation curves rather than true steady-state curves. Nonetheless, they are likely to provide a good approximation of true $V_{1/2}$ values, especially in the absence of cAMP or in the presence of relatively high cAMP levels (Wang et al., 2002) and have been routinely used in the literature because of problems with membrane breakdown with longer hyperpolarizations (Wainger et al., 2001; Zhou and Siegelbaum, 2007; Zolles et al., 2009).

The Hill equation was fitted to the cAMP dose–response data (Figs. 1, 3, and 7): $\Delta V_{1/2} = \Delta V_{max}/\{1 + (K_{1/2}/[cAMP])^h\}$, where $\Delta V_{1/2}$ is the $V_{1/2}$ shift produced by a given cAMP concentration, ΔV_{max} is the maximal $V_{1/2}$ shift produced by saturating cAMP, $K_{1/2}$ is the concentration of cAMP producing half of the maximal shift, and h is the Hill coefficient. In Fig. 5 F, the Hill equation was fitted to the TRIP8b$_{core}$ peptide dose–response data. The data analysis and function fitting were performed in PULSE FIT (HEKA) and Igor Pro (WaveMetrics).

Model fitting

The modulation of HCN2 channel opening by voltage, cAMP, and TRIP8b was described by a 12-state allosteric model (Fig. 6). Definitions of all terms are described in Fig. 6. The open probability of the channel is determined from the equation

$$P_V(A,T) = \frac{\sum O}{\sum O + \sum C_R + \sum C_A} = \left\{ 1 + L \cdot (1 + K_V) \cdot \frac{1 + \frac{A}{K_C^A} + \frac{T}{K_C^T} + \frac{A \cdot T}{K_C^A \cdot K_{TC}^A}}{1 + \frac{A}{K_O^A} + \frac{T}{K_O^T} + \frac{A \cdot T}{K_O^A \cdot K_{TO}^A}} \right\}, \quad (1)$$

where

$$K_V = Q_0 \cdot e^{V/s}. \quad (2)$$

Solving Eqs. 1 and 2 yields the voltage shift produced by a given concentration of cAMP (A) in the presence of a given concentration of TRIP8b (T)

$$\Delta V_{1/2}(A,T) = s \cdot \left\{ \ln\left(1 + \frac{1}{L} \cdot \frac{1 + \frac{A}{K_O^A} + \frac{T}{K_O^T} + \frac{A \cdot T}{K_O^A \cdot K_{TO}^A}}{1 + \frac{A}{K_C^A} + \frac{T}{K_C^T} + \frac{A \cdot T}{K_C^A \cdot K_{TC}^A}} \right) - \ln\left(1 + \frac{1}{L} \cdot \frac{1 + \frac{T}{K_O^T}}{1 + \frac{T}{K_C^T}} \right) \right\}. \quad (3)$$

The relationship in Eq. 3 for $\Delta V_{1/2}$ as a function of cAMP concentration and TRIP8b concentration was used in the model fitting of Fig. 7.

At extreme negative voltages in the absence of cAMP, the maximal open probability is given by

$$P_\infty(0,T) = \frac{1}{1 + L \cdot \frac{1 + \frac{T}{K_C^T}}{1 + \frac{T}{K_O^T}}}.$$

The current reduction caused by the TRIP8b$_{core}$ polypeptide can be described from the following relationship:

$$1 - \frac{P_\infty(0,T)}{P_\infty(0,0)} = 1 - \frac{1 + L}{1 + L \cdot \frac{1 + \frac{T}{K_C^T}}{1 + \frac{T}{K_O^T}}}.$$

Fitting of the current reduction as a function of TRIP8b$_{core}$ peptide concentration (data in Fig. 4 B) by the model yields the following values: K_C^T = 0.34 µM and K_O^T = 1.90 µM. The fitting of the model was conducted in MATLAB with the *fitnlm* function.

Online supplemental material

Detailed derivations and fitting procedures are provided in the supplemental text. Online supplemental material is available at http://www.jgp.org/cgi/content/full/jgp.201311013/DC1.

Published November 25, 2013

RESULTS

TRIP8b exerts opposing actions on the ability of cAMP to shift voltage-dependent gating and increase maximal current through HCN2 channels

In this study, we examined the biophysical mechanisms that underlie the action of TRIP8b to alter the response of HCN channels to cAMP by addressing two questions: (1) How does the binding of TRIP8b to HCN channels inhibit the effect of cAMP to shift HCN channel voltage gating to more positive voltages, and (2) does TRIP8b alter the action of cAMP to enhance the maximal tail current carried by HCN channels after steps to extreme negative voltages? We focused on the interaction of TRIP8b with HCN2 because this α-subunit forms channels that respond to cAMP with a large depolarizing voltage shift and noticeable enhancement in maximal current.

In a previous study, our laboratory found that the action of TRIP8b to antagonize the cAMP-dependent shift in HCN1 voltage gating observed in intact cells was greatly diminished upon patch excision when TRIP8b and HCN1 were expressed independently, perhaps because of instability of the complex and/or loss of some intracellular modulatory factor (Santoro et al., 2009). In contrast, we found that the regulatory effect of TRIP8b was robustly maintained in cell-free patches with a TRIP8b-HCN1 fusion protein (Santoro et al., 2009). In our present study of the action of TRIP8b on HCN2, we have therefore covalently linked the N terminus of HCN2 to either the C terminus of TRIP8b or to GFP (as a control).

As shown in Fig. 1, application of cAMP to GFP-HCN2 channels in inside-out patches produces a large, dose-dependent depolarizing shift in the voltage dependence of channel activation and increases the rate of channel opening, actions which are identical to those seen in WT HCN2 channels (Pian et al., 2006). In cell-free patches in the absence of cAMP, TRIP8b-HCN2 channels exhibit a similar voltage dependence and rate of activation compared with GFP-HCN2 channels (Fig. 1, A–C). However, TRIP8b-HCN2 channels show a marked reduction in sensitivity to cAMP compared with GFP-HCN2 channels (Fig. 1, A–C). An examination of the cAMP dose–response curves for GFP-HCN2 and TRIP8b-HCN2 demonstrates that the presence of TRIP8b causes a 40-fold increase in the concentration of cAMP required to produce a half-maximal shift in the voltage

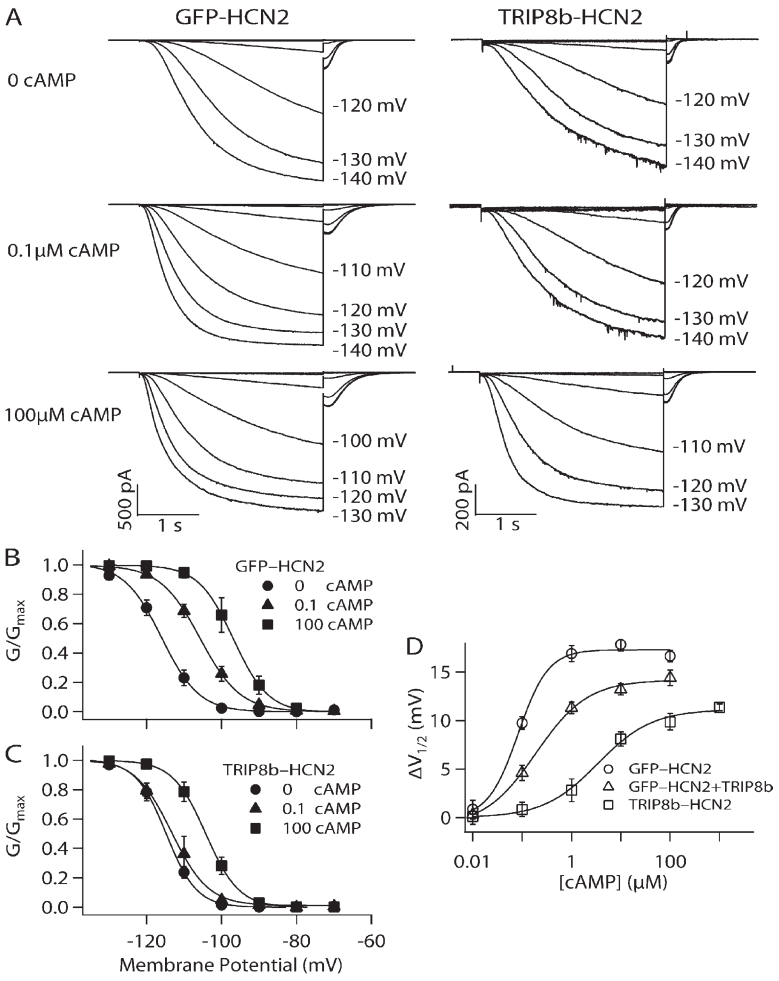

Figure 1. Effect of fusion of TRIP8b to HCN2 on relationship between [cAMP] and voltage dependence of channel gating. (A) Currents elicited by hyperpolarizing voltage steps in inside-out patches from oocytes expressing TRIP8b-HCN2 fusion channels or GFP-HCN2 channels in 0, 0.1, or 100 μM [cAMP]. The membrane was held at −40 mV for 0.5 s and then stepped for 3 s to test potentials from −70 to −140 mV in 10-mV decrements. (B and C) Normalized tail current G-V relationship for GFP-HCN2 (B) or TRIP8b-HCN2 (C) channels in the presence of 0, 0.1, or 100 μM [cAMP]. Fits of Boltzmann relation yield the following values for $V_{1/2}$ and slope with different [cAMP]. GFP-HCN2 0 cAMP: $V_{1/2}$ = −116.0 mV, s = 4.98; 0.1 cAMP: $V_{1/2}$ = −105.7 mV, s = 5.33; and 100 cAMP: $V_{1/2}$ = −96.9 mV, s = 4.65. TRIP8b-HCN2 0 cAMP: $V_{1/2}$ = −114.8mV, s = 4.05; 0.1 cAMP: $V_{1/2}$ = −113.3 mV, s = 4.91; and 100 cAMP: $V_{1/2}$ = −104.2 mV, s = 4.42. (D) $\Delta V_{1/2}$ as a function of [cAMP] for GFP-HCN2, GFP-HCN2 + TRIP8b expressed as independent proteins, and TRIP8b-HCN2 fusion channels in inside-out patches. Solid lines show fits of Hill equation. Fits of the Hill equation yield GFP-HCN2: ΔV_{max} = 17.3 mV, $K_{1/2}$ = 0.08 μM, h = 1.43; GFP-HCN2 + TRIP8b: ΔV_{max} = 14.2 mV, $K_{1/2}$ = 0.19 μM, h = 0.83; and TRIP8b-HCN2: ΔV_{max} = 11.1 mV, $K_{1/2}$ = 3.42 μM, h = 0.79. Error bars indicate SEM.

Published November 25, 2013

dependence of channel activation ($K_{1/2}$; Fig. 1 D). Moreover, there is a 40% decrease in the maximal shift in the $V_{1/2}$ in response to saturating concentrations of cAMP (ΔV_{max}), a measure of ligand efficacy (Fig. 1 D).

We found a qualitatively similar inhibitory action on the modulatory effects of cAMP when TRIP8b is coexpressed with GFP-HCN2 as independent proteins (Fig. 1 D). However, similar to our previous results with HCN1 (Santoro et al., 2009), the quantitative extent of inhibition produced by the independent TRIP8b protein is much less than with the TRIP8b-HCN2 fusion. Thus, expression of TRIP8b with GFP-HCN2 causes only a 2.5-fold increase in the $K_{1/2}$ for cAMP and a 20% decrease in ΔV_{max}. Our results differ slightly from those of Zolles et al. (2009), who found that coexpression of TRIP8b with HCN2 caused a somewhat larger decrease in ΔV_{max} (~40%) and produced a slight decrease in the $K_{1/2}$ (~40%) for cAMP. These discrepancies may reflect small differences in recording conditions or relative levels of protein expression. We also found that the Hill coefficient is reduced by ~44% by TRIP8b coexpression or fusion to HCN2 (from 1.43 to ~0.8), suggesting that TRIP8b might inhibit the cooperativity of cAMP binding. Neither TRIP8b coexpression or fusion to HCN2 alters the voltage dependence of HCN2 channel gating in the absence of cAMP, indicating that this regulatory subunit has minimal effect on the basal channel voltage gating ($V_{1/2}$ values: GFP-HCN2, −116.2 ± 0.86 mV; GFP-HCN2 + TRIP8b, −116.0 ± 0.98 mV; and TRIP8b-HCN2, −114.7 ± 0.74 mV).

Next we asked whether TRIP8b alters the action of cAMP to enhance maximal HCN2 current after voltage steps to extreme hyperpolarized potentials. Unexpectedly, we found that fusion of TRIP8b to HCN2 increases the extent to which cAMP enhances I_{max} (Fig. 2). Thus, whereas cAMP increases maximal current in GFP-HCN2 channels by only 37 ± 9%, the nucleotide enhances maximal current in TRIP8b-HCN2 channels by 83 ± 9%, more than a twofold increase ($P < 0.05$; $n = 10$). Thus, TRIP8b exerts opposing actions on the two modulatory effects of cAMP: TRIP8b inhibits the ability of cAMP to shift voltage gating to more positive potentials, whereas it increases the action of cAMP to enhance maximal current.

An 81–amino acid domain in the conserved core of TRIP8b is both necessary and sufficient to produce the opposing actions of TRIP8b on cAMP-dependent modulation of HCN2

Are the two distinct actions of TRIP8b mediated by the same region of the molecule? We previously found that an 81–amino acid core region of TRIP8b, $TRIP8b_{core}$ corresponding to residues 223–303 in TRIP8b(1a-4), is sufficient to fully reproduce the effect of full-length TRIP8b to antagonize the actions of cAMP on HCN1 channel voltage gating, based on the action of the $TRIP8b_{core}$-HCN1 fusion protein in intact oocytes (Santoro et al., 2011). However, these experiments did not quantify the effect of the TRIP8b core region on the relation between cAMP concentration and the voltage shift in HCN channel gating. Moreover, these experiments did not examine whether the core region could mimic the effect of full-length TRIP8b to enhance the ability of cAMP to increase HCN channel maximal current.

We therefore next examined the effect of cAMP on voltage gating and maximal current of $TRIP8b_{core}$-HCN2 fusion protein channels. We found that the relatively small core region is necessary and sufficient to both inhibit the ability of cAMP to alter voltage gating

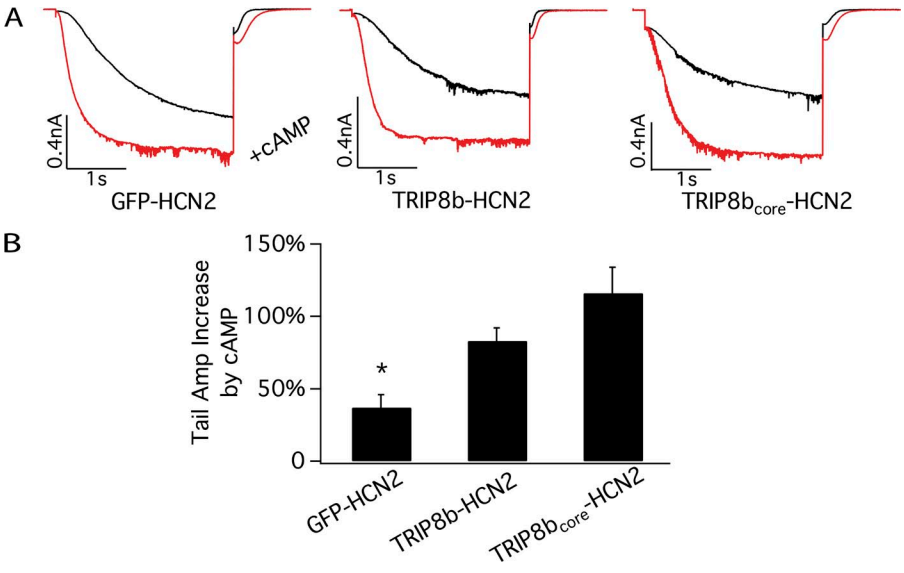

Figure 2. cAMP causes a larger increase in maximal current with TRIP8b-HCN2 and $TRIP8b_{core}$-HCN2 channels than with GFP-HCN2 channels. The membrane was held at −40 mV and then hyperpolarized to −140 mV with a 3-s test pulse, followed by a depolarizing pulse to −40 mV to measure the tail current. (A) Representative currents for GFP-HCN2, TRIP8b-HCN2, and $TRIP8b_{core}$-HCN2 channels before (black traces) and after (red traces) application of saturating concentrations of cAMP (100 µM for GFP-HCN2 and 1 mM for the other two channels) to inside-out patches. (B) Percent increase in maximal tail current amplitude in response to cAMP for GFP-HCN2, TRIP8b-HCN2, and $TRIP8b_{core}$-HCN2; error bars indicate SEM. Mean percent increases in maximal current ± SEM are as follows: GFP-HCN2: 37 ± 9% ($n = 9$); TRIP8b-HCN2: 83 ± 9% ($n = 10$); and $TRIP8b_{core}$-HCN2: 116 ± 18% ($n = 9$). Current amplitude increase with GFP-HCN2 by cAMP is significantly less than that seen with TRIP8b-HCN2 and $TRIP8b_{core}$-HCN2 (*, $P < 0.05$, ANOVA). There is no significant difference in current increase between the latter two constructs ($P > 0.05$, *t* test).

Published November 25, 2013

and facilitate the action of cAMP to increase maximal current (Figs. 2 and 3 A). Surprisingly, the magnitude of some of the effects of TRIP8b$_{core}$ on the cAMP-dependent modulation of HCN2 are even greater than those seen with full-length TRIP8b-HCN2. Thus, TRIP8b$_{core}$-HCN2 fusion protein channels exhibit a >2,000-fold increase in the $K_{1/2}$ for cAMP relative to HCN2 alone, a 50-fold larger effect than seen with the full-length TRIP8b-HCN2 fusion (Fig. 3 A). The TRIP8b$_{core}$-HCN2 channels also display a decrease in ΔV_{max} with saturating cAMP (~27% decrease). cAMP increased the maximal current carried by TRIP8b$_{core}$-HCN2 channels by 116 ± 18%, slightly greater than the 83% increase in maximal current seen with cAMP with full-length TRIP8b fusion protein channels ($P > 0.05$; $n = 9$; Fig. 2). We next confirmed previous results obtained using HCN1 channels in intact oocytes, that the TRIP8b core is necessary for the action of full-length TRIP8b to inhibit the effects of cAMP on voltage gating (Santoro et al., 2011). Thus, a fusion protein consisting of HCN2 plus full-length TRIP8b lacking only 22 amino acids in the core domain (TRIP8b$_{\Delta Int}$-HCN2) generates channels whose response to cAMP is identical to that of HCN2 expressed alone without TRIP8b (Fig. 3 A). These results further suggest that the alterations in the regulatory

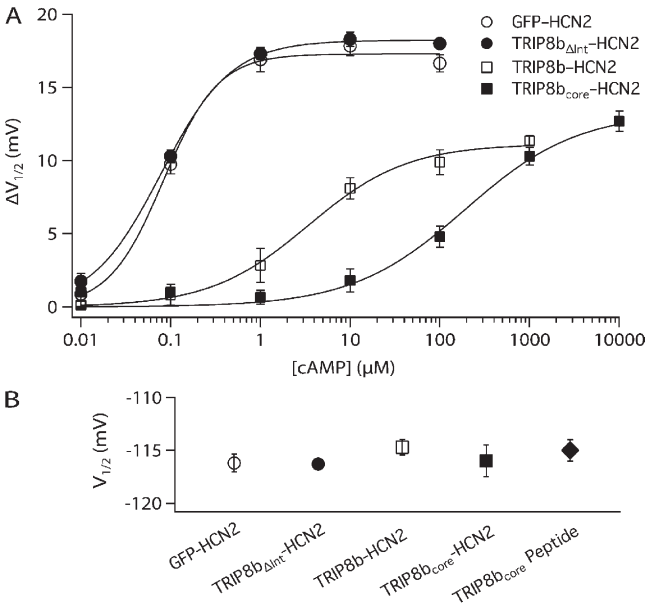

Figure 3. TRIP8b core domain is necessary to antagonize action of cAMP on HCN2. (A) $\Delta V_{1/2}$ as a function of [cAMP] for TRIP8b$_{\Delta Int}$-HCN2 and TRIP8b$_{core}$-HCN2 channels in inside-out patches, compared with GFP-HCN2 and TRIP8b-HCN2 channels. Solid lines show fits of the Hill equation. Fits of the Hill equation yield TRIP8b$_{\Delta Int}$-HCN2: ΔV_{max} = 18.2 mV, $K_{1/2}$ = 0.08 μM, h = 1.11; and TRIP8b$_{core}$-HCN2: ΔV_{max} = 13.3 mV, $K_{1/2}$ = 190 μM, h = 0.69. Note that TRIP8b$_{\Delta Int}$, with internal deletion of 22 residues of the core domain, fails to alter cAMP dose–response relation. (B) $V_{1/2}$ values of various indicated constructs in the absence of cAMP show no significant differences ($P > 0.05$, ANOVA). Error bars indicate SEM.

actions of cAMP with TRIP8b fusion proteins are not the result of some nonspecific effects of the fusion per se, as the effects are completely dependent on the short internal stretch of 22 amino acids. Consistent with results using full-length TRIP8b, neither the TRIP8b$_{\Delta Int}$ nor the TRIP8b$_{core}$ fusion proteins show altered voltage-dependent gating in the absence of cAMP (Fig. 3 B), further indicating that basal voltage gating is not affected by this regulatory subunit.

Effects of acute application of a TRIP8b$_{core}$ peptide to HCN2 channels

How does TRIP8b exert its opposing effects on the cAMP-dependent modulation of HCN2, inhibiting the action of cAMP to shift voltage gating while enhancing the action of cAMP to increase maximal current? Previous studies have suggested that channel opening involves a voltage-dependent activation step followed by a voltage-independent opening reaction. cAMP binding is thought to stabilize the open state of the channel, thereby enhancing maximal open probability and, thereby, maximal current (Shin et al., 2004; Chen et al., 2005; Zhou and Siegelbaum, 2007). The relatively large maximal open probability of HCN2 in the absence of cAMP (>0.5) normally limits the extent to which cAMP can enhance maximal current (Zhou and Siegelbaum, 2007). We therefore hypothesized that TRIP8b might enhance the ability of cAMP to increase maximal current by depressing maximal channel open probability in the absence of cAMP, thereby providing a larger dynamic range by which cAMP can increase channel opening.

To directly address this possibility, we examined the effect of acute application of a soluble, purified TRIP8b core peptide (TRIP8b residues 223–303) to HCN2 channels in cell-free inside-out patches (using oocytes where TRIP8b was not coexpressed with HCN2). Consistent with the above hypothesis, application of 4 μM TRIP8b core peptide to HCN2 channels in the absence of cAMP causes a marked, ~40%, decrease in current amplitude in response to a hyperpolarizing voltage step to −140 mV, a potential at which voltage-dependent activation is complete (Fig. 4 A). In contrast, the core peptide produces no detectable change in the voltage dependence of channel gating (Fig. 3 B). Over a range of concentrations, the core peptide causes a dose-dependent reduction in HCN2 channel maximal current (in the absence of cAMP), resulting in a 60% decrease in current at 40 μM, the maximum concentration of core peptide that was soluble (Fig. 4 B).

To determine whether the effects of TRIP8b$_{core}$ on maximal current are specific, we examined the action of a mutant core peptide in which a conserved pentapeptide sequence (EEEFE) is replaced with a charge-reversed sequence (RRRAR; Fig. 4, C and D). In a yeast two-hybrid assay, we find that this mutation abolishes the ability of TRIP8b to bind to the HCN1 CNBD

Published November 25, 2013

(Fig. 4 C). Application of this mutant peptide to HCN2 channels has no effect on maximal current, arguing for a specific action dependent on the conserved core sequence (Fig. 4 D).

Is the effect of the core peptide to reduce maximal current related in any way to the action of cAMP to enhance maximal current? The two processes do indeed interact as the application of 100 µM cAMP fully reverses the inhibitory action of the core peptide on maximal current. Thus, cAMP application is able to increase maximal current to a level similar to that seen when cAMP is applied in the absence of core peptide (Fig. 4 A). As a result, cAMP application in the presence of core peptide produces a larger percentage increase in maximal current amplitude compared with that seen when cAMP is applied in the absence of core peptide. This action therefore accounts for the increased effect of cAMP to enhance maximal current observed above with TRIP8b-HCN2 or TRIP8b$_{core}$-HCN2 channels (Fig. 2).

We next asked whether acute application of the core peptide also inhibits the ability of cAMP to shift the voltage dependence of HCN2 opening to more positive potentials, similar to what we observe when the core peptide is fused to HCN2. Indeed, application of the core peptide rapidly antagonizes the ability of cAMP to shift HCN2 gating to more positive potentials (Fig. 5). At a concentration of 4 µM, TRIP8b$_{core}$ almost fully abolishes the voltage shift in response to 0.1 µM cAMP and significantly reduces the voltage shift with 10 µM cAMP (Fig. 5, A–C). Importantly, the effect of cAMP recovers rapidly after wash-out of the peptide (Fig. 5 A), indicating that the binding between TRIP8b and HCN2 is reversible. This rapid reversibility may explain the finding that the modulatory action of TRIP8b on HCN channel function is diminished after patch excision when TRIP8b and HCN subunits are coexpressed as independent proteins (Santoro et al., 2009, 2011). Importantly, the action of the core peptide to inhibit the effect of cAMP to shift HCN2 voltage gating results from a specific action of the peptide as it is prevented by the EEEFE to RRRAR mutation (Fig. 5 D).

Examination of the action of a range of cAMP concentrations reveals that, at a concentration of 4 µM, the TRIP8b$_{core}$ peptide shifts the cAMP dose–response

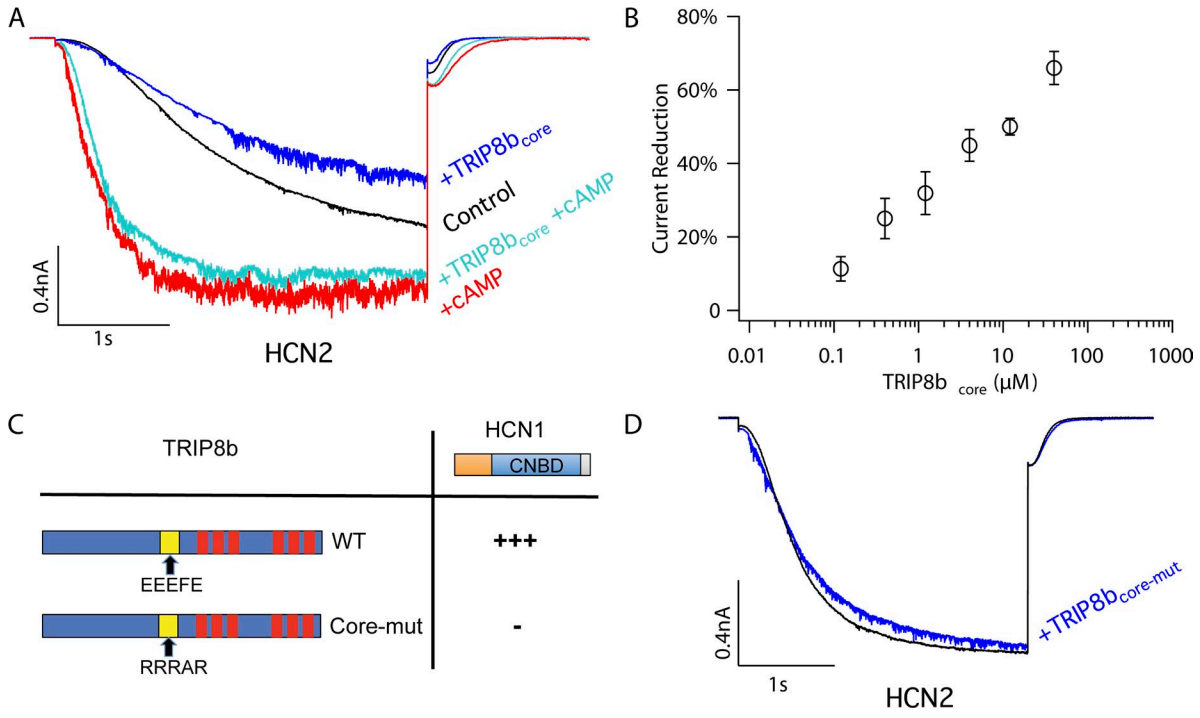

Figure 4. Direct application of TRIP8b$_{core}$ polypeptide to inside-out patches suppresses HCN2 maximal current in the absence of cAMP. (A) Representative experiment showing effects of TRIP8b$_{core}$ polypeptide on HCN2 currents in inside-out patches elicited by a hyperpolarization to −140 mV, either in the absence or presence of cAMP. The current recording protocol is described in Fig. 3. The internal bath solution contained control solution, 4 µM TRIP8b$_{core}$ with no cAMP, 4 µM TRIP8b$_{core}$ plus 100 µM cAMP, or 100 µM cAMP with no TRIP8b. (B) Dose–response curve for the percent reduction in current amplitude at extreme negative voltages as a function of TRIP8b$_{core}$ polypeptide concentration (in the absence of cAMP). Error bars show SEM. (C) The binding activity of the HCN1 C-linker/CNBD (residues 390–611) with WT and mutant TRIP8b (constant region, exons 5–16) assessed using a yeast two-hybrid assay. For TRIP8b, the yellow square represents the conserved core region. In TRIP8b$_{core\text{-}mut}$, the WT EEEFE core residues are substituted by RRRAR. The red colors denote the TPR domains. Activity was detected by transactivation of a GFP reporter gene. "+++" indicates very strong fluorescence; "−" indicates no detectable fluorescence (see Santoro et al. [2011]). (D) Representative HCN2 currents before (black trace) and after (blue trace) the application of TRIP8b$_{core\text{-}mut}$ polypeptide to inside-out patches. The current recording protocol is described in Fig. 3.

Published November 25, 2013

curve to higher agonist concentrations, causing a 70-fold increase in the $K_{1/2}$ for cAMP and a small decrease in ΔV_{max} (Fig. 5 E). The shift in $K_{1/2}$ with 4 μM $TRIP8b_{core}$ is intermediate between the results with TRIP8b-HCN2 and $TRIP8b_{core}$-HCN2 fusion protein channels, suggesting that the local effective concentration of TRIP8b in the two fusion proteins may be, respectively, lower and higher than 4 μM. Alternatively, the efficacy or affinity of the core peptide may differ from that observed with the two fusion protein channels.

We next explored the effect of a range of concentrations of $TRIP8b_{core}$ on the action of cAMP. The core peptide produces a dose-dependent inhibition of the effect of a given concentration of cAMP to shift the $V_{1/2}$ to more positive potentials (Fig. 5 F). Moreover, as the cAMP concentration is increased, higher concentrations of $TRIP8b_{core}$ are required to produce a given level of inhibition of the cAMP response. Thus, TRIP8b and cAMP exert reciprocal inhibitory effects on each other's action. TRIP8b shifts the dose–response curve for cAMP to higher concentrations, and conversely, cAMP produces a concentration-dependent shift in the dose–response curve for TRIP8b. Although these results are consistent with a competition of cAMP and TRIP8b for a single binding site, the finding that TRIP8b reduces the maximal response to saturating concentrations of cAMP is more consistent with an allosteric interaction, as discussed in the next section.

TRIP8b inhibits the effect of cAMP to facilitate HCN2 voltage gating through an allosteric mechanism

To explore the mechanism by which TRIP8b alters the function of HCN2 channels, we examined whether the actions of TRIP8b are consistent with an extension of a six-state cyclic allosteric model previously used to describe the modulatory action of cAMP on HCN2 gating in the absence of TRIP8b (Fig. 6; Zhou and Siegelbaum, 2007). According to this model, in the absence of cAMP, membrane hyperpolarization causes the channel to undergo a voltage-dependent transition from a closed resting state (C_R) to a closed active state (C_A), from which the channel undergoes a voltage-independent conformational change to the open state (O). cAMP (A) can bind and unbind the CNBD in all three states, yielding three

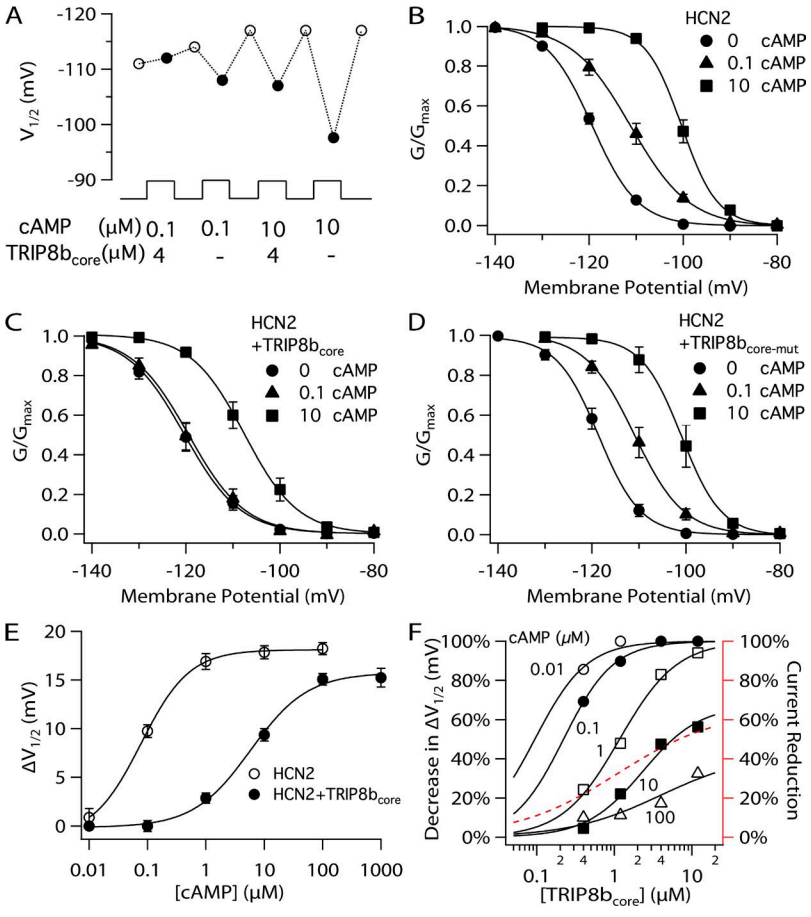

Figure 5. Effects of $TRIP8b_{core}$ polypeptide on action of cAMP on HCN2 channel voltage gating. (A) Representative experiment showing $V_{1/2}$ of HCN2 channels in inside-out patches with solutions containing the indicated [cAMP] in the absence or presence of 4 μM $TRIP8b_{core}$ polypeptide. Open circles indicate $V_{1/2}$ in the absence of both cAMP and $TRIP8b_{core}$; closed circles indicate $V_{1/2}$ in the presence of 0.1 or 10 μM cAMP, with or without 4 μM $TRIP8b_{core}$ polypeptide, as indicated. (B) Normalized G-V relationship for HCN2 channel tail currents in 0, 0.1, or 10 μM cAMP. (C) Normalized G-V relationship for HCN2 channel tail currents in the presence of 4 μM $TRIP8b_{core}$ polypeptide plus 0, 0.1, or 10 μM cAMP. (D) Normalized G-V relationship for HCN2 tail currents in the presence of 4 μM $TRIP8b_{core-mut}$ polypeptide plus 0, 0.1, or 10 μM cAMP. (E) Shift in $V_{1/2}$ as a function of [cAMP] in the absence (open circles) or presence (closed circles) of 4 μM $TRIP8b_{core}$ polypeptide. Solid lines show fits of the Hill equation, which yield HCN2: ΔV_{max} = 18.1 mV, $K_{1/2}$ = 0.08 μM, h = 0.86; and HCN2 plus 4 μM $TRIP8b_{core}$: ΔV_{max} = 15.8 mV, $K_{1/2}$ = 5.64 μM, h = 0.86. (F) Percent decrease in $\Delta V_{1/2}$ produced by the indicated concentrations of cAMP as a function of $TRIP8b_{core}$ concentration (left ordinate). Fits of the Hill equation (solid lines) yield 0.1 μM cAMP: $K_{1/2}$ = 0.22 μM, h = 1.35, percent maximal decrease in $\Delta V_{1/2}$ = 100%; 1 μM cAMP: $K_{1/2}$ = 1.57 μM, h = 1.69, percent maximal decrease in $\Delta V_{1/2}$ = 97%; 10 μM cAMP: $K_{1/2}$ = 2.34 μM, h = 1.19, percent maximal decrease in $\Delta V_{1/2}$ = 69%; and 100 μM cAMP: $K_{1/2}$ = 3.96 μM, h = 0.74, percent maximal decrease in $\Delta V_{1/2}$ = 42%. The Hill fit to the TRIP8b dose–response curve for HCN2 maximal current reduction from Fig. 4 B is replicated here for comparison (red dashed line, right ordinate). Error bars indicate SEM.

Published November 25, 2013

corresponding agonist bound states: AC_R, AC_A, and AO. The key property of this model is that the opening transition is allosterically coupled to a conformational change in the CNBD that enhances the affinity of the open state for cAMP (dissociation constant K_O^A), relative to the affinity of the two closed states (identical dissociation constant K_C^A). Thus, cAMP binding to the open state is energetically more favorable than binding to the closed state, causing agonist binding to shift the equilibrium toward the open transition by the factor K_C^A / K_O^A. Because the voltage-independent opening reaction is kinetically coupled to the voltage-dependent activation step, the cAMP-dependent enhancement of channel opening both shifts the apparent voltage dependence of channel gating to more positive potentials and increases maximal open probability.

We incorporated TRIP8b (T) into this model by assuming it binds to the open and closed states of the channel, in both the cAMP-bound or unbound states. This results in an additional six states for the TRIP8b-bound channel, three states with the CNBD unoccupied by cAMP (TC_R, TC_A, and TO; Fig. 6, top face), and three states with the CNBD occupied by cAMP (AC_RT, AC_AT, and AOT; Fig. 6, back face). According to the model, TRIP8b binding may, in principle, alter the affinity of both the closed and open states for cAMP. Our finding that TRIP8b decreases ΔV_{max} implies that TRIP8b must reduce cAMP binding to the open state more than it reduces cAMP binding to the closed state. Finally, as the various states are incorporated in a cyclic reaction scheme, cAMP binding must necessarily reduce the affinity of the channel for TRIP8b. We adjusted the parameters of the model to obtain the best fit to the measured relation between [cAMP] and $\Delta V_{1/2}$, in the presence of 0–12 µM $TRIP8b_{core}$ peptide (Fig. 7; see supplemental text for details).

The model provides a good fit to the cAMP dose–response curves in both the absence and presence of increasing concentrations of TRIP8b. In particular, the model reproduces the effect in which increasing concentrations of TRIP8b cause both a progressive shift in the cAMP dose–response curve to higher concentrations of cAMP and a progressive decrease in the maximal response to saturating cAMP (Fig. 7). Based on the parameters obtained from the fit (see legend to Fig. 7), we infer that binding of TRIP8b produces a 70-fold decrease in the affinity of the closed channel for cAMP. Conversely, binding of cAMP produces an identical decrease in the affinity of the closed channel for TRIP8b. For the open channel, cAMP or TRIP8b binding produces an even greater 300-fold decrease in affinity for the antagonistic ligand. The finding that the K_{TC}^A / K_{TO}^A ratio (9.6) is much smaller than the K_C^A / K_O^A ratio (105) indicates that TRIP8b binding does indeed reduce the

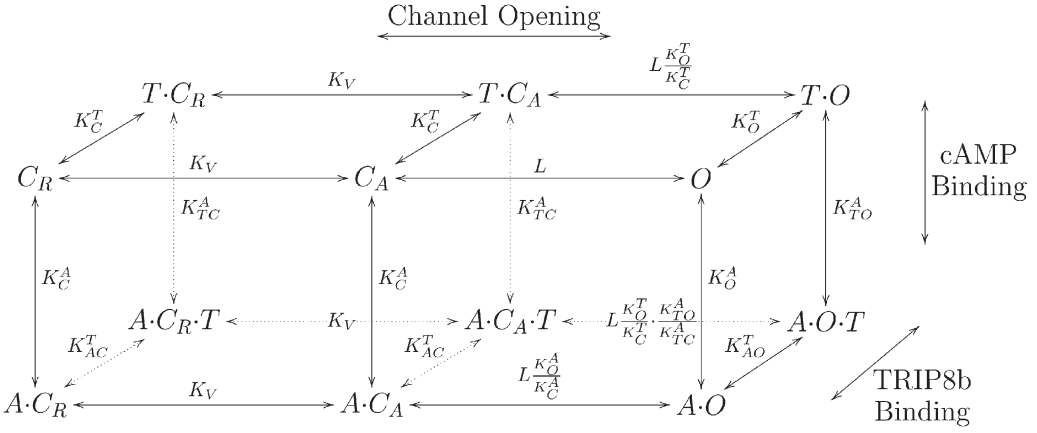

Figure 6. 12-state allosteric model for regulation of HCN2 channel opening by voltage, cAMP, and TRIP8b. The vertical and front-back transitions of the cubic scheme represent the cAMP and TRIP8b binding reactions to the channel, respectively. The two horizontal transitions are the voltage-dependent activation step reflecting voltage sensor movement, followed by a voltage-independent opening step. The front face of the cube is the six-state cyclic allosteric model that represents the effects of voltage and cAMP on channel opening in the absence of bound TRIP8b (Zhou and Siegelbaum, 2007); the top face is a six-state cyclic allosteric model that represents the actions of voltage and TRIP8b binding on channel opening in the absence of bound cAMP. TRIP8b and cAMP can both bind to the channel at the same time, as represented by the back and bottom faces of the cube. Definition of states and ligands: C_R, unliganded closed channel with voltage sensor in the resting state; C_A, unliganded closed channel with voltage sensor in the activated state; O, unliganded channel in the open state; A, cAMP; T, TRIP8b. Definition of parameters: K_V, equilibrium constant for transition of closed channel transition between resting state and activated state; L, intrinsic equilibrium constant for channel opening; K_C^A and K_O^A, dissociation equilibrium constants for cAMP binding to closed and open states, respectively; K_C^T and K_O^T, dissociation equilibrium constants of TRIP8b binding to channel in closed and open states, respectively; K_{TC}^A and K_{TO}^A, dissociation equilibrium constants for cAMP binding to TRIP8b-bound channels in closed and open states, respectively; K_{AC}^T and K_{AO}^T, dissociation equilibrium constants for TRIP8b binding to cAMP-bound channels in closed and open states, respectively.

Published November 25, 2013

affinity of the open state for cAMP to a greater extent than it reduces affinity of the closed state for cAMP. Moreover, this accounts for the action of TRIP8b to inhibit the efficacy with which cAMP shifts the voltage dependence of channel gating, resulting in the decrease in ΔV_{max}.

In principle, the model could also account for our observation that TRIP8b reduces HCN2 maximal current in the absence of cAMP (as shown in Fig. 4), if TRIP8b were to bind to the cAMP-free closed state more tightly than it were to bind to the cAMP-free open state. However, the best fit of the model yields nearly identical values for K_C^T (0.089 ± 0.027 µM) and K_O^T (0.064 ± 0.010 µM). A second discrepancy is seen when we independently adjusted K_C^T and K_O^T to fit the observed reduction in I_{max} (Fig. 4 B). In this case, the model predicts that TRIP8b should produce a −3-mV shift in the voltage dependence of gating in the absence of cAMP, an effect we do not observe (Fig. 3 B). Moreover the estimates of K_C^T and K_O^T obtained from the fits in the absence of cAMP are 4- to 30-fold larger (K_C^T = 0.34 µM; K_O^T = 1.90 µM) than those obtained when we fit the relation between TRIP8b core polypeptide concentration and the magnitude of the shift in voltage gating with cAMP (compare Fig. 4 B with Fig. 5 F; see Model fitting subsection of Materials and methods).

The above discrepancies suggest that the effects of TRIP8b to inhibit maximal current amplitude in the absence of cAMP are mediated through an interaction with a separate low-affinity binding site on the channel distinct from the high-affinity site responsible for the action of TRIP8b to antagonize the cAMP-dependent shift in HCN2 voltage gating. Consistent with such a dissociation, we find that a point mutation in a conserved arginine, $HCN2_{R591E}$, which profoundly disrupts the binding to the CNBD of both cAMP (Chen et al., 2001; Zhou and Siegelbaum, 2007) and TRIP8b (Han et al., 2011), has no effect on the ability of the TRIP8b core polypeptide to reduce HCN2 maximal current (Fig. 8). Collectively, these observations strongly argue that TRIP8b reduces maximal current through a kinetic and structural mechanism that is distinct from its action to antagonize the effect of cAMP on HCN2 voltage gating. We next explore in more detail the mechanism for this second action of TRIP8b to suppress maximal current.

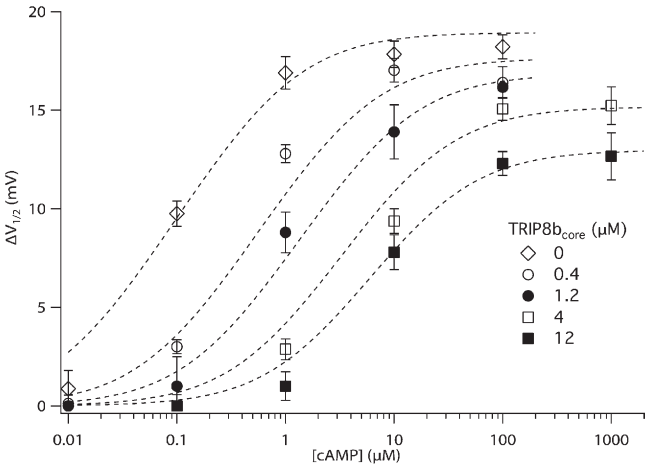

Figure 7. $\Delta V_{1/2}$ as a function of [cAMP] and [$TRIP8b_{core}$] polypeptide, fitted by the 12-state allosteric model. The $TRIP8b_{core}$ polypeptide concentrations are indicated. The parameters of the front face of the model (corresponding to the six-state cyclic model) are adopted from Zhou and Siegelbaum (2007): $L = 0.43$, $s = 4.4$, K_C^A = 0.844 µM, K_O^A = 0.008 µM. The best fit of the model yields the following values for the other parameters: K_C^T = 0.089 ± 0.027 µM, K_O^T = 0.064 ± 0.010 µM, K_{TC}^A = 33.58 ± 8.18 µM, K_{TO}^A = 3.53 ± 1.33 µM. K_{AC}^T and K_{AO}^T are then derived from the other parameters: $K_{AC}^T = K_{TC}^A \cdot K_C^T / K_C^A$ = 3.54 µM and $K_{AO}^T = K_{TO}^A \cdot K_O^T / K_O^A$ = 28.24 µM. Error bars show SEM. See supplemental text for further details.

Molecular mechanism underlying the action of TRIP8b to reduce HCN2 channel current

TRIP8b and HCN1 have been previously found to interact at two sites (Lewis et al., 2009; Han et al., 2011; Santoro et al., 2011). At an upstream site the core region of TRIP8b binds to the CNBD of the channel; at a downstream site the C-terminal TPR domain of TRIP8b binds the extreme C-terminal SNL tripeptide of the channel. Which channel domains are required for the action of the TRIP8b core peptide to regulate HCN2 maximal current? We find that truncation of HCN2 at the N terminus of the CNBD blocks the ability of TRIP8b to reduce HCN2 channel current ($HCN2_{\Delta CNBD}$; Fig. 8). In contrast, as stated above, the $HCN2_{R591E}$ point mutation does not alter the action of 4 µM TRIP8b to reduce maximal HCN2 current (Fig. 8). These results suggest that, although a direct interaction of TRIP8b with the CNBD may not be required and some other previously unrecognized low-affinity binding site may be important for the reduction in channel current, the presence of the CNBD is still essential for TRIP8b to exert its effect to reduce maximal current amplitude (either by contributing to the integrity of the low affinity binding site or by acting as an effector domain).

If the action of TRIP8b to reduce HCN2 maximal channel current does not depend directly on its interaction with the CNBD, how does cAMP antagonize this action? A previous study has suggested that cAMP binding enhances HCN channel opening by relieving an inhibitory action of the CNBD on channel gating (Wainger et al., 2001). At a structural level, cAMP is thought to act by promoting assembly of the four CNBDs in a channel into a tetrameric gating ring (Zagotta et al., 2003). We thus hypothesized that the inhibitory action of TRIP8b on channel current is only manifest when the gating ring is disassembled, that is, in the absence of cAMP. To test this hypothesis, we took advantage of a triple point mutation our laboratory previously identified in the first (A′) helix of the cytoplasmic C-linker region of the channel, which

Published November 25, 2013

connects the S6 transmembrane segment to the CNBD. We found that this mutation promotes gating ring assembly in the absence of cAMP (Zhou et al., 2004). We therefore predicted that this mutation should also block the action of TRIP8b to reduce channel current. As shown in Fig. 8 ($HCN2_{FPN}$), the triple point mutation does indeed block the effect of TRIP8b to inhibit HCN2 maximal current, supporting the hypothesis outlined above.

DISCUSSION

In this study, we report that TRIP8b exerts multiple effects on HCN2 channel function. The auxiliary subunit shifts the relation between $\Delta V_{1/2}$ and [cAMP] to higher concentrations, decreasing the sensitivity of the channel to cAMP. TRIP8b also decreases the maximal voltage shift in response to a saturating concentration of cAMP (ΔV_{max}), reflecting a reduction in cAMP efficacy. Finally, in the absence of cAMP, TRIP8b inhibits the maximal current through the channel. Because this latter effect is antagonized by cAMP, TRIP8b enhances the action of cAMP to increase maximal current through the channel.

An allosteric mechanism accounts for the action of TRIP8b to inhibit the effect of cAMP to shift the voltage dependence of HCN2 channel opening

The effect of TRIP8b to inhibit the cAMP-dependent modulation of HCN2 voltage gating can be accounted for by an expansion of a six-state allosteric model that has been previously used to describe the dual actions of voltage and cAMP to promote HCN2 channel opening in the absence of TRIP8b (Zhou and Siegelbaum, 2007). In this model, cAMP facilitates channel opening by binding more tightly to the open than to the closed state of the channel. In the expanded 12-state model, TRIP8b exerts an allosteric action that reduces the affinity of both the closed and open states of the channel for cAMP. Conversely, cAMP binding produces an allosteric effect to reduce the affinity of the closed and open channel for TRIP8b. Because TRIP8b also reduces ΔV_{max}, its binding must reduce the cAMP affinity of the open state to a greater extent than it reduces the cAMP affinity of the closed state, a prediction which was confirmed by our detailed modeling results. In contrast, unlike cAMP, which binds much more favorably to the open state than the closed state, TRIP8b binds with similar affinity to the open and closed states of the channel.

A recent biochemical study focused on the nature of the interaction between TRIP8b and HCN1 at the upstream interaction site, using a channel in which the C-terminal SNL tripeptide was deleted to prevent the interaction at the downstream site (Han et al., 2011). Under these conditions the binding between TRIP8b and HCN1 is reduced by cAMP in a concentration-dependent manner. Moreover the binding of TRIP8b to the $HCN1_{\Delta SNL}$ truncation mutant is abolished when a highly conserved arginine residue in the CNBD, which interacts with the cyclized phosphate of cAMP, is mutated to glutamate (R538E in HCN1 and R591E in HCN2). This led Han et al. (2011) to conclude that the core region of TRIP8b may directly bind to this conserved arginine, thereby competing with cAMP for the CNBD.

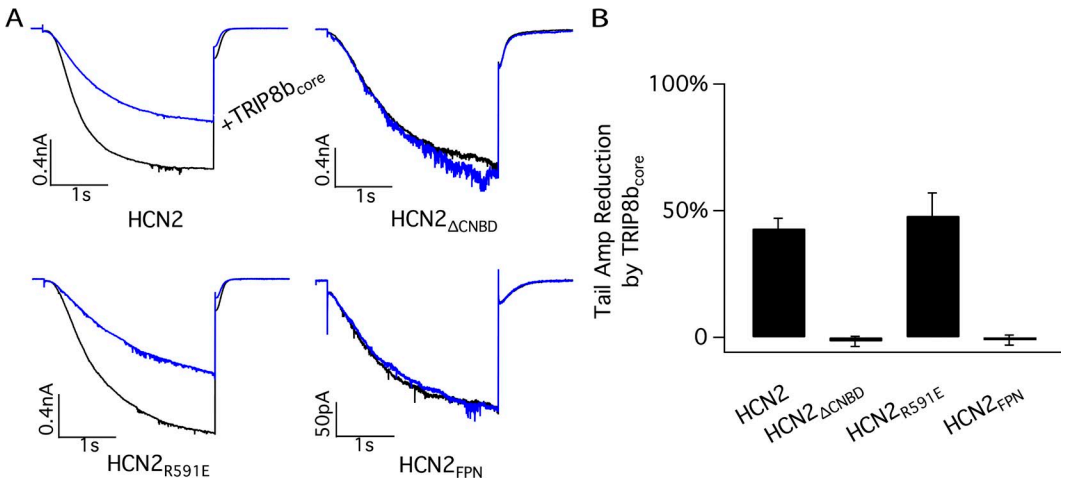

Figure 8. Importance of C-terminal regions of HCN2 for the ability of TRIP8b to reduce maximal current. (A) Representative currents through HCN2 WT and mutant channels before (black traces) and after (blue traces) the application of 4 µM $TRIP8b_{core}$ polypeptide to inside-out patches (no cAMP present). $HCN2_{\Delta CNBD}$, truncation after residue V526 removing entire CNBD and all downstream residues; $HCN2_{R591E}$, point mutation of conserved arginine in CNBD required for high-affinity cAMP binding; $HCN2_{FPN}$, triple point mutation substituting FPN sequence for residues QEK in A′ helix of C-linker (residues 450–452 in HCN2). The recording protocol is described in Fig. 2. (B) Percent reduction in maximal tail current amplitude for HCN2 WT and mutant channels in response to 4 µM $TRIP8b_{core}$ polypeptide. Error bars indicate SEM. Mean percent reductions ± SEM are as follows: HCN2, 43 ± 4% ($n = 9$); $HCN2_{\Delta CNBD}$, −1.6 ± 2% ($n = 3$); $HCN2_{R591E}$, 48 ± 9% ($n = 3$); and $HCN2_{FPN}$, −1 ± 2% ($n = 3$).

Published November 25, 2013

However, the finding that TRIP8b reduces the maximal voltage shift with saturating concentrations of cAMP (Zolles et al., 2009) indicates that the auxiliary subunit does not directly compete with cAMP for the channel but acts through an allosteric mechanism to decrease the affinity of the CNBD for ligand. Moreover, several additional lines of evidence make it unlikely that TRIP8b directly interacts with the binding domain arginine (R591 in HCN2). First, the crystal structure of the HCN2 CNBD with cAMP bound shows that the arginine is embedded in the binding pocket and surrounded by the CNBD β-roll (Zagotta et al., 2003). Although cAMP or cGMP are small enough to enter the pocket and interact with the arginine, it is unclear how the internal core domain of TRIP8b would have ready access to this site. Second, we find that the binding of TRIP8b to HCN1 is not altered when the corresponding arginine (R538) is substituted with alanine (HCN1 R538A), although we confirmed that the R538E mutation does weaken the binding of TRIP8b to the channel (Fig. 9). These results can be reconciled if the conserved arginine of the CNBD does not directly interact with TRIP8b, but rather its substitution by glutamate results in a local disruption of the CNBD, thereby weakening the binding of TRIP8b. We further hypothesize that this local structural change in the CNBD may not occur with the less disruptive alanine substitution. More detailed structural studies, including x-ray crystallography, are needed to identify the precise location of the TRIP8b binding site.

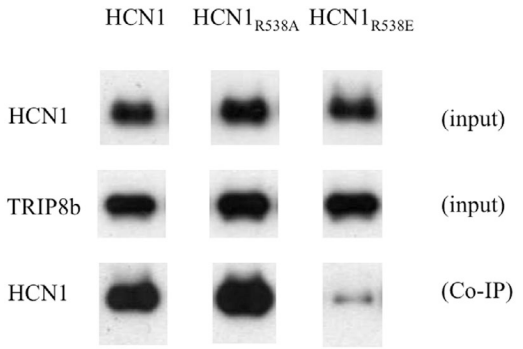

Figure 9. The effect of mutations in the HCN1 key CNBD residue R538 on TRIP8b binding. Western blot analysis shows binding of HCN1, $HCN1_{R538A}$, and $HCN1_{R538E}$ mutants to WT TRIP8b(1b-2) assessed by coimmunoprecipitation from *Xenopus* oocyte extracts coinjected with TRIP8b and HCN1 cRNA. The top row shows the HCN1 input signal using an HCN1 antibody. The middle row shows the TRIP8b input signal using an anti-TRIP8b antibody. The bottom row shows the amount of HCN1 protein coimmunoprecipitated with the TRIP8b antibody (Western blot probed using HCN1 antibody). Note that exposure times are directly comparable along each row but not down each column. Individual bands have been cut from intact gel pictures and aligned to allow direct comparison of intensities for WT and mutant constructs.

TRIP8b inhibits maximal current through HCN2 channels through a second action

What is the relation between the action of TRIP8b to reduce maximal Ih in the absence of cAMP and the action of TRIP8b to decrease the affinity of the CNBD for cAMP? As discussed in the Results, although in principle the 12-state allosteric model can account for both of these actions through TRIP8b binding more tightly to the closed than open state of the channel, this single mode of action is not consistent with our experimental and modeling results. Rather, the reduction in maximal macroscopic current appears to be caused by a second, low-affinity action of TRIP8b to reduce maximal channel current. Such an effect could result from a reduction in channel open probability or from a reduction in single channel conductance.

One important caveat with our modeling results is that the 12-state allosteric reaction scheme does not take into account the tetrameric nature of the channel and its interaction with cAMP (Ulens and Siegelbaum, 2003) and TRIP8b (Bankston et al., 2012). Furthermore, a recent study suggests that the gating of HCN2 channels is much more complex than our model, involving a profound cooperative interaction (Kusch et al., 2012). Although our initial attempts to fit a model with multiple equivalent cAMP and TRIP8b binding sites did not yield a significant improvement in our ability to describe the two effects of TRIP8b through a single mechanistic action, some more complex model with nonequivalent binding sites (Ulens and Siegelbaum, 2003; Kusch et al., 2012) may prove adequate to explain our results based on a single underlying action of TRIP8b.

If TRIP8b does indeed exert separate high- and low-affinity actions at two distinct binding sites that, respectively, antagonize the action of cAMP on voltage gating and reduce maximal current in the absence of cAMP, where are these sites located? One possibility is that TRIP8b binds to two separate sites within the CNBD. However it is unclear as to how the relatively compact CNBD could accommodate multiple TRIP8b proteins. Also, any interaction of TRIP8b with a second CNBD-binding site that reduces maximal current must be impervious to the R591E mutation, which disrupts high-affinity binding of TRIP8b to the CNBD (Fig. 9; Han et al., 2011). Rather, we favor a model in which the core region of TRIP8b binds to two separate sites on the channel, a high-affinity site on the CNBD that allosterically reduces cAMP binding and a low-affinity site located elsewhere in the channel that reduces maximal current, perhaps by decreasing apparent single channel conductance. As we previously failed to detect an interaction between the TRIP8b core peptide and the C-terminal downstream HCN1 binding site using a yeast two-hybrid–based assay (Santoro et al., 2011), this second site is likely to be located either within the C-linker or within the channel's intracellular loops.

Published November 25, 2013

Our finding that cAMP antagonizes the ability of TRIP8b to reduce maximal current indicates that the low-affinity TRIP8b binding site must be allosterically coupled to the CNBD. We further postulate that this allosteric coupling may be mediated by the action of cAMP to promote assembly of the four CNBDs of the tetrameric HCN2 channel into a fourfold symmetric gating ring (Zagotta et al., 2003). Some support for this idea comes from our finding that a triple point mutation in the A′ helix of the HCN2 C-linker, previously shown to promote gating ring assembly in the absence of cAMP (Zhou et al., 2004), blocks the action of TRIP8b to inhibit HCN2 maximal current (Fig. 8). However, this result is also consistent with the possibility that the A′ helix of the C-linker may help form the TRIP8b low-affinity binding site.

Implications of the dual actions of TRIP8b for the physiological effects of cAMP to modulate Ih

Our finding that TRIP8b exerts opposing actions on the modulatory effects of cAMP, enhancing the action of cAMP to increase maximal current while inhibiting the action of cAMP to shift voltage gating to more positive potentials, has interesting potential implications for the physiological consequences of the diverse modulatory actions of cAMP on Ih as previously reported in different neurons. Our results suggest that in neurons with high levels of TRIP8b expression, cAMP will exert a larger action to enhance maximal current and a smaller action to alter the voltage dependence of channel gating compared with neurons in which TRIP8b expression is low. Differences in TRIP8b expression among different neuronal types could help explain the varied results reported in the literature for the modulatory effects of neurotransmitters on the hyperpolarization-activated Ih (Bobker and Williams, 1989; McCormick and Williamson, 1991; Kiehn and Harris-Warrick, 1992; Larkman and Kelly, 1992; Erickson et al., 1993; Gasparini and DiFrancesco, 1999; Bickmeyer et al., 2002; Schweitzer et al., 2003; Heys and Hasselmo, 2012). Whereas in most neurons the predominant effect of neurotransmitter actions results from a cAMP-dependent alteration in the voltage-dependent gating of Ih, the extent to which transmitters also regulate maximal current amplitude varies greatly. In some instances, the predominant effect of transmitter is to enhance maximal current, with little or no change in channel voltage-dependent gating (e.g., Bickmeyer et al., 2002). Further studies using manipulations of TRIP8b expression in intact neurons may help in characterizing the role of this auxiliary subunit in the modulatory control of Ih function under more physiological conditions.

We thank John Riley and Claudia Corso for their excellent technical support.

This work was partially supported by grant NS36658 from the National Institutes of Health (to S. Siegelbaum) and by grant SAL-49 ASTIL Regione Lombardia (to A. Moroni).

Sharona E. Gordon served as editor.

Submitted: 22 April 2013
Accepted: 18 October 2013

REFERENCES

Arikkath, J., and K.P. Campbell. 2003. Auxiliary subunits: essential components of the voltage-gated calcium channel complex. *Curr. Opin. Neurobiol.* 13:298–307. http://dx.doi.org/10.1016/S0959-4388(03)00066-7

Bankston, J.R., S.S. Camp, F. DiMaio, A.S. Lewis, D.M. Chetkovich, and W.N. Zagotta. 2012. Structure and stoichiometry of an accessory subunit TRIP8b interaction with hyperpolarization-activated cyclic nucleotide-gated channels. *Proc. Natl. Acad. Sci. USA.* 109:7899–7904. http://dx.doi.org/10.1073/pnas.1201997109

Battefeld, A., C. Bierwirth, Y.C. Li, L. Barthel, T. Velmans, and U. Strauss. 2010. I(h) "run-up" in rat neocortical neurons and transiently rat or human HCN1-expressing HEK293 cells. *J. Neurosci. Res.* 88:3067–3078. http://dx.doi.org/10.1002/jnr.22475

Bickmeyer, U., M. Heine, T. Manzke, and D.W. Richter. 2002. Differential modulation of I(h) by 5-HT receptors in mouse CA1 hippocampal neurons. *Eur. J. Neurosci.* 16:209–218. http://dx.doi.org/10.1046/j.1460-9568.2002.02072.x

Biel, M., C. Wahl-Schott, S. Michalakis, and X. Zong. 2009. Hyperpolarization-activated cation channels: from genes to function. *Physiol. Rev.* 89:847–885. http://dx.doi.org/10.1152/physrev.00029.2008

Bobker, D.H., and J.T. Williams. 1989. Serotonin augments the cationic current Ih in central neurons. *Neuron.* 2:1535–1540. http://dx.doi.org/10.1016/0896-6273(89)90041-X

Chen, S., J. Wang, and S.A. Siegelbaum. 2001. Properties of hyperpolarization-activated pacemaker current defined by coassembly of HCN1 and HCN2 subunits and basal modulation by cyclic nucleotide. *J. Gen. Physiol.* 117:491–504. http://dx.doi.org/10.1085/jgp.117.5.491

Chen, X., J.E. Sirois, Q. Lei, E.M. Talley, C. Lynch III, and D.A. Bayliss. 2005. HCN subunit-specific and cAMP-modulated effects of anesthetics on neuronal pacemaker currents. *J. Neurosci.* 25:5803–5814. http://dx.doi.org/10.1523/JNEUROSCI.1153-05.2005

Craven, K.B., and W.N. Zagotta. 2004. Salt bridges and gating in the COOH-terminal region of HCN2 and CNGA1 channels. *J. Gen. Physiol.* 124:663–677. http://dx.doi.org/10.1085/jgp.200409178

DiFrancesco, D., and P. Tortora. 1991. Direct activation of cardiac pacemaker channels by intracellular cyclic AMP. *Nature.* 351:145–147. http://dx.doi.org/10.1038/351145a0

Erickson, K.R., O.K. Ronnekleiv, and M.J. Kelly. 1993. Electrophysiology of guinea-pig supraoptic neurones: role of a hyperpolarization-activated cation current in phasic firing. *J. Physiol.* 460:407–425.

Frère, S.G.A., and A. Lüthi. 2004. Pacemaker channels in mouse thalamocortical neurones are regulated by distinct pathways of cAMP synthesis. *J. Physiol.* 554:111–125. http://dx.doi.org/10.1113/jphysiol.2003.050989

Gasparini, S., and D. DiFrancesco. 1999. Action of serotonin on the hyperpolarization-activated cation current (Ih) in rat CA1 hippocampal neurons. *Eur. J. Neurosci.* 11:3093–3100. http://dx.doi.org/10.1046/j.1460-9568.1999.00728.x

Han, Y., Y. Noam, A.S. Lewis, J.J. Gallagher, W.J. Wadman, T.Z. Baram, and D.M. Chetkovich. 2011. Trafficking and gating of hyperpolarization-activated cyclic nucleotide-gated channels are regulated by interaction with tetratricopeptide repeat-containing Rab8b-interacting protein (TRIP8b) and cyclic AMP at distinct sites. *J. Biol. Chem.* 286:20823–20834. http://dx.doi.org/10.1074/jbc.M111.236125

Heys, J.G., and M.E. Hasselmo. 2012. Neuromodulation of I(h) in layer II medial entorhinal cortex stellate cells: a voltage-clamp study.

J. Neurosci. 32:9066–9072. http://dx.doi.org/10.1523/JNEUROSCI.0868-12.2012

Kiehn, O., and R.M. Harris-Warrick. 1992. 5-HT modulation of hyperpolarization-activated inward current and calcium-dependent outward current in a crustacean motor neuron. *J. Neurophysiol.* 68:496–508.

Kusch, J., S. Thon, E. Schulz, C. Biskup, V. Nache, T. Zimmer, R. Seifert, F. Schwede, and K. Benndorf. 2012. How subunits cooperate in cAMP-induced activation of homotetrameric HCN2 channels. *Nat. Chem. Biol.* 8:162–169.

Larkman, P.M., and J.S. Kelly. 1992. Ionic mechanisms mediating 5-hydroxytryptamine- and noradrenaline-evoked depolarization of adult rat facial motoneurones. *J. Physiol.* 456:473–490.

Lewis, A.S., E. Schwartz, C.S. Chan, Y. Noam, M. Shin, W.J. Wadman, D.J. Surmeier, T.Z. Baram, R.L. Macdonald, and D.M. Chetkovich. 2009. Alternatively spliced isoforms of TRIP8b differentially control h channel trafficking and function. *J. Neurosci.* 29:6250–6265. http://dx.doi.org/10.1523/JNEUROSCI.0856-09.2009

McCormick, D.A., and A. Williamson. 1991. Modulation of neuronal firing mode in cat and guinea pig LGNd by histamine: possible cellular mechanisms of histaminergic control of arousal. *J. Neurosci.* 11:3188–3199.

Pian, P., A. Bucchi, R.B. Robinson, and S.A. Siegelbaum. 2006. Regulation of gating and rundown of HCN hyperpolarization-activated channels by exogenous and endogenous PIP2. *J. Gen. Physiol.* 128:593–604. http://dx.doi.org/10.1085/jgp.200609648

Piskorowski, R., B. Santoro, and S.A. Siegelbaum. 2011. TRIP8b splice forms act in concert to regulate the localization and expression of HCN1 channels in CA1 pyramidal neurons. *Neuron.* 70:495–509. http://dx.doi.org/10.1016/j.neuron.2011.03.023

Robinson, R.B., and S.A. Siegelbaum. 2003. Hyperpolarization-activated cation currents: from molecules to physiological function. *Annu. Rev. Physiol.* 65:453–480. http://dx.doi.org/10.1146/annurev.physiol.65.092101.142734

Santoro, B., B.J. Wainger, and S.A. Siegelbaum. 2004. Regulation of HCN channel surface expression by a novel C-terminal protein-protein interaction. *J. Neurosci.* 24:10750–10762. http://dx.doi.org/10.1523/JNEUROSCI.3300-04.2004

Santoro, B., R.A. Piskorowski, P. Pian, L. Hu, H. Liu, and S.A. Siegelbaum. 2009. TRIP8b splice variants form a family of auxiliary subunits that regulate gating and trafficking of HCN channels in the brain. *Neuron.* 62:802–813. http://dx.doi.org/10.1016/j.neuron.2009.05.009

Santoro, B., L. Hu, H. Liu, A. Saponaro, P. Pian, R.A. Piskorowski, A. Moroni, and S.A. Siegelbaum. 2011. TRIP8b regulates HCN1 channel trafficking and gating through two distinct C-terminal interaction sites. *J. Neurosci.* 31:4074–4086. http://dx.doi.org/10.1523/JNEUROSCI.5707-10.2011

Schweitzer, P., S.G. Madamba, and G.R. Siggins. 2003. The sleep-modulating peptide cortistatin augments the h-current in hippocampal neurons. *J. Neurosci.* 23:10884–10891.

Shin, K.S., C. Maertens, C. Proenza, B.S. Rothberg, and G. Yellen. 2004. Inactivation in HCN channels results from reclosure of the activation gate: desensitization to voltage. *Neuron.* 41:737–744. http://dx.doi.org/10.1016/S0896-6273(04)00083-2

Ulens, C., and S.A. Siegelbaum. 2003. Regulation of hyperpolarization-activated HCN channels by cAMP through a gating switch in binding domain symmetry. *Neuron.* 40:959–970. http://dx.doi.org/10.1016/S0896-6273(03)00753-0

Vacher, H., and J.S. Trimmer. 2011. Diverse roles for auxiliary subunits in phosphorylation-dependent regulation of mammalian brain voltage-gated potassium channels. *Pflugers Arch.* 462:631–643. http://dx.doi.org/10.1007/s00424-011-1004-8

Wainger, B.J., M. DeGennaro, B. Santoro, S.A. Siegelbaum, and G.R. Tibbs. 2001. Molecular mechanism of cAMP modulation of HCN pacemaker channels. *Nature.* 411:805–810. http://dx.doi.org/10.1038/35081088

Wang, J., S. Chen, M.F. Nolan, and S.A. Siegelbaum. 2002. Activity-dependent regulation of HCN pacemaker channels by cyclic AMP: signaling through dynamic allosteric coupling. *Neuron.* 36:451–461. http://dx.doi.org/10.1016/S0896-6273(02)00968-6

Zagotta, W.N., N.B. Olivier, K.D. Black, E.C. Young, R. Olson, and E. Gouaux. 2003. Structural basis for modulation and agonist specificity of HCN pacemaker channels. *Nature.* 425:200–205. http://dx.doi.org/10.1038/nature01922

Zhou, L., and S.A. Siegelbaum. 2007. Gating of HCN channels by cyclic nucleotides: residue contacts that underlie ligand binding, selectivity, and efficacy. *Structure.* 15:655–670. http://dx.doi.org/10.1016/j.str.2007.04.012

Zhou, L., N.B. Olivier, H. Yao, E.C. Young, and S.A. Siegelbaum. 2004. A conserved tripeptide in CNG and HCN channels regulates ligand gating by controlling C-terminal oligomerization. *Neuron.* 44:823–834. http://dx.doi.org/10.1016/j.neuron.2004.11.012

Zolles, G., D. Wenzel, W. Bildl, U. Schulte, A. Hofmann, C.S. Müller, J.-O. Thumfart, A. Vlachos, T. Deller, A. Pfeifer, et al. 2009. Association with the auxiliary subunit PEX5R/Trip8b controls responsiveness of HCN channels to cAMP and adrenergic stimulation. *Neuron.* 62:814–825. http://dx.doi.org/10.1016/j.neuron.2009.05.008

PART III

MATERIALS AND METHODS

Preparation of proteins

The cDNA fragment encoding residues 521–672 of human HCN2 (HCN2 CNBD) was cloned into a modified pET-24b downstream of a double His_6-maltose-binding protein (MBP) tag and transformed into *Escherichia coli* Rosetta strain under Kanamycin and chloramphenicol selection. In order to uniformly label HCN2 CNBD with ^{15}N or $^{15}N/^{13}C$, cells were grown in M9 minimal medium containing 1.0 g/L $^{15}NH_4Cl$ (*Isotec*), 3% glucose or ^{13}C-U, 1 mM $MgSO_4$, 0.01 mg/mL thiamine-HCl, 18.5 μM $FeCl_3$ $6H_2O$, 0.1 mM $CaCl_2$ $2H_2O$. HCN2 CNBD was expressed and purified using the protocol described in reference 31, with an additional step of purification. After the size exclusion chromatography the fractions containing HCN2 CNBD were combined and buffer exchanged using PD10 column to buffer A (5 mM KCl, 20 mM potassium phosphate, pH 6). A cation-exchange chromatography column Mono S G 5/5 (GE Healthcare) was used to remove remaining protein contaminants. Buffer A was used as binding buffer and elution was directed with buffer B (500 mM KCl, 20 mM potassium phosphate, pH 6). The constructs encompassing residues 188–268 (miniTRIP8b) and 188-240 (microTRIP8b) of TRIP8b (1a) were expressed and purified as described in reference 26.

Purification of protein complexes

The modified pET-24b containing $HCN2_{470-672}$ (C-linker + CNBD), previously described in reference 31, was co-transformed with vector pET-52b containing miniTRIP8b (see reference 26) into *Escherichia coli* Rosetta strain under Kanamycin and Ampicillin selection. Cells were grown at 37°C in Luria Broth to a OD_{600nm} of 0.6 and induced with 0.4 mM isopropyl-1-thioβ-D-galactopyranoside. After 3 h cells were collected by centrifugation and resuspended in ice-cold lysis buffer (500 mM KCl, 30 mM Hepes, pH 7.4, 10% w/v glycerol) with the addition of 1 mM β-mercaptoethanol, 10 µg/ml DNase, 0.25 mg/ml lysozyme, 100 µM phenylmethylsulfonyl fluoride, 5 µM leupeptin, and 1 µM pepstatin. The cells were sonicated on ice 12 times for 20 s each, and the lysate was cleared by centrifugation. The HCN2 C-linker/CNBD was purified by affinity chromatography on Ni^{2+}-NTA and

eluted in lysis buffer plus 300 mM imidazole and cAMP at different concentrations: from 0 to 1 mM.

The cDNA fragments encoding $HCN2_{521-645}$, $HCN2_{521-651}$, $HCN2_{521-657}$ and $HCN2_{521-663}$, $HCN2_{521-666}$, $HCN2_{521-669}$ were cloned into the same modified pET-24b described above. Each of these plasmids (including the one containing HCN2 CNBD earlier described) was co-transformed with pET-52b containing miniTRIP8b into *Escherichia coli* Rosetta strain under Kanamycin and Ampicillin selection. Cells were grown at 37°C in Luria broth to OD_{600nm} of 0.8 and induced with 0.1 mM isopropyl-1-thioβ-D-galactopyranoside for 3 h. The copurifications were performed using the protocol described in reference 26. Samples were analyzed by SDS-PAGE using a 8-16% Precise™ Tris-Glycine Gel (12 well) (Thermo scientific), in Tris-Glycine-SDS buffer.

Isothermal Titration Calorimetry

Measurements were carried out at 25 °C using an microcalorimeter (MicroCal VP-ITC System, GE Healthcare). The volume of sample cell was 2 ml; the reference cell contained water. The proteins were buffer exchanged with a PD10 column to PBS buffer. HCN2 CNBD (20 µM) was titrated with miniTRIP8b (200 µM) using injection volumes of 1 µl. Calorimetric data were analyzed with Origin software (version7, MicroCal), using equations described for the single-site binding model [63].

Circular Dichroism Measurements

Circular dichroism (CD) spectra were recorded with Jasco J-810 spectropolarimeter (Jasco Europe) at 22 °C using a 1 mm pathlength cuvette. Data were acquired every 1 nm. For the CD experiments the proteins were were buffer exchanged with a PD10 column to PBS buffer.

NMR Spectroscopy

Resonance Assignment of the cAMP-unbound CNBD

For NMR experiments the protein samples were buffer exchanged with a PD10 column to the following buffer: 150 mM KCl, 20 mM potassium phosphate, pH 7, 10 % (v/v) ^2H_2O (Sigma). The protein concentration used in the NMR experiments was 1 mM. NMR experiments were carried

out at 298 K on a Bruker AvanceIII 800 MHz NMR spectrometer equipped with a QXI-HCN gradient probe and a Bruker AvanceIII 600 MHz NMR spectrometer equipped with a TCI-cryoprobe. The sequence specific assignment of the protein backbone resonances were obtained by analyzing the 2D [^{1}H, ^{15}N]-HSQC, 3D HNHA, 3D HNCO, 3D HN(CA)CO, 3D CBCA(CO)NH, 3D HNCACB spectra [64]. For the side chain assignment 2D [^{1}H, ^{13}C]-HSQC and 3D (H)CCH-TOCSY experiments were performed [64]. The side chain of the aromatic residues were assigned using the [^{1}H-^{13}C] HSQC-NOESY experiment. The Nδ1 and Nε2 of histidine imidazole ring were assigned by performing 2J 2D NMR experiments, using a standard [^{1}H, ^{15}N]-HSQC experiment with 1/(2J) = 36 ms, an offset of 170 ppm, and a spectral width of 200 ppm for the ^{15}N dimension. Most of the aromatic ring protons HD and HE were assignment by acquiring 2D (HB)CB(CGCD)HD and (HB)CB(CGCD)HE spectra, which correlates CB with either HD or HE aromatic protons, together with the analysis of [^{1}H, ^{13}C] HSQC and [^{1}H, ^{13}C] HSQC -NOESY.

^{15}N NMR relaxation measurements

^{15}N R1 (=1/T1) and R2(=1/T2) experiments were acquired using the pulse sequences described in reference 54, at 800 MHz spectrometer described above. R1 and R2 delay times were set as 128, 256 (x2), 384, 512, 40 8x2), 769, 897 ms and 20, 40, 60, (x2), 80, 100, 120 (x2), 140, 160 ms respectively. The ^{15}N heteronuclear NOE (nuclear Overhauser effect) experiments were collected with a relaxation delay of 5 s with and without saturation of the amide protons that was achieved using 120° high-power pulses. [65]. The spectra was analysed in Analysis-CCPN [66], and the relaxation times were calculated using the scripts present in the software, as exponential fit of single exponential decays to peak intensity values: I=I0exp(−t/Tx) where Tx=T1 or T2, and I=resonance intensity at time t. Heteronuclear NOEs were calculated using the expression:

$$NOE = \frac{Isat}{Iunsat}$$

The standard deviation of NOE value, σNOE can be determined using the measured background noise levels:

$$\sigma NOE = \sqrt{\frac{\sigma \mathrm{Isat}^2}{Isat^2} + \frac{\sigma Iunsat^2}{Iunsat^2}}$$

2D NMR titrations

Sample preparation

Both ^{15}N-CNBD and mini or microTRIP8b proteins were buffer exchanged with a PD10 column to the following buffer: 150 mM KCl, 20 mM potassium phosphate, pH 7, 10 % (v/v) $^{2}H_2O$ (Sigma). The protein concentration used in the NMR experiments was 0.1 mM of CNBD.

2D NMR titrations

Each of the titration points was prepared independently by adding an aliquot of miniTRIP8b (or microTRIP8b) to a solution of ^{15}N-CNBD until a ratio of [mini or micro]/[HCN2] of 2.0 and keeping constant the concentration of CNBD. [^{15}N, ^{1}H] HSQC spectra were obtained using a phase sensitive and water flip-back pulse sequence. The spectral widths were 14 ppm for 1H and 27 ppm for ^{15}N. A total of 2048 data points in t2 and 4 transients for each of the 256 t1 were used. Spectra were acquired at 298 K on a Bruker Avance 600 MHz spectrometer equipped with a TCI Z-Grad cryo-probe. The NMR spectra were processed with TOPSPIN 2.1 provided by Bruker and analyzed with CARA 1.8.4 [67]. Chemical shift perturbation for each amide resonance, ΔδHN (ppm), was calculated as a combination of the changes in the proton (ΔδH) and nitrogen (ΔδN) dimensions according to the following equation:

$$\Delta\delta_{HN} = \sqrt{\frac{\Delta\delta_H^2 + \frac{\Delta\delta_N^2}{5}}{2}}$$ [68].